MICROWAVE SPECTROSCOPY OF JAHN-TELLER CRYSTALS

MICROWAVE SPECTROSCOPY OF JAHN-TELLER CRYSTALS

by

Abraham Jesion

A thesis submitted to the Faculty of Graduate Studies and Research of McGill University in partial fulfillment of the requirements for the Degree of Doctor of Philosophy

Eaton Electronics Research Laboratory, Department of Physics, McGill University, Montreal, Quebec, Canada

July 1976

© Abraham Jesion 1977

DEDICATED

TO

MY PARENTS

ABSTRACT

Accurate electron paramagnetic resonance (EPR) and spin-lattice relaxation measurements on the Jahn-Teller system Ti^{3+} as a dilute substitutional impurity for Al^{3+} in cesium aluminum alum were performed at X-band below 3°K. The quasi-Γ_8 ground state is a consequence of the almost exact cancellation of the effective trigonal field due to the dynamic Jahn-Teller coupling of the orbital triplet Γ_5 to the Γ_{3g} vibrational mode. An energy level splitting of 7 ± 1 cm^{-1} was measured between the ground state and the excited Γ_7 state.

The Jahn-Teller system Cu^{2+} as a dilute substitutional impurity for Zn^{2+} in zinc bromate hexahydrate was also studied using the same type of measurements below 4.2°K. From the angular variation of the EPR spectra, the ground state has been found to be a strain-stabilized vibronic doublet with the g-tensor principal axis displaced from the rhombohedral [100] axis. A concentration-independent, resonant two-phonon spin-lattice relaxation mechanism with an average energy level splitting to the first excited state of 3.1 cm^{-1} was determined. This has been interpreted in terms of a Jahn-Teller model based on random strain with dominant tetragonal components.

RESUME

La résonance paramagnétique (EPR) et la relaxation spin-réseau ont été mesurées pour le système Jahn-Teller Ti^{3+}: CsAl alum à 9.46 GHz pour des températures entre 1.27 et 2.63°K. L'état fondamental quasi-Γ_8 est causé par l'annulation presque complète du champ trigonal dû au couplage Jahn-Teller de l'état orbital triplet Γ_5 et le mode vibrionien Γ_{3g}. On a mesuré une différence d'énergie de 7±1 cm^{-1} entre l'état fondamental et l'état excité Γ_7.

On a étudié également le système Jahn-Teller Cu^{2+}: zinc bromate hexahydrate avec la même méthode au-dessous de 4.2°K. D'après la variation angulaire des spectres EPR, l'état fondamental est un doublet vibrionien, stabilisé par la tension, et l'axe principal du tenseur-g est déplacé de l'axe [100] rhomboèdral. On a trouvé un mécanisme de la relaxation spin-réseau résonnante de deux phonons, indépendante de la concentration de Cu^{2+}, avec le premier état excité à une énergie moyenne de 3.1 cm^{-1}. Ceci peut être interprété par un modèle Jahn-Teller basé sur la tension tétragonale aléatoire.

ACKNOWLEDGEMENTS

The author would like to thank Professor D. Walsh for his continuing guidance and encouragement throughout the course of this work. In addition, the author is indebted to Dr. Y.H. Shing for his constant aid, advice and numerous suggestions for the improvement of the research. Professors G. Donnay and J.D.H. Donnay of the Department of Geological Sciences have been very helpful with crystallographic problems. Mr. R. Schaeren supplied technical assistance in the laboratory while Mr. D. Jeffries of the Chemistry Department provided a chemical analysis of some of the samples. Thanks are also due to Joan Proudfoot and Debbie Terry for the rapid and skilled typing of the manuscript. The author would also like to thank the staff and students of the Eaton Electronics Research Laboratory for their assistance in all phases of this work.

The author gratefully acknowledges the National Research Council for the grant which supported the research project and for it's financial assistance in the form of a scholarship during his residence at McGill University.

STATEMENT OF ORIGINALITY

The Jahn-Teller model of a quasi-Γ_8 ground state has been used to consistently explain the EPR properties of the Ti^{3+}: CsAl alum system at liquid helium temperatures. Measurement of the almost exact cancellation of the effective trigonal field has led to an estimate of the orbital reduction factor $\gamma \sim 0.03$ and the energy level splitting $\Delta \sim 6$ cm^{-1} between the ground state and the excited Γ_7 state. Accurate spin-lattice relaxation measurements were used to determine for the first time the details of the relaxation process over the temperature range 2.63 to 1.27°K. This data confirmed the Γ_7 energy level splitting to be 7 ± 1 cm^{-1}.

Large numbers of single crystals of zinc bromate hexahydrate have been grown with various concentrations of the single isotope $^{65}Cu^{2+}$ as a dilute substitutional impurity for Zn^{2+}. For the first time the complicated EPR spectra (and spin-Hamiltonian parameters) of this Jahn-Teller system have been measured and explained at liquid helium temperatures. The angular variation of the EPR spectra shows that the ground state is a strain-stabilized vibronic doublet. An angular displacement of the g-tensor principal axis from the rhombohedral [100] axis was experimentally confirmed for the first time. The temperature dependence of the spin-lattice relaxation rate was measured between 4.2 and 1.3°K for samples with Cu^{2+} concentrations varying by a factor of 18. A consistent resonant two-phonon relaxation mechanism has been observed for all concentrations which supports a Jahn-Teller model based on random strain with dominant tetragonal components.

TABLE OF CONTENTS

1. BACKGROUND

The primary objective of this work is to investigate the nature of two paramagnetic ions, octahedrally co-ordinated Ti^{3+} and Cu^{2+} as impurities in insulating crystals which are subject to "Jahn-Teller" effects. Previously, at the Eaton Laboratory of McGill University, Shing et al. (1974) studied Ti^{3+} in methylammonium aluminum alum while Vincent and Walsh (1973) investigated Cu^{2+} in lanthanum magnesium nitrate. To test their models and compare the general properties of such systems, their electron paramagnetic resonance (EPR) and spin-lattice relaxation measurements have been extended to two similar Jahn-Teller systems; Ti^{3+} in cesium aluminum alum and Cu^{2+} in zinc bromate hexahydrate. Before beginning the discussion of the theoretical and experimental aspects of this work, a general background to the subject material is presented in Chapter 1. Here the fundamental concepts and terminology are briefly outlined. Chapter 2 provides a review of some of the previous work in the literature which is relevant to the following discussion. The next two chapters survey the theory of Jahn-Teller effects for orbital triplet and doublet electronic states respectively, while the apparatus is described in Chapter 5. Chapter 6 details the EPR and relaxation data obtained for Ti^{3+} in cesium aluminum alum as well as discussing the results. This is repeated in the following chapter for Cu^{2+} in zinc bromate hexahydrate. Chapter 8 summarizes the results and gives our conclusions.

1.1 Definition of Paramagnetism

A paramagnetic substance may be defined as one that possesses no resultant magnetic moment in the absence of an applied external magnetic field. However it acquires a magnetic moment in the direction of the applied external magnetic field, whose size is a function of the field. In general, it can be said that all magnetic effects are due to magnetic moments $\vec{\mu}$, through their interaction with each other and with an external magnetic field. In a particular material, the combined effect of all the individual moments is referred to as the magnetization $\vec{M}$ and the ratio of this quantity to an external magnetic field $\vec{H}$ is called the magnetic susceptibility χ. Of interest here are atoms or ions which have permanent magnetic moments which tend to align themselves with an applied field, giving rise to a positive χ. The tendency for alignment is hindered by thermal agitation according to Curie's Law,

$$\chi=\frac{C}{T} \tag{1.1}$$

where C is the Curie contant. This constant may be evaluated by using a quantum mechanical approach based on the quantization of the total angular momentum $\vec{J}$ of the ion or atom. The result, for a system of N magnetic moments is,

$$C=\frac{g^2\beta^2N\ J(J+1)}{3k} \tag{1.2}$$

where g is the spectroscopic splitting factor and $\beta=\frac{eh}{2mc}$ is the Bohr magneton.

1.2 Paramagnetic Resonance

Permanent magnetic dipoles occur only when an atom or ion possesses a resultant angular momentum $\vec{J}$ ($J=\frac{\hbar}{2}, \hbar, \frac{3\hbar}{2}\ldots$). These are related by

$$\vec{\mu}=\gamma\vec{J} \tag{1.3}$$

where γ is the gyromagnetic ratio of the order of (e/mc). When such a dipole is exposed to an external magnetic field $\vec{H}$, it experiences a couple $\vec{\mu} \times \vec{H}$, so that the equation of motion is

$$\frac{d\vec{J}}{dt}=\vec{\mu} \times \vec{H} \tag{1.4}$$

Hence the motion of $\vec{J}$ and $\vec{\mu}$ consists of a uniform precession about $\vec{H}$ with an angular velocity

$$\vec{\omega}=-\gamma\vec{H} \tag{1.5}$$

where the negative sign means that the precession is in the direction of a left-handed screw advancing along $\vec{H}$ if γ is positive and vice versa. The component of $\vec{J}$ or $\vec{\mu}$ along $\vec{H}$ remains fixed in magnitude so that the Zeeman energy of the dipole in the field $\vec{H}$, namely $-\vec{\mu}.\vec{H}$ is a constant of the motion.

The gyromagnetic ratio for a free ion or atom which has a resultant electronic angular momentum is

$$\gamma=-g\left(\frac{e}{2mc}\right) \tag{1.6}$$

where the negative sign occurs because of the negative charge on the electron, while e and m represent the charge and mass respectively on the electron. The g-factor, as it is usually referred to, is a pure number of order unity whose value depends on the relative contributions of orbit and spin to the total angular momentum. For a free atom with an orbital angular momentum the g-factor is given by

$$g = 1 + \frac{J(J+1)+S(S+1)-L(L+1)}{2\ J(J+1)} \qquad (1.7)$$

where the resultant angular momentum $\vec{J}=\vec{L}+\vec{S}$ and L, S are the quantum numbers of the total orbital and total spin momentum respectively.

When a magnetic dipole precesses about an external field $\vec{H}$ with an angular velocity $\vec{\omega}_L=-\gamma\vec{H}$, this precession produces an oscillatory magnetic moment, in any direction normal to the field $\vec{H}$, which can interact with an oscillatory magnetic field, $H_1 \cos \omega t$, which is also normal to $\vec{H}$. The interaction has an important effect only when ω is close to the natural precession frequency ω_L, so that we are concerned with a resonance phenomenon. When $\omega=\omega_L$, the component of the dipole along the external magnetic field can be altered even by oscillatory fields whose amplitude $H_1 << H$. This effect is known as "magnetic resonance".

A change in the component of $\vec{\mu}$ in the direction of $\vec{H}$ means a change in the energy of the dipole which can be written as

$$W = -\gamma J H \cos \alpha \qquad (1.8)$$

where α is the angle between $\vec{\mu}$ and $\vec{H}$. The component of the angular momentum in the direction of $\vec{H}$, namely $J \cos \alpha$, may take on the discrete values $\hbar M$, $\hbar(M-1)$, etc. where the magnetic quantum number M has a series of integral or half-integral values differing by unity between successive values. In this case, the allowed transitions are given by the selection rule $\Delta M = \pm 1$ when a suitably oriented oscillatory magnetic field is applied. The electronic magnetic dipole moment for a free atom can be written in the form,

$$\vec{\mu}_J = -g_J \, \beta \, \vec{J} \qquad (1.9)$$

and the Hamiltonian for its Zeeman interaction with a field $\vec{H}$ is,

$$\mathcal{H} = -(\vec{\mu}_J \cdot \vec{H}) = g_J \, \beta (\vec{H} \cdot \vec{J}). \qquad (1.10)$$

A quantum of energy is thus required of size

$$\hbar\omega = W_M - W_{M-1} = -\gamma \hbar H \qquad (1.11)$$

For a state with magnetic quantum number M, corresponding to a component $\hbar M$ of angular momentum in the direction of $\vec{H}$, the energy is

$$W_M = g_J \, \beta \, HM \qquad (1.12)$$

and allowed transitions of the type $\Delta M=\pm 1$ require an energy quantum

$$h\nu=g_J\ \beta\ H \qquad (1.13)$$

This form of Zeeman interaction is valid for a group of (2J+1) levels, degenerate when H=0, and well separated from other levels. Partly filled electron shells, with permanent dipole moments due to the orbital motion of the electrons, are the cause of paramagnetism which is of interest in this work. In particular, Ti^{3+} has only one electron in the 3d shell while Cu^{2+} has only one electron vacancy or "hole" in the 3d shell.

1.3 The Crystalline Electric Field

In the solid state, a paramagnetic ion is by no means "free". It is embedded in a complex of diamagnetic neighbour ions which form part of an extended lattice. These charged neighbour or ligand ions have a strong interaction with the paramagnetic ion, producing a strong electrostatic field (the ligand field), through which the paramagnetic electrons must move. This ligand interaction is in addition to the spin-orbit and electron-electron interactions of the central ion which complicate the problem.

In the "crystal field" approach, the ligand ions are regarded as setting up an additional electrostatic potential which reflects the symmetry of the complex and its immediate surroundings. The magnetic electrons, which are localized on the central ion and move in the effective potential, experience a "Stark splitting" of their orbital levels. The lowest energy levels are associated with the negatively charged electrons avoiding negatively charged ligand ions and hence minimizing the energy due to their mutual electrostatic repulsion.

The degeneracy within groups of energy levels depends on the symmetry within the complex and can thus be predicted by group theory. An important theorem concerning the residual degeneracy is due to Kramers (1930). In a system containing an odd number of electrons, at least twofold degeneracy must remain in the absence of a magnetic field. The pairs of states or "Kramers doublets" are time conjugate (one can be obtained from the other by use of a time-reversal operator) and can be split only by a time-odd operator such as a magnetic field but not by an electrostatic perturbation which is even under time reversal.

1.4 The Spin-Hamiltonian

The most general form of the Hamiltonian to represent the interaction energy of a paramagnetic ion in a constant magnetic field is given by, (Abragam and Pryce, 1951; Bleany and Stevens, 1953)

$$\mathcal{H} = \mathcal{H}_{\mathrm{elect}} + \mathcal{H}_{\mathrm{CF}} + \mathcal{H}_{\mathrm{LS}} + \mathcal{H}_{\mathrm{SS}} + \mathcal{H}_{\mathrm{Zee}} + \mathcal{H}_{\mathrm{hfs}} + \mathcal{H}_{\mathrm{Q}} + \mathcal{H}_{\mathrm{N}} \quad (1.13)$$

$\mathcal{H}_{\mathrm{elect}}$ represents the electronic energy of the paramagnetic ion in the free state with a magnitude approximately 10^4-10^5cm^{-1}.

$\mathcal{H}_{CF}$ is the energy of the interaction between the free ion's electronic structure and the crystalline electric field ($\approx 10^3$-10^4 cm^{-1}). $\mathcal{H}_{LS}$ is the spin-orbit interaction ($\approx 10^2$ cm^{-1}). $\mathcal{H}_{SS}$ is the spin-spin interaction (≈ 1 cm^{-1}). $\mathcal{H}_{Zee}$ is the Zeeman energy (≈ 1 cm^{-1}). $\mathcal{H}_{hfs}$ is the hyperfine interaction with the nuclear spin (≈ 0-10^{-2} cm^{-1}). $\mathcal{H}_{Q}$ is the nuclear quadrupole energy (≈ 0-10^{-2} cm^{-1}) while $\mathcal{H}_{N}$ is the nuclear spin energy (≈ 0-10^{-3} cm^{-1}).

In EPR measurements, at microwave frequencies transitions are detected between levels whose splitting is on the order of 1 cm^{-1}. Hence the interest lies only in groups of levels which are degenerate or very close to degenerate in zero magnetic field. A convenient method which represents the behaviour of such a group of levels when a magnetic field is applied involves the use of the concept of an "effective spin" $\tilde{S}$, which is a fictitious angular momentum. The value of $\tilde{S}$ is selected so that the degeneracy of the groups of levels involved is set equal to $(2\tilde{S}+1)$. This concept can be then extended to the use of an "effective spin-Hamiltonian" that may be used to describe the behaviour of a group of levels in the same manner as is common for free atoms or ions. The fictitious spin $\tilde{S}$ may or may not be the actual angular momentum of the paramagnetic ion or atom depending on factors such as the local symmetry of the complex.

The simplest form of the Zeeman interaction for example is,

$$\mathcal{H}_{Zee}=\beta(\vec{H}\cdot\overleftrightarrow{g}\cdot\vec{\tilde{S}}) \tag{1.14}$$

where $\overleftrightarrow{g}$ is the g tensor and $\tilde{S}$ is the effective spin. This is shorthand notation for,

$$\mathcal{H}_{Zee}=\beta\{g_{xx}H_x\tilde{S}_x+g_{yy}H_y\tilde{S}_y+g_{zz}H_z\tilde{S}_z$$

$$+\ g_{xy}H_x\tilde{S}_y+g_{yx}H_y\tilde{S}_x+g_{yz}H_y\tilde{S}_z \qquad (1.15)$$

$$+\ g_{zy}H_z\tilde{S}_y+g_{xz}H_x\tilde{S}_z+g_{zx}H_z\tilde{S}_x\}$$

In the majority of cases where there is some crystal symmetry, the cross terms can be eliminated with a suitable choice of X, Y and Z axes known as the "principal axes", giving the interaction the form,

$$\mathcal{H}_{Zee}=\beta(g_{xx}H_x\tilde{S}_x+g_{yy}H_y\tilde{S}_y+g_{zz}H_z\tilde{S}_z) \qquad (1.16)$$

For axial symmetry $g_{xx}=g_{yy}=g_{\perp}$ and $g_{zz}=g_{\parallel}$ so that equation (1.16) reduces to

$$\mathcal{H}_{Zee}=g_{\parallel}\ \beta H_z\tilde{S}_z+\ g_{\perp}\beta(H_x\tilde{S}_x+H_y\tilde{S}_y) \qquad (1.17)$$

where

$$g=\sqrt{g_{\parallel}^2\cos^2\theta+g_{\perp}^2\sin^2\theta} \qquad (1.18)$$

is the value required to maintain the form of the resonance transition (1.13) and θ is the angle between $\vec{H}$ and the Z-axis. This g or "spectroscopic g-factor" is one of the family of parameters used to describe the behaviour of paramagnetic resonance phenomena by means of the spin-Hamiltonian.

1.5 Paramagnetic Relaxation

From the most general considerations, spin-lattice relaxation may be thought of as the process by which the energy absorbed by the spin system in a magnetic field is dissipated to the lattice when the magnetic field is removed. A large number of models have been used over the years to explain the wideranging results obtained for the temperature dependence of the relaxation rate. Appendix 1 provides a short bibliography of some important references in this field.

Figure 1.1 shows schematically the three most common relaxation mechanisms quoted in the literature. Consider a pair of states $|a>$ and $|b>$ of the paramagnetic ion having energy E_a and E_b respectively where $E_a<E_b$ and $\delta=E_b-E_a$. The direct process of Figure 1.1a, involving phonons of the same energy as the magnetic resonance quantum $h\nu$, is merely the downward transition from the excited state $|b>$ to the ground state accompanied by the simultaneous creation of an energy conserving phonon. The spin-Lattice relaxation rate $1/\tau$ of such a mechanism has the form,

$$\frac{1}{\tau}=A \coth \frac{h\nu}{2kT} \qquad (1.19)$$

where A is a constant. When $kT>>h\nu$, the direct process exhibits a linear temperature dependence. For the case when $h\nu>>kT$, this process tends to give a constant spin-lattice relaxation rate

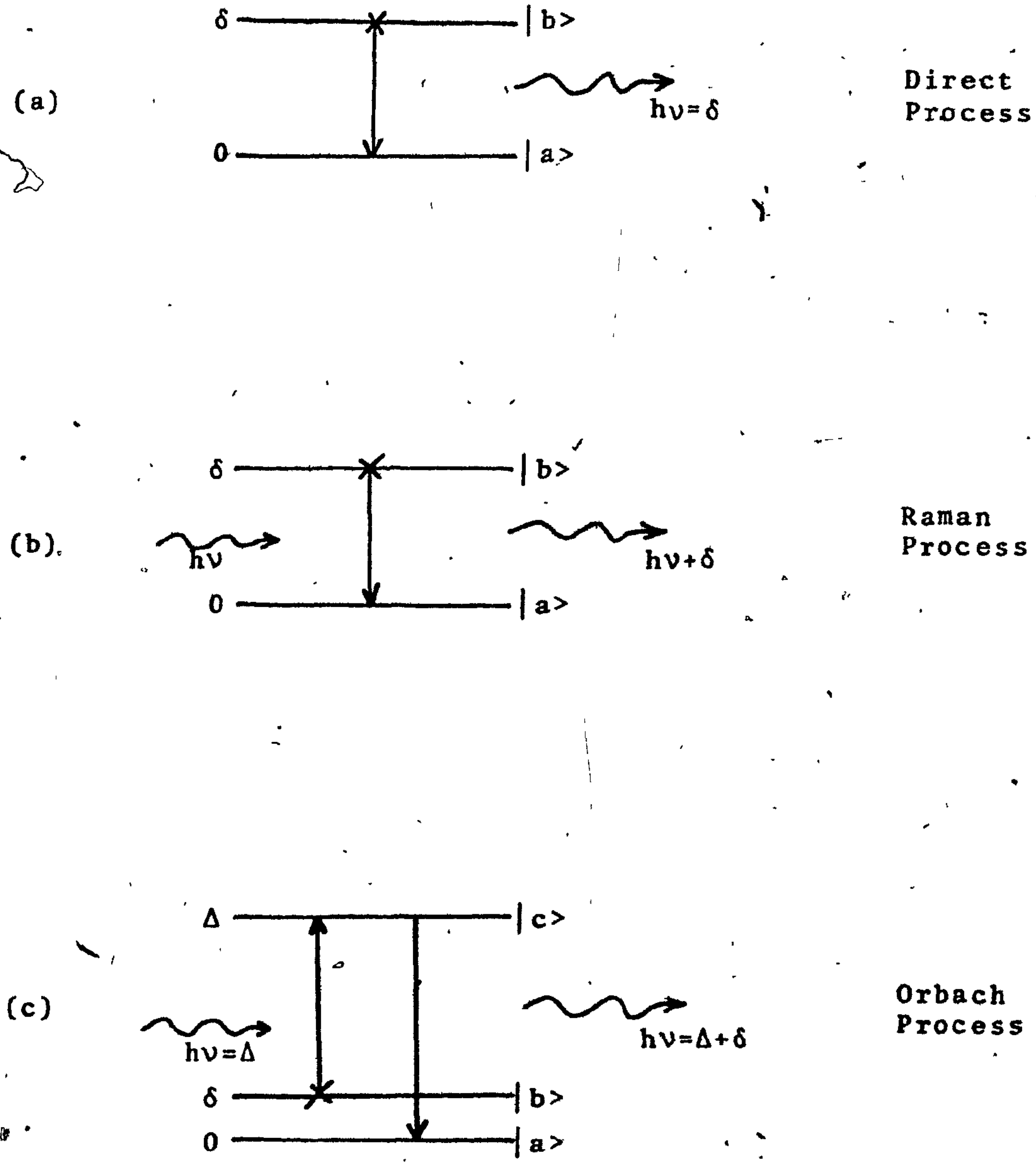

FIGURE 1.1

Pictorial representation of three spin-lattice relaxation mechanisms.

determined by the rate of spontaneous emission of phonons from the upper state when phonons of energy hν are no longer thermally excited.

The Raman process is shown schematically in Figure 1.1b. A phonon of energy hν interacts with a spin, causing a transition from $|b\rangle$ to $|a\rangle$ within the spin system, the phonon being scattered with a different energy $h\nu+\delta$ where δ is the energy splitting between the Zeeman levels of the transition. The temperature dependence of the Raman relaxation process is

$$\frac{1}{\tau} = B\,T^{n} \qquad (1.20)$$

where B is a constant and n=9 for a Kramers doublet of states, n=7 for a non-Kramers doublet and n=5 for a multiplet with small splitting.

Figure 1.1c represents the resonant Raman or Orbach relaxation mechanism. This involves the absorption of a phonon by a direct process to excite the spin system to a higher energy level $|c\rangle$ at Δ above the ground doublet, followed by the emission of another phonon of slightly different energy so that the magnetic ion is indirectly transferred from one level to the other of the ground doublet. The temperature dependence of the Orbach process is

$$\frac{1}{\tau} = C\left[\exp\left(\frac{\Delta}{kT}\right)-1\right]^{-1} \qquad (1.21)$$

where C is a constant.

These three mechanisms are by no means the only ones by which spin-lattice relaxation may proceed. The problem of measuring and determining the temperature dependence of the relaxation rate is complicated by the superposition of more than one relaxation mechanism and/or the interference between these mechanisms as they compete for the phonon spectrum. The review by Manenkov and Orbach (1966) for example includes a number of aspects of the problem.

1.6 The Jahn-Teller Theorem

The fundamental theorem of the Jahn-Teller effect may be stated as follows: When an atom, ion or crystalline defect has orbital electronic degeneracy and its neighbours are in a symmetric (non-linear) configuration, then the atom, ion or defect is unstable with respect to at least one assymmetric displacement of the neighbours which lifts the degeneracy. This theorem was proved by Jahn and Teller (1937) from an examination of the properties of all the point symmetry groups and is merely an existence theorem concerning the availability in all cases of at least one mode of distortion that can cause some energy level splitting.

The simplest example of a situation where the theorem is applicable is illustrated in Figure 1.2. Consider a doubly degenerate electronic state in a symmetric configuration with energy E_o. According to the Jahn-Teller theorem, there is some distortion denoted by Q which splits the electronic degeneracy and causes the lower split-off state to have an energy E_a such that (E_o-E_a) increases linearly for small values of Q. Since

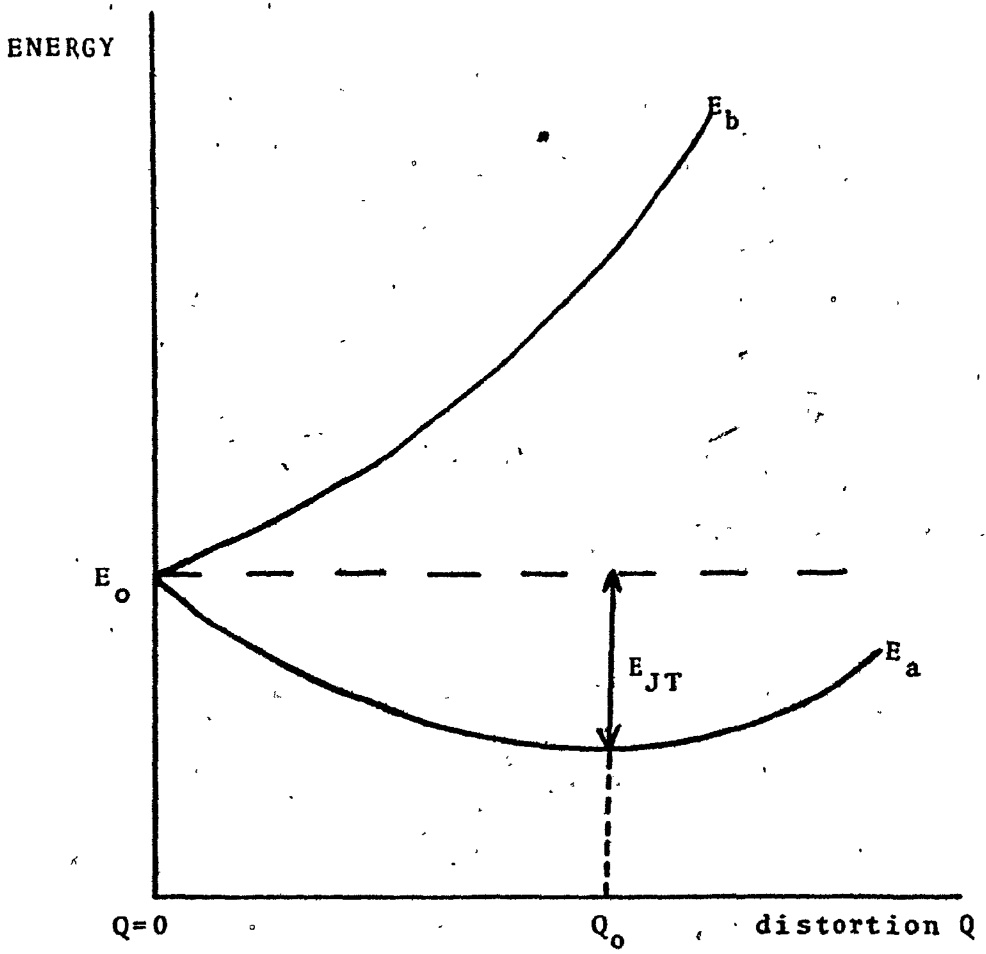

FIGURE 1.2

Energy splitting of a doubly degenerate electronic state under a distortion that lifts the degeneracy to first order.

the elastic energy associated with this distortion is proportional to Q^2 there will be a position of minimum (E_o-E_a). Thus, the symmetric configuration is unstable and the system can lower its energy by distorting to a finite $Q=Q_o$. The energy difference E_{JT} by which the lower split-off state's energy lies below the energy of the symmetric configuration is the "Jahn-Teller" or stabilization energy of the distorted configuration and usually has a magnitude of the order of 1000 cm^{-1}.

Although an individual complex may be spontaneously distorted into a particular configuration, there may still be significant dynamic corrections (O'Brien, 1964). These are due to zero point ionic motion in the ground state and reorientation by tunneling through or thermal activation over a barrier from one distorted configuration to another. A measurement made in a time short compared to the time for reorientation will indicate a static distortion, while one taking a longer time may yield an average over the configurations and thus correspond to a dynamic effect. A second type of dynamic effect was introduced by Moffitt and Liehr (1957) and Longuet-Higgins et al. (1958). It arises when the electronic and vibrational motions of the system are coupled, hence mixing the electronic and vibrational parts of the wave function of the coupled system. Eigenstates of such a coupled system are labelled "vibronic" eigenstates.

2. INTRODUCTION

This thesis reports the EPR spectra and spin-lattice relaxation rates of Ti^{3+} in cesium aluminum alum and Cu^{2+} in zinc bromate hexahydrate at liquid helium temperatures. Since transition metal ions have been under extensive investigation for some time, it is the aim of this chapter to review some of the theoretical and experimental papers found in the literature.

2.1 Review: Ti^{3+} in Alum

The Ti^{3+} ion has only one 3d electron in its outermost shell. This makes the analysis of its properties from basic principles somewhat simpler than other transition metal ions. However, since Ti^{3+} is readily oxidized to Ti^{4+}, it has been difficult to study the ion in the majority of crystal hosts. Nevertheless, the study of Ti^{3+} both in concentrated and dilute form within alum crystals has been a subject of considerable interest during the past twenty-five years. Paramagnetic resonance, relaxation and magnetic susceptibility data have been the basis of much theoretical analysis.

Van Vleck (1939a) first pointed out the special place occupied by the alums in the understanding of the subject of paramagnetic relaxation. The next year, Van Vleck (1940) called attention to the difficulties experienced in relating the experimental results to theory for a "pure" or undiluted titanium alum. It was in that paper in relation to titanium that he wrote:

"The agreement with experiment is miserable."

Bijl (1950) first observed electron paramagnetic resonance of Ti^{3+} in concentrated CsTi alum powder over a range of temperatures between 6.33°K and 7.88°K. He measured the effective g-factors to be 1.35 at the lower and 1.53 at the higher temperature. Bleaney et al. (1955a) investigated the spectrum of a single crystal of CsTi alum at temperatures between 2.5°K and 4.2°K. They found a wide line of width 250±50 gauss for which they give the g-factors $g_{\parallel}=1.25\pm0.02$ and $g_{\perp}=1.14\pm0.02$. They interpreted their results as indicating that Ti^{3+} exists in four differently oriented, but otherwise equivalent, trigonally distorted magnetic complexes with the z-axis directed along the <111> crystal directions. They concluded that simple crystalline field theory was inadequate to explain their results. Gladney and Swalen (1965) have discussed the results of Bleaney et al. and have applied their own computations to explain them. It was only by using an unusually large Stevens orbital reduction factor (Stevens, 1953) that they were able to bring experiment and theory into agreement. In a series of reports on Ti^{3+} substituting for Al^{3+} in CsAl alum (Woonton and MacKinnon, 1968), RbAl alum (Dionne, 1964) and TlAl alum (Dionne, 1966a) the appearance in the spectrum of more than four EPR lines with an unexpected anisotropy was interpreted as evidence of lower-than-trigonal site symmetry for the Ti^{3+} site. The lower symmetry was considered to be due to an effective displacement of the $[Ti(H_2O)_6]^{3+}$ octahedron perpendicular to the trigonal symmetry axis, giving rise to twelve magnetic complexes in the unit cell. Gladney and

Swalen (1965) criticized this model on symmetry grounds, and the unusual interpretation arose because the ground state was assumed to be described by an effective spin $S=\frac{1}{2}$.

The first reported spin-lattice relaxation experiments with Ti^{3+} in an alum lattice were by Gorter et al. (1938) at 77°K and by de Haas and du Pré (1938) in the liquid helium range of 4.2°K and lower using non-resonant techniques. In the latter, the value of τ was established as less than a millisecond at 1.2°K. However, no insight into the type of relaxation process was derived since there was no way of determining the temperature dependence of τ because no dispersion was observed. It should also be noted that these measurements were carried out with undiluted CsTi alum, with the result that τ cannot be equated to the spin-lattice relaxation time since dipole-dipole interaction undoubtedly influenced the result. Van Vleck (1940) also questioned the reliability of these previous measurements because the samples studied may have been affected by dehydration. Dionne (1966b) reported continuous wave saturation measurements on titanium-doped rubidium alum after unsuccessfully preparing samples of Ti^{3+} in CsAl alum. He only succeeded in obtaining 3 experimental points, which prevented the determination of the relaxation mechanism with any certainty. As reported in that paper the data was influenced by the presence of Cr^{3+} impurity.

Moffitt and Thorson (1957) and Opik and Pryce (1957) were the first to consider the details of the theory of Jahn-Teller effects for a triplet state. They discussed the vibronic Hamiltonian of an orbital triplet electronic state coupled to vibrational modes of the complex and gave the corresponding vibronic eigenstates. Ham (1965) extended this analysis to calculate orbital reduction factors for matrix elements of interactions within the electronic triplet. Macfarlane et al. (1968) and Bates and Bentley (1969) also considered a Jahn-Teller model in which the triplet orbital state is coupled to the lattice vibrations. This model was used by Rumin et al. (1973) to explain the ground state g-values of Ti^{3+} in methylammonium aluminum alum. Their values of $g_{\parallel}=1.37 \pm 0.01$ and $g_{\perp}=1.16 \pm 0.01$ cannot be explained using static crystal field theory.

Since more accurate data is required to further the understanding of the $[Ti(H_2O)_6]^{3+}$ system, this thesis describes the EPR and spin-lattice relaxation measurements which were carried out on Ti^{3+} in CsAl alum at liquid helium temperatures. The data obtained is then used to construct a model for the energy level structure based on the Jahn-Teller model described in Chapter 3.

2.2 Review: Cu^{2+} in Octahedral Co-ordination

The ground state of a cubic octahedrally co-ordinated Cu^{2+} ion is the orbital doublet ^2E_g. The only excited state is the $^2T_{2g}$ orbital triplet at approximately $10^4 cm^{-1}$ above the ground state. The Cu^{2+} configuration possesses one hole in the filled d shell so that the spectral behaviour of the complex should be as found in octahedrally co-ordinated Ti^{3+} complexes, only with the level order inverted.

Considerable theoretical work on Cu^{2+} followed the enunciation of the Jahn-Teller Theorem (Jahn and Teller, 1936, 1937). Van Vleck (1939a,b) predicted that Cu^{2+} when in an octahedral environment would suffer a Jahn-Teller distortion to a state of lower symmetry. A more detailed treatment of this problem was given by Opik and Pryce (1957) who also gave estimates for some of the important parameters of the theory.

The first unambiguous experimental evidence of the Jahn-Teller effect was found by Bleaney and Ingram (1950) in an EPR study of Cu^{2+} in zinc fluosilicate. They found a spectrum which was anomalous from the standpoint of ordinary crystal field theory but which could be explained as a result of the Jahn-Teller instability for the orbital doublet ground state of the Cu^{2+} ion. Abragam and Pryce (1950) explained this nearly isotropic EPR spectrum at 90°K as corresponding to an average of the anisotropic spectra expected for the various possible Jahn-Teller distortions of the Cu^{2+} complex. The high temperature (90°K) spectrum resulted from the rapid reorientation of the complex between these various distorted configurations. Bleaney and Bowers (1952) reported the EPR spectra of Cu^{2+} in zinc fluosilicate, copper bismuth double nitrate and copper bromate at 20°K. In each case the anisotropic EPR spectra of the individual static Jahn-Teller-distorted configurations of Cu^{2+} were observed.

Other experimental EPR data have reinforced the Jahn-Teller model for Cu^{2+} in octahedral co-ordination. Notable among the systems studied are Cu^{2+} within MgO and CaO (Reynolds et al. 1974; Low and Suss, 1963; and Coffman, 1968). Of most interest here is the work of Bleaney et al. (1955c) who reported the EPR spectra of Cu^{2+} as a dilute substitutional impurity for Mg^{2+} or Zn^{2+} in magnesium bismuth double nitrate, deuterated lanthanum magnesium double nitrate, zinc fluosilicate and zinc bromate. Since little understanding of the bromate system was achieved through their measurements at 90°K, this system was chosen for further investigation at liquid helium temperatures within this thesis. In addition the anisotropic spectrum of Cu^{2+} in zinc bromate was not investigated sufficiently to determine the spin-Hamiltonian parameters.

After Moffitt and Liehr (1957) had examined Jahn-Teller effects as fundamental consequences of the coupling between electronic energy states and nuclear displacements, the Cu^{2+} or $3d^9$ electronic configuration served as a model for such calculations. O'Brien (1964) supplemented the earlier treatments of the static Jahn-Teller effect for the case of the orbital doublet by examining the dynamic effects resulting from ionic motion in the ground state and low-energy vibronic states of the distorted complex. As a result of tunneling from one distorted configuration to another, the vibronic energy levels are split in proportion to the tunneling frequency, with the vibronic ground state remaining a degenerate doublet. For a strong Jahn-Teller coupling, O'Brien showed how the tunneling splittings of low energy vibronic states depend on the barrier heights between the configurations. Earlier, Bersuker (1963) had also investigated the dynamic effects of this tunneling in strongly distorted Jahn-Teller systems.

Recognition that the theory of dynamic Jahn-Teller effects held widespread implications in the interpretation of EPR and optical spectra of paramagnetic complexes was in the work of Ham (1965, 1968). He showed that a dynamic Jahn-Teller effect can cause large changes in the matrix elements of electronic operators such as the orbital angular momentum operator, the spin-orbit interaction and the operators governing the splitting of the electronic degeneracy under applied strain. This is due to the mixing of the vibrational and electronic wave functions that occurs even in the vibronic ground state. In the limiting case of a strong Jahn-Teller coupling, in which some of these matrix elements are quenched effectively to zero, the system exhibits the behaviour expected for a static Jahn-Teller effect. Ham's review (1972) gives an excellent summary of both theoretical and experimental aspects of the problem.

It has been found in several Jahn-Teller systems involving Cu^{2+} in hydrated host crystals, that spin-lattice relaxation rates are considerably faster than in similar systems in which there is no orbital degeneracy. An enhanced spin-lattice relaxation rate has been found by Lee and Walsh (1968) and Breen et al. (1969) for Cu^{2+} in $La_2Mg_3(NO_3)_{12}.24H_2O$ to be at liquid helium temperatures, four to five orders of magnitude faster than that of Cu^{2+} in potassium zinc Tutton salt (Gill, 1965), in which a strong tetragonal crystal field removes the orbital degeneracy thus suppressing the Jahn-Teller effect. Even faster spin-lattice relaxation rates for the $Cu^{2+}(H_2O)_6$ complex in zinc fluosilicate were measured by Dang et al. (1974). Preliminary spin-lattice relaxation data on Cu^{2+} in zinc bromate below 10°K were also reported in the paper of Breen et al. (1969) although the EPR spectrum had never been reported at these temperatures. Only a qualitative comment was made on their data which was not analysed in detail. As was the case for Ti^{3+} in CsAl alum, more EPR and spin-lattice relaxation data for the Cu^{2+}: zinc bromate hexahydrate system must be obtained before a consistent model is constructed.

3. JAHN-TELLER EFFECTS FOR AN ORBITAL TRIPLET STATE

3.1 Normal Co-ordinates

In this chapter and the next, molecular clusters of the form XY_6 are examined. Here X signifies a paramagnetic ion and Y a water molecule. Jahn and Teller (1937) have shown that if the X ion has a degenerate electronic ground state (excluding Kramers degeneracy), the water group distorts itself so that it is not cubically arranged and the degeneracy is lifted. The reason for this is that in a degenerate system, the electronic charge cloud has different orientations for different components of the degenerate family of levels. This means that linear terms in the normal co-ordinates cannot be simultaneously eliminated for all components which implies a distortion and a lowering of the symmetry.

The modes of distortion of an octahedron of six ions have been discussed by Van Vleck (1939b). He numbered Y ions at the corners of the octahedron 1-6 and placed them at the positions (R,0,0), (0,R,0), (0,0,R), (-R,0,0), (0,-R,0) and (0,0,-R) respectively, while the central or X ion was placed at the origin of the co-ordinate system. The displacement of the n^th^ ion is denoted by (X_n, Y_n, Z_n). Thus the six Y ions occupy the face centers of a cube of width 2R.

A cluster such as XY_6 has 21 degrees of freedom characterized by normal co-ordinates which are usually classified as even (g) or odd (u). Normal co-ordinates are odd if they change sign under reflection in the origin. These introduce no linear terms in the Hamiltonian and need not be considered in the problem. Ignoring translations or rotations, the only even normal co-ordinates of an octahedral complex XY_6 can be written,

$$Q_1=1/\sqrt{6}[X_1-X_4+Y_2-Y_5+Z_3-Z_6]$$

$$Q_2=\frac{1}{2}[X_1-X_4-Y_2+Y_5]$$

$$Q_3=(1/\sqrt{3})[\frac{1}{2}(X_1-X_4+Y_2-Y_5)-Z_3+Z_6] \qquad (3.1)$$

$$Q_4=\frac{1}{2}[Z_1-Z_4+X_3-X_6]$$

$$Q_5=\frac{1}{2}[Z_1-Z_4+X_3-X_6]$$

$$Q_6=\frac{1}{2}[Z_2-Z_5+Y_3-Y_6]$$

only $Q_2,\ldots, Q_6$ can give rise to linear terms in the Hamiltonian while Q_1 adds a constant term which can merely shift the set of energy levels without causing any splitting. The corresponding modes of vibration are shown schematically in Figure 3.1.

The Hamiltonian for such an isolated cluster can be written

$$\mathcal{H}=V_o+\sum_{i=2}^{6}V_iQ_i \qquad (3.2)$$

where V_o is a function of the co-ordinates of the d electrons of the central ion and has cubic symmetry while $V_2,\ldots,V_6$ are coefficients depending on the co-ordinates and forces between the X and Y ions. These coefficients characterize the Jahn-

FIGURE 3.1

The symmetrical modes of vibration of an octahedral complex.

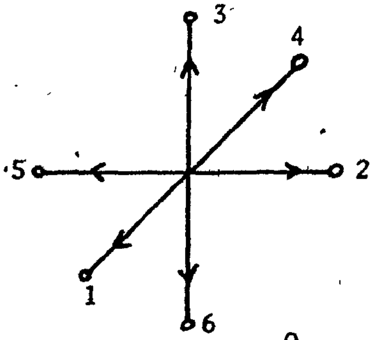

Q_1

Γ_{1g}

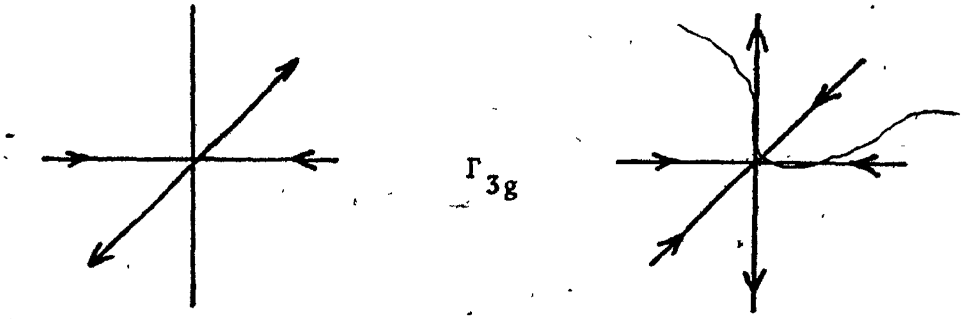

Q_2 Γ_{3g} Q_3

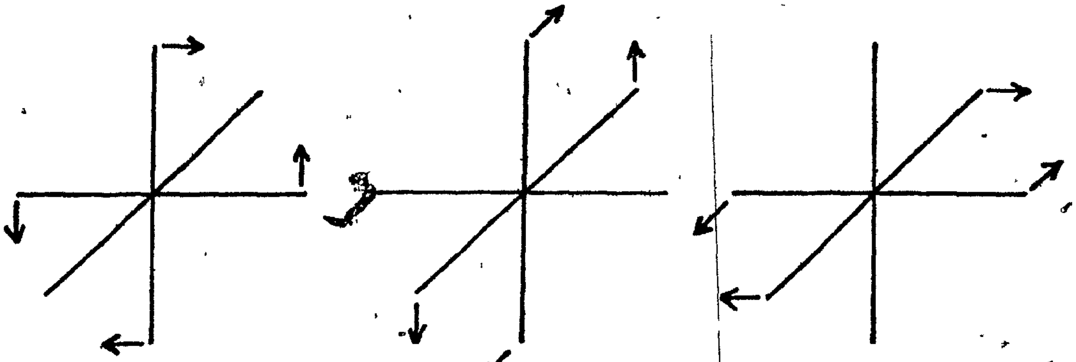

Q_4 Q_5 Q_6

Γ_{5g}

Teller effect since they are linear in the normal co-ordinates. The transformation of these normal co-ordinates and their coefficients can be classified according to the irreducible representations of the cubic group as follows:

	Bethe's Notation (1929)	Mulliken's Notation (1933)
Q_1	Γ_{1g}	A_{1g}
$\left.\begin{matrix}Q_2\\Q_3\end{matrix}\right\}$	Γ_{3g}	E_g
$\left.\begin{matrix}Q_4\\Q_5\\Q_6\end{matrix}\right\}$	Γ_{5g}	T_{2g}

The coefficients V_2, V_3 will be nonvanishing if the degenerate orbital state is either Γ_3 or Γ_5 while V_4, V_5 and V_6 will differ from zero only for Γ_5. This was shown in detail by Van Vleck (1939b). He also pointed out that if the vibration corresponding to Q is of a type contained in the direct product of the representation of the orbital state with itself, the coefficient will be nonvanishing. These direct products can be decomposed into irreducible representations as follows:

$$[\Gamma_3 x \Gamma_3]=\Gamma_{1g}+\Gamma_{2u}+\Gamma_{3g}$$

$$[\Gamma_4 x \Gamma_4]=\Gamma_{1g}+\Gamma_{3g}+\Gamma_{4u}+\Gamma_{5g} \qquad (3.3)$$

$$[\Gamma_5 x \Gamma_5] = \Gamma_{1g} + \Gamma_{3g} + \Gamma_{4u} + \Gamma_{5g}$$

3.2 The Orbital Triplet

As shown in the previous section, an orbital triplet state can couple to both Γ_{3g} and Γ_{5g} normal modes of vibration. For Ti^{3+} in such an octahedral environment, the dominant cubic crystal field splits the ^2D ground state of the free ion into an orbital triplet ground state (T_{2g} or Γ_{5g})* and an excited orbital doublet (E_g or Γ_{3g}) at about 20,000 cm^{-1} above the ground level. Although the Γ_{5g} electronic ground state can couple to either the Γ_{3g} or Γ_{5g} mode of vibration (equation 3.3), Ham (1965) and Macfarlane et al. (1968) assumed that the Γ_{3g} mode is more strongly coupled. It can be shown that if the coupling is to the mode Γ_{5g} or both Γ_{3g} and Γ_{5g}, the difficulty of the problem is greatly increased. (See for example Abragam and Bleaney, 1970, p. 841.) The EPR and spin-lattice relaxation measurements on Ti^{3+} as an impurity in methylammonium aluminum alum are consistent with a Jahn-Teller model which considers the Γ_{5g} ground state of the Ti^{3+} ion to interact with a Γ_{3g} mode of vibration only (Rumin et al. 1973). Ham (1965) used the cluster approximation of section 3.1 to show that the vibronic spectrum remains the same as that in the absence of the Jahn-Teller interaction except for the reduction by the Jahn-Teller energy E_{JT} common to all states.

*Note: Both notations are in common usage and appear in this thesis.

For an orbital triplet electronic state Γ_{5g} in cubic symmetry, the Jahn-Teller coupling to a Γ_{3g} vibrational mode (Q_2,Q_3) is given by the vibronic Hamiltonian, (Moffitt and Thorson, 1957)

$$\mathcal{H} = \mathcal{H}_o I + V[Q_2\varepsilon_2 + Q_3\varepsilon_3] \tag{3.4}$$

where

$$\mathcal{H}_o = E_o + (1/2\mu)[P_2^2 + P_3^2 + \mu^2\omega^2(Q_2^2+Q_3^2)] \quad ,$$

P_2 and P_3 are momenta conjugate to the normal co-ordinates Q_2 and Q_3, ω is the angular frequency appropriate to the Γ_{3g} mode of vibration and V is a constant corresponding to the strength of the Jahn-Teller coupling. I is the 3x3 unit matrix and ε_2 and ε_3 are two standard electronic orbital operators belonging to E and taking the matrix form

$$\varepsilon_2 = \begin{pmatrix} \frac{1}{2} & 0 & 0 \\ 0 & \frac{1}{2} & 0 \\ 0 & 0 & -1 \end{pmatrix} \qquad \varepsilon_3 = \begin{pmatrix} -\sqrt{3}/2 & 0 & 0 \\ 0 & +\sqrt{3}/2 & 0 \\ 0 & 0 & 0 \end{pmatrix} \tag{3.5}$$

with respect to the basis ψ_4, ψ_5 and ψ_6. These basis functions are taken to transform respectively as YZ, ZX and XY for Γ_5. Since the matrices ε_2 and ε_3 are diagonal, the Hamiltonian (3.4) does not admix the states ψ_4, ψ_5, ψ_6 for any Q_2, Q_3. The resulting energy surfaces describing the static Jahn-Teller effect are thus three disjoint paraboloids (Van Vleck, 1939b; Opik and Pryce, 1957) corresponding to ψ_4, ψ_5, ψ_6 with vertices lying respectively at the points

$$Q_{2i}=\frac{-Ve_{i2}}{\mu\omega^2} \quad , \quad Q_{3i}=\frac{-Ve_{i3}}{\mu\omega^2} \qquad (3.6)$$

where e_{i2} and e_{i3} are the diagonal matrix elements, respectively of ε_2 and ε_3 corresponding to $i=4, 5, 6$. These vertices thus correspond to the three energetically equivalent stable configurations of the static Jahn-Teller effect and the Jahn-Teller energy is

$$E_{JT}=V^2/2\mu\omega^2 \quad . \qquad (3.7)$$

The stable configurations have tetragonal symmetry and represent an elongation or contraction along one of the cubic axes.

The vibronic eigenstates of (3.4) are given exactly by (Ham, 1965; Moffitt and Thorson, 1957)

$$\Psi_{in}=\psi_i F_{n_2}[Q_2+(\frac{Ve_{i2}}{\mu\omega^2})]\, F_{n_3}[Q_3+(\frac{Ve_{i3}}{\mu\omega^2})] \qquad (3.8)$$

corresponding to the energy eigenvalues

$$E_{in}=E_o-E_{JT}+(n_2+n_3+1)\hbar\omega \qquad (3.9)$$

where n_2, $n_3=0, 1, 2, 3, \ldots$ and $F_n(y)$ is the one-dimensional simple harmonic oscillator wave function for the energy $(n+\frac{1}{2})\hbar\omega$. The energy spectrum (3.9) is thus displaced by $-E_{JT}$ but otherwise is unchanged by the Jahn-Teller coupling, while the vibrational parts of the wave functions (3.8) are appropriate to a displaced two-dimensional harmonic oscillator. The ground state is a degenerate triplet belonging to Γ_{5g} (the same representation as the electronic triplet) for arbitrary strength of the Jahn-Teller coupling. The exact vibronic wave functions (3.8) have the form of simple Born-Oppenheimer products, but the vibrational factor is different for the three electronic states even for states of the same energy. The equilibrium position (3.6) for the displaced oscillators is different for the different electronic functions $\psi_i (i=4, 5, 6)$. Their separation increases in proportion to $V/_{2\mu\omega^2}$ and hence the region of overlap between corresponding oscillator states associated with different electronic functions is diminished, and matrix elements between such states fall off accordingly. Any eigenstate of the system is a linear combination of the three vibronic functions and retains the cubic symmetry of that system.

Matrix elements of various operators between the vibronic eigenstates (3.8) may be evaluated explicitly using the generating relation for the harmonic oscillator functions (Ham, 1965). Consider an electronic operator 0 which is independent of Q_2, Q_3. Then a vibronic matrix element of 0 is simply the product of an electronic matrix element and the oscillator overlap integrals:

$$\langle \Psi_{in_2n_3} | 0 | \Psi_{in_2'n_3'} \rangle = \langle \psi_i | 0 | \psi_j \rangle \langle in_2 | jn_2' \rangle \langle in_3 | jn_3' \rangle \qquad (3.10)$$

where

$$<in_2|jn_2' >=\int_{-\infty}^{\infty}dQ_2\ F_{n_2}(Q_2+\frac{Ve_{i2}}{\mu\omega^2})F_{n_2'}(Q_2+\frac{Ve_{j2}}{\mu\omega^2})$$

and similarly for $< in_3|jn_3' >$.

An electronic operator O_A that has only off-diagonal matrix elements among the states ψ_4, ψ_5, ψ_6 has matrix elements within the vibronic ground-state triplet

$$<\Psi_{ioo}|O_A|\Psi_{joo}>=<\psi_i|O_A|\psi_j>\exp[-3E_{JT}/2\hbar\omega] \qquad (3.11)$$

However, an electronic operator O_B having only diagonal matrix elements between ψ_4, ψ_5, ψ_6 is unaffected by the Jahn-Teller coupling:

$$<\Psi_{inm}|O_B|\Psi_{jn'm'}>=<\psi_i|O|\psi_j>\delta_{ij}\delta_{nn'}\delta_{mm'} \qquad (3.12)$$

Thus, the direct effect of O_A within the ground state triplet of the vibronic system is gradually quenched as the overlap (of the oscillator wave functions of the different states) diminishes as the strength of the Jahn-Teller interaction is increased. The exponential factor

$$\gamma=\exp(-3E_{JT}/2\hbar\omega) \qquad (3.13)$$

is the orbital reduction caused by the dynamical Jahn-Teller quenching of the operator O_A.

Operators transforming as Γ_{3g} or Γ_{1g} are diagonal in the above representation and are thus unaffected by the Jahn-Teller coupling (when the coupling is solely with modes belonging to Γ_{3g}). On the other hand, operators transforming as Γ_{4g} or Γ_{5g} are of the O_A type and are quenched by the orbital reduction factor (3.13). In the limiting case $E_{JT} \gg \hbar\omega$, the direct effect of these operators is entirely quenched as expected for the static Jahn-Teller effect.

The electronic orbital angular momentum $\vec{L}$ is an operator of the type O_A with only off-diagonal matrix elements between the states ψ_4, ψ_5, and ψ_6. Then, its matrix elements within the vibronic ground state triplet are reduced as in (3.11)

$$<\Psi_{i00}|L_k|\Psi_{j00}>=<\psi_i|L_k|\psi_j>\exp[-3E_{JT}/2\hbar\omega] \; . \; . \qquad (3.14)$$

We see that the orbital angular momentum of the ground state triplet is partially quenched by the Jahn-Teller interaction. In the limiting form of a strong J-T interaction, this quenching is complete for the large static tetragonal distortion. The quenching is only partial in the dynamical regime, when there is still appreciable overlap of the oscillator wave functions for different states.

Exactly the same considerations apply to the spin-orbit coupling operator $\lambda\vec{S}.\vec{L}$. Since $\vec{S}$ does not operate on the Ψ_{inm}, the spin-orbit matrix elements are reduced in the same proportion as those of $\vec{L}$. The same is true of any operator whose orbital part is exclusively off-diagonal in the representation in which the Jahn-Teller interaction is diagonal. Other orbital interactions, such as the orbital contribution to the hyperfine interaction and the effects of Γ_{5g} type strain, are also partially quenched by a dynamic Jahn-Teller effect as in equation (3.14). This general reduction in off-diagonal elements was first recognized by Ham (1965) and has been called the Ham effect in recognition.

The potential due to a trigonal distortion has Γ_{5g} symmetry (Tanabe and Kamimura, 1958) and all its matrix elements are off diagonal in the (ψ_4, ψ_5, ψ_6) basis. Their values are therefore reduced by the same factor γ. The orbital triplet T_{2g} state is still split to first order into E_g and A_{1g} states, when the direction of quantization is the trigonal axis, but the splitting is reduced by the factor γ. In the limit $\gamma \to 0$, a trigonal field cannot distinguish between the three equivalent [100]-type distortions, so that there can be no trigonal splitting. On the other hand diagonal operators, such as a tetragonal field, are not quenched, and so produce a splitting.

4. JAHN-TELLER EFFECTS FOR AN ORBITAL DOUBLET STATE

4.1 Static Jahn-Teller Effects

Since the first unambiguous observation of the Jahn-Teller effect for Cu^{2+} in zinc fluosilicate by Bleaney and Ingram (1950), the coupling of the orbital doublet electronic state to vibrational modes of the crystal has been studied in great detail. An octahedral cubic crystal field splits the ^2D ground state of the free ion Cu^{2+} $(3d^9)$ into an orbital doublet E ground state with an excited orbital triplet at least $10^4 cm^{-1}$ above the ground level. This is the inversion of the energy levels of Ti^{3+} $(3d^1)$ in an octahedral crystal field.

An orbital doublet state in cubic symmetry belongs to the two dimensional irreducible representation Γ_{3g} of the rotation group of the cube. In accordance with section 3.1, the two electronic states comprising the doublet are labeled ψ_2 and ψ_3 and transform as $(2Z^2-X^2-Y^2)$ and (X^2-Y^2) respectively. Here, X, Y and Z denote Cartesian co-ordinates with respect to the cubic axes. From equation (3.3) we find that the orbital doublet can be split only by the Γ_{3g} mode of vibration.

The splitting of the Γ_{3g} doublet by the Jahn-Teller effect is described by the effective Hamiltonian (see for example Ham, 1972)

$$\mathcal{H} = E_0 + V\begin{pmatrix} Q_2 & Q_3 \\ Q_3 & -Q_2 \end{pmatrix} + \frac{K}{2}(Q_2^2+Q_3^2) . \qquad (4.1)$$

E_o is the energy of the degenerate electronic state in the symmetrical configuration while V is the linear Jahn-Teller coupling coefficient which is negative for an electron-hole as for Cu^{2+}. The third term represents the elastic energy associated with the distortions Q_2 and Q_3. As illustrated in Figure 1.2, it is this elastic force that limits the Jahn-Teller distortion to a finite value. Letting $Q_2=\rho\cos\theta$ and $Q_3=\rho\sin\theta$, the eigenvalues of the Hamiltonian (4.1) become

$$E=E_o\pm V\rho+\frac{K\rho^2}{2} \tag{4.2}$$

with corresponding eigenstates

$$\begin{aligned}\psi_+&=\psi_2\sin(\theta/2)+\psi_3\cos(\theta/2)\\ \psi_-&=\psi_2\cos(\theta/2)-\psi_3\sin(\theta/2)\end{aligned} \tag{4.3}$$

These energy surfaces are shown in Figure 4.1a. The energy surface is obtained by rotating the curves of Figure 1.2 through 360°. In this case E is independent of θ and the corresponding Jahn-Teller stabilization energy is $E_{JT}=\frac{V^2}{2K}$ at $\rho_o=\frac{V}{K}$ as shown by Van Vleck (1939b).

A more realistic Hamiltonian should not allow this full rotational symmetry but only the three-fold symmetry of the cube. Liehr and Ballhausen (1958) included the quadratic Jahn-Teller coupling

FIGURE 4.1a

Energy sufaces $E_{\pm}$ for the orbital doublet electronic state with linear Jahn-Teller coupling in cubic symmetry. The surfaces have rotational symmetry about the energy axis.

FIGURE 4.1b

A fold-out view of the potential well at $\rho=\rho_0$ when the effect of the higher-order coupling terms are taken into account.

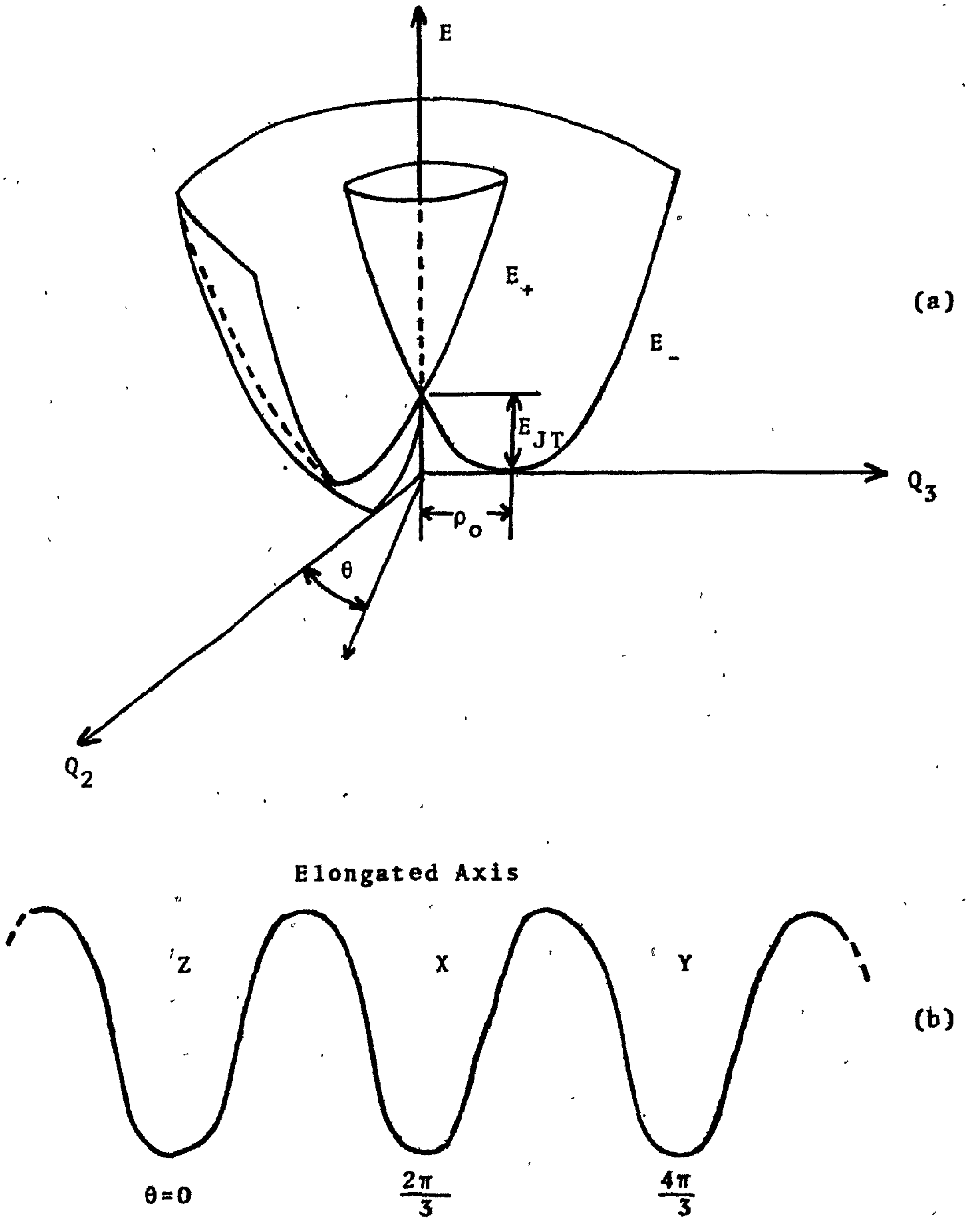
E
E+
E-
(a)
E JT
Q3
ρo
θ
Q2
Elongated Axis
Z
X
Y
(b)
θ=0
2π/3
4π/3

$$V_q \begin{pmatrix} -Q_2^2+Q_3^2 & 2Q_2Q_3 \\ 2Q_2Q_3 & Q_2^2-Q_3^2 \end{pmatrix} \tag{4.4}$$

while Opik and Pryce (1957) considered the anharmonic term

$$V_aQ_2(Q_2^2-3Q_3^2) \ . \tag{4.5}$$

When these "warping" terms are added to the Hamiltonian (4.1) the eigenvalues are given by

$$E=E_o+\frac{K}{2}\rho^2+V_a\rho^3 \cos 3\theta \pm (V^2\rho^2+V_q^2\rho^4-2V\ V_q\rho^3\cos 3\theta)^{1/2} \tag{4.6}$$

Minima of the potential energy occur for discrete values of θ, namely $\theta=0$, $\frac{2\pi}{3}$, and $\frac{4\pi}{3}$ or $\theta=\frac{\pi}{3}$, π, and $\frac{5\pi}{3}$ depending on the relative signs and magnitude of V_q and V_a. In either case, the result is three energetically equivalent configurations (corresponding to either elongations or contractions along the X, Y, and Z axes) which are separated by low barriers, when the higher-order coupling terms are taken into account. (See Figure 4.1b.) If the barriers between the wells are sufficiently high, the static Jahn-Teller effect for the doublet will therefore correspond to the three stable configurations at the bottoms of these wells. However, the system is dynamic unless it is sufficiently perturbed, which may happen in a measurement (see section 4.2 below). The electronic orbital ground state is ψ_+ for $V<0$ as is the case for Cu^{2+}. Typical values for the barrier height and Jahn-Teller energy for Cu^{2+} in lanthanum magnesium double nitrate

(LMN) are 312cm^{-1} and 1420cm^{-1} respectively (Vincent and Walsh, 1973).

4.2 The Effect of Strain and Tunneling

The importance of crystal strain in connection with the Jahn-Teller effect was noted by Ham (1965, 1968). A uniform strain can be defined by its six components belonging respectively to

$$\begin{aligned} &\Gamma_1 \quad (e_1 = e_{xx} + e_{yy} + e_{zz}) \\ &\Gamma_3 \quad \left(e_2 = \frac{3e_{zz} - e_1}{2}\ ,\ e_3 = \frac{\sqrt{3}}{2}(e_{xx} - e_{yy})\right) \qquad (4.7) \\ &\Gamma_5 \quad (e_4 = e_{xy},\ e_5 = e_{yz},\ e_6 = e_{zx}) \end{aligned}$$

where $e_{ij} = \frac{1}{2}\left(\frac{\partial u_i}{\partial x_j} + \frac{\partial u_j}{\partial x_i}\right)$ and u is the displacement. Within an orbital doublet Γ_3 the components e_2 and e_3 are the only ones that split the energy level of the ion to first order. This splitting is described by the Hamiltonian

$$\mathcal{H}_s = V_s \begin{pmatrix} -e_2 & e_3 \\ e_3 & e_2 \end{pmatrix} \qquad (4.8)$$

where V_s is the strain coupling coefficient. This term in the Hamiltonian increases in significance with the strength of the Jahn-Teller coupling. A tetragonal crystal strain along the Z axis would cause one of the equivalent distortions of Figure 4.1b to have a lower energy as shown in Figure 4.2. This would

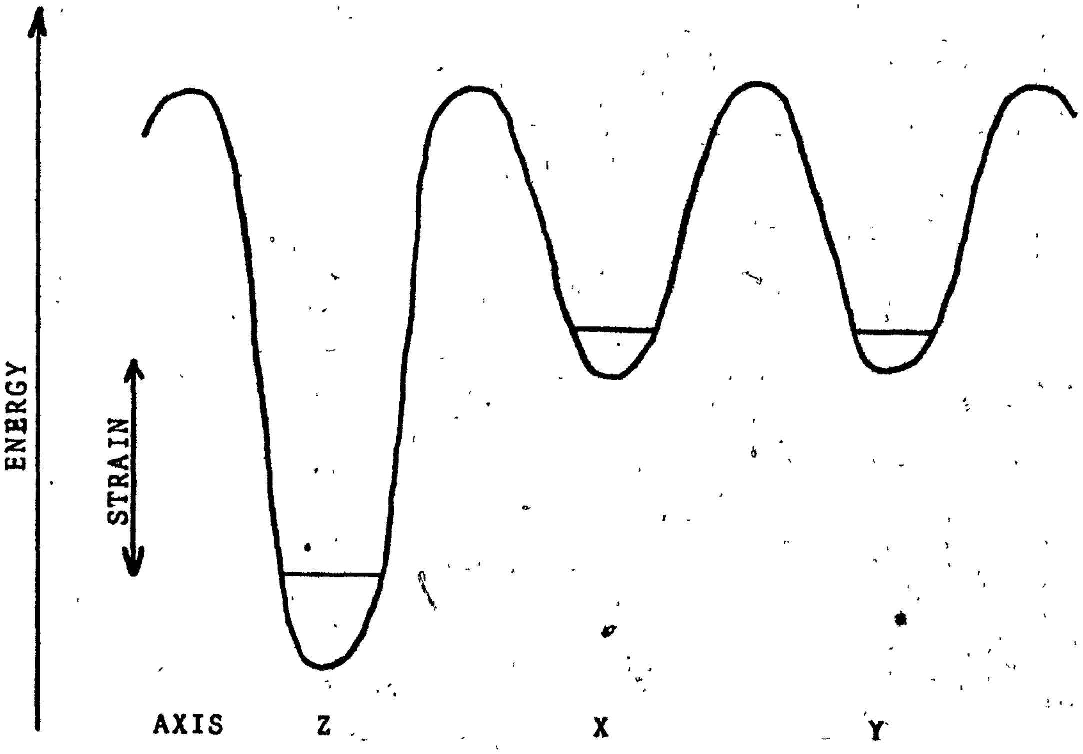

FIGURE 4.2

The effect of a tetragonal strain along Z on the corrugated potential well.

tend to localize a particular Cu^{2+} ion in this potential well. In reality, the Cu^{2+} ions of the crystal will be distributed among the X, Y and Z strain-stabilized wells since the tetragonal strain does not distinguish between these directions.

So far the discussion has ignored the zero-point motion and tunneling through finite barriers. A more realistic approach always takes into account the kinetic energy T of the nuclei which adds a term to the Hamiltonian of the form

$$T=\frac{1}{2\mu}(P_2^2+P_3^2) \qquad (4.9)$$

where μ is the effective mass of the ligand ions for the Γ_{3g} mode of vibration and P_i is the momentum operator conjugate to Q_i. As a first approximation the eigenfunctions of the combined Hamiltonian can be considered to be linear combinations of Born-Oppenheimer products. These products are electronic wave functions multiplied by harmonic oscillator wave functions. Moffitt and Thorson (1957) give explicit expressions for these eigenfunctions.

When the barrier height between minima of the potential is very high, the wave-functions are well localized. For smaller barriers, quantum mechanical tunneling can occur between the wells. This configuration interaction results in the separation of the three degenerate vibronic levels into a singlet and a ground doublet separated by a tunneling or "inversion" splitting δ (Bersuker, 1962). This compares with the effect of a local strain which causes the three degenerate vibronic levels to split into an excited doublet and a ground

Singlet.

When both strain and tunneling are present and comparable in magnitude, an effective Hamiltonian approach may be used to superimpose their contributions to the splitting of the three-fold degenerate vibronic ground states. This triplet can be described by a pseudospin T=1 representation with allowed T_z values ± 1 and 0. If a tetragonal strain along Z is present, for example, the strain operators in the pseudospin representation are

$$e_2=\frac{F}{2}(3T_z^2-2);\quad e_3=0 \tag{4.10}$$

where F is the tetragonal strain parameter. When the following choice of basis states is made

$$\begin{aligned}
|z\rangle &= |T_z=0\rangle \\
|x\rangle &= \frac{1}{\sqrt{2}}(|T_z=1\rangle-|T_z=-1\rangle) \\
|y\rangle &= \frac{1}{\sqrt{2}}(|T_z=1\rangle+|T_z=-1\rangle)
\end{aligned} \tag{4.11}$$

the matrix elements of e_2 are diagonal:

$$\begin{array}{c} |x\rangle \\ |y\rangle \\ |z\rangle \end{array} \begin{pmatrix} \frac{F}{2} & 0 & 0 \\ 0 & \frac{F}{2} & 0 \\ 0 & 0 & -F \end{pmatrix} \tag{4.12}$$

The effect of tunneling between equivalent potential wells causes mixing of the wave-functions. Thus matrix elements representing tunneling must be off-diagonal. The matrix representing both tunneling and strain may be written in the above basis as

$$\begin{array}{c} |x\rangle \\ |y\rangle \\ |z\rangle \end{array} \begin{pmatrix} \frac{F}{2} & \Gamma & \Gamma \\ \Gamma & \frac{F}{2} & \Gamma \\ \Gamma & \Gamma & -F \end{pmatrix} \qquad (4.13)$$

where Γ is a tunneling parameter. The eigenvalues are given by

$$E_1 = (\frac{F}{2} - \Gamma)$$

$$E_2 = -\frac{1}{2}(\frac{F}{2} - \Gamma) + \frac{1}{2}\sqrt{\frac{9F^2}{4} + 3F\Gamma + 9\Gamma^2} \qquad (4.14)$$

$$E_3 = -\frac{1}{2}(\frac{F}{2} - \Gamma) - \frac{1}{2}\sqrt{\frac{9F^2}{4} + 3F\Gamma + 9\Gamma^2}$$

Figure 4.3 shows qualitatively how these energy levels split as a function of strain. The strain and Jahn-Teller distortion were assumed to be parallel as was observed in the measurements in Chapter 7. The result is three vibronic singlets whose separation is a function of F and Γ. When F>>Γ, a strain along Z tends to localize a state in this direction, and EPR is observed within the Kramers doublet when an external magnetic

FIGURE 4.3

Energy splitting of the pseudospin T=1 triplet due to tunneling and tetragonal strain.

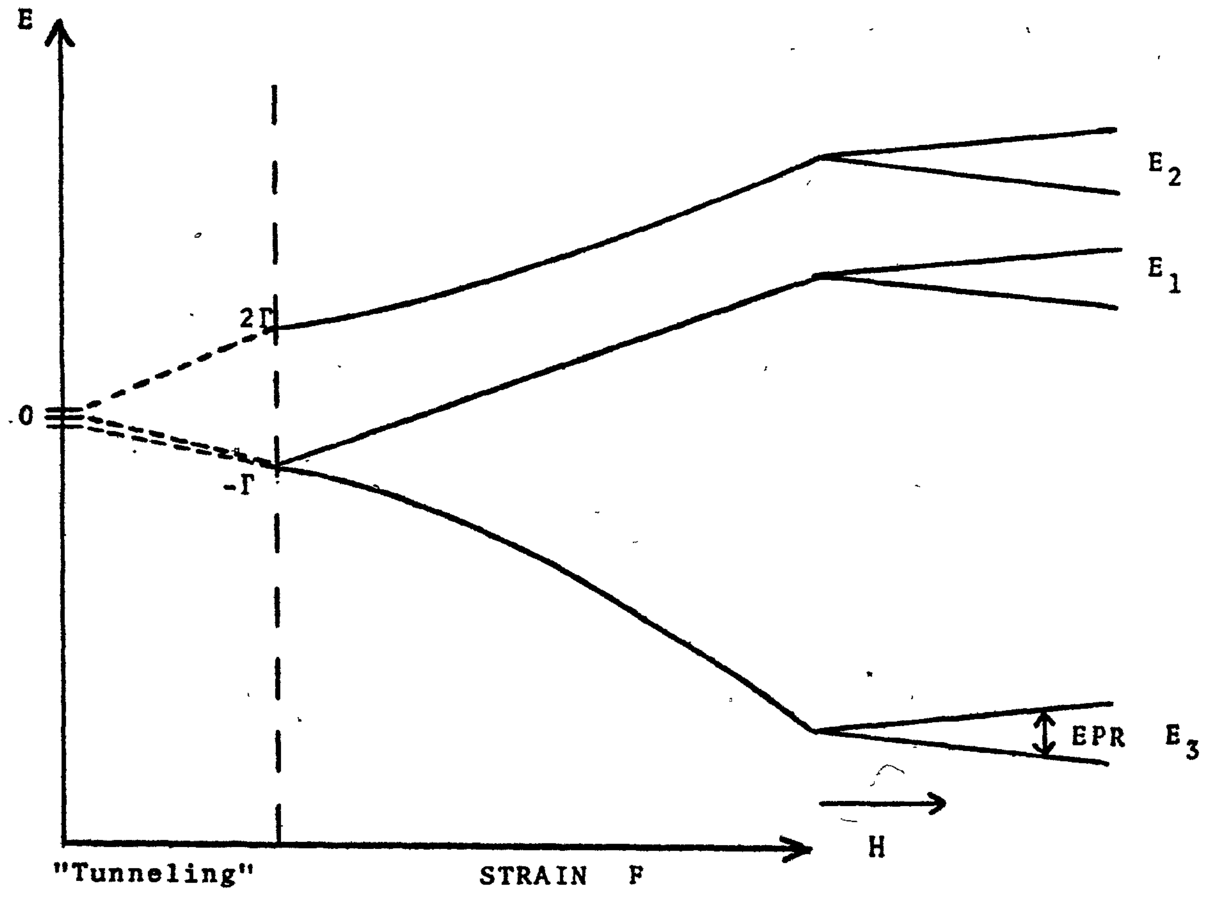
E
0
2Γ
-Γ
E$_2$
E$_1$
EPR
E$_3$
H
"Tunneling"
STRAIN F

field is applied. Three such EPR spectra are to be expected since at any particular time there will be a random distribution of X, Y and Z strains.

4.3 Phonon-Assisted Tunneling

As pointed out in the previous section, a strongly coupled Jahn-Teller complex in a particular distorted configuration will reorient to another distorted configuration by tunneling through the barrier. The reorientation rate depends on the interaction of the Jahn-Teller ion with phonons of the lattice as well as the size of the potential barrier between the wells. When a magnetic field is applied, tunneling matrix elements (or other residual interactions between vibronic wave functions) can induce more rapid transitions between states of opposite spin belonging to different configurations than between the Kramers conjugate states of a single configuration.

The above hypothesis has been advanced by several authors (Lee and Walsh, 1968; Williams et al., 1969) to explain the anomalous relaxation rates mentioned at the end of Chapter 2 which were observed for the Cu^{2+} ion in an orbitally degenerate state. These rates are at least four orders of magnitude faster than that of Cu^{2+} in potassium zinc Tutton salt at liquid helium temperatures, (Stoneham, 1965). In the Tutton salt, the relaxation occurs between the component states of a single Kramers doublet in a permanently distorted crystal field. Here, Van Vleck's theory successfully describes the relaxation data (Van Vleck, 1940). However, when the Cu^{2+} ion is within a Jahn-Teller system, the ground state is a Kramers doublet for each of the energetically equivalent configurations. As shown in the previous section, in the presence of both tunneling and strain, the ground state in which EPR is observed is a Kramers doublet. Spin-phonon coupling is weak between this Kramers conjugate pair resulting in a relatively small direct relaxation rate. However, a spinless transition (corresponding to a reorientation of the complex) can take place by phonon assisted tunneling to upper state as shown in Figure 4.4. The phonon-assisted process which returns the state to the ground and simultaneously flips the spin has a strong spin-phonon coupling, since the pair of states involved in the process is not a Kramers conjugate pair. The spinless transition has been observed by the spin-echo decay measurements of Breen et al. (1969) who estimated it to have a rate 100 times faster than that for the corresponding spin-flip transition which consequently governs entirely the spin-echo decay.

FIGURE 4.4

Pictorial representation of two relaxation mechanisms illustrating the process of phonon-assisted tunneling.

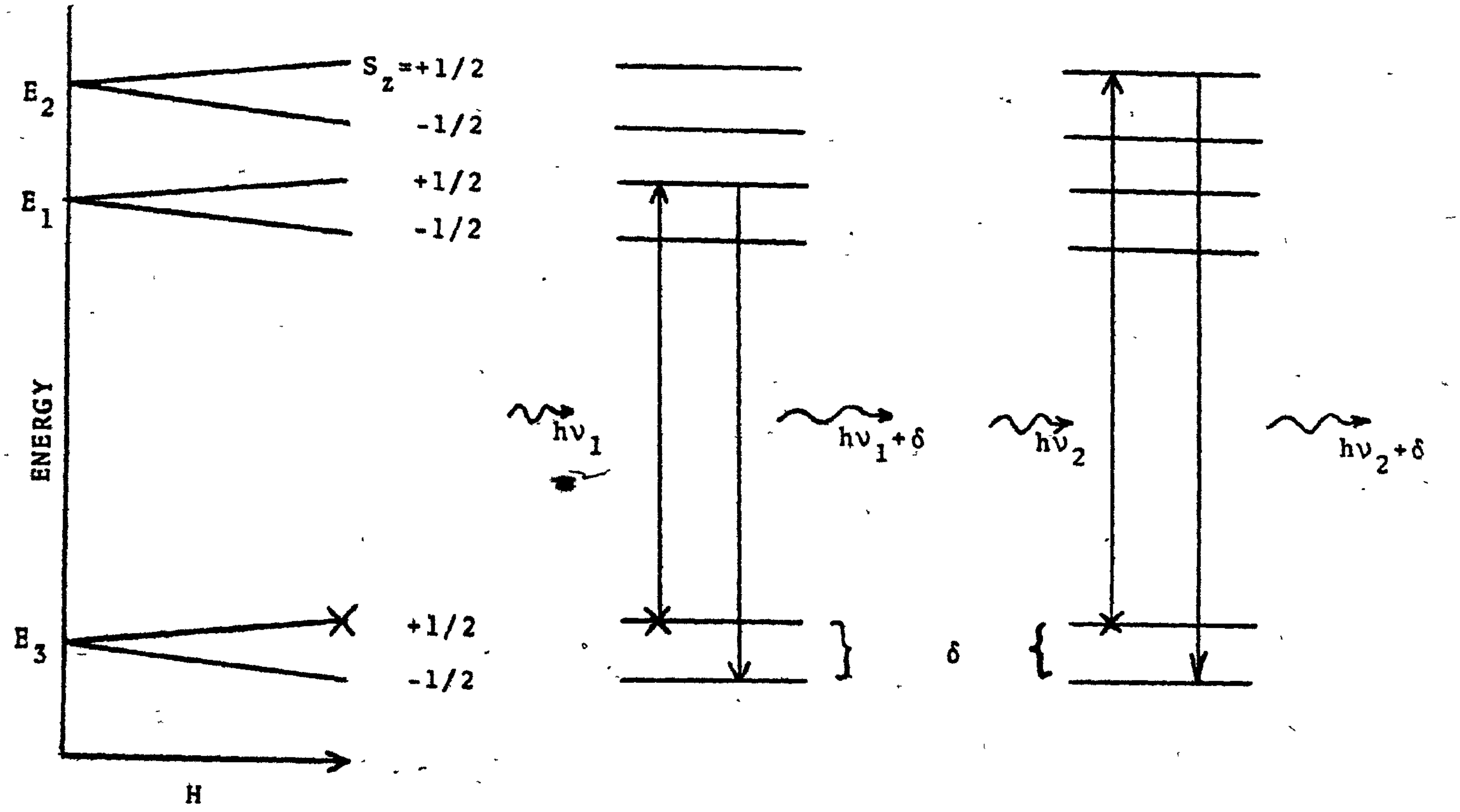

E_2
E_1
E_3
ENERGY
H
$S_z = +1/2$
$-1/2$
$+1/2$
$-1/2$
$+1/2$
$-1/2$
$h\nu_1$
$h\nu_1 + \delta$
$h\nu_2$
$h\nu_2 + \delta$
δ

5. APPARATUS

The EPR and relaxation measurements that are reported in Chapters 6 and 7 were made with a standard superheterodyne reflection spectrometer operating at X-band frequencies. The apparatus is basically the same as that described by Feher (1957) and Poole (1967), and is shown schematically in Figure 5.1.

Samples are placed on an externally rotatable platform at the center of a rectangular resonant cavity operating in the TE_{102} mode. The position of the sample corresponds to the microwave field maximum. The angle of rotation of the platform was read on a calibrated dial to within 0.15 degree. The cavity was enclosed in an evacuated jacket of stainless steel tubing, vacuum sealed at one end by means of indium wire.

Paramagnetic resonance measurements were carried out using two Varian Reflex V-58 Klystrons. Both were frequency stabilized to one part in 10^6 for several hours using a Curry McLaughlin and Len Inc. frequency stabilizer and a Dymec Model 2650A oscillator synchronizer. Power from signal Klystron 1 was fed to the resonant cavity by means of a magic tee. The magnetic field was provided by a rotatable 12" DC magnet with a homogeneity of approximately one tenth of a gauss over the crystal dimensions. This DC magnetic field was modulated by a 200 Hz audio frequency field produced by Helmholtz coils at the magnet pole faces. This resulted in a 200 Hz envelope on the microwave signal reflected from the cavity, the amplitude of which was proportional to the derivative of χ'' with respect

FIGURE 5.1

Block diagram of the X-band microwave spectrometer. Symbols used are shown below.

	FERRITE ISOLATOR
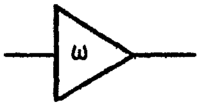	AMPLIFIER AT FREQUENCY ω
	CRYSTAL DIODE DETECTOR
	VARIABLE ATTENUATOR
	CAVITY
	PHASE SHIFTER
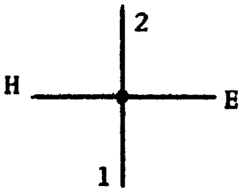	MAGIC TEE
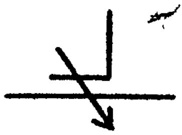	DIRECTIONAL COUPLER
	SHORT CIRCUIT TERMINATION
	PHASE SENSITIVE DETECTOR

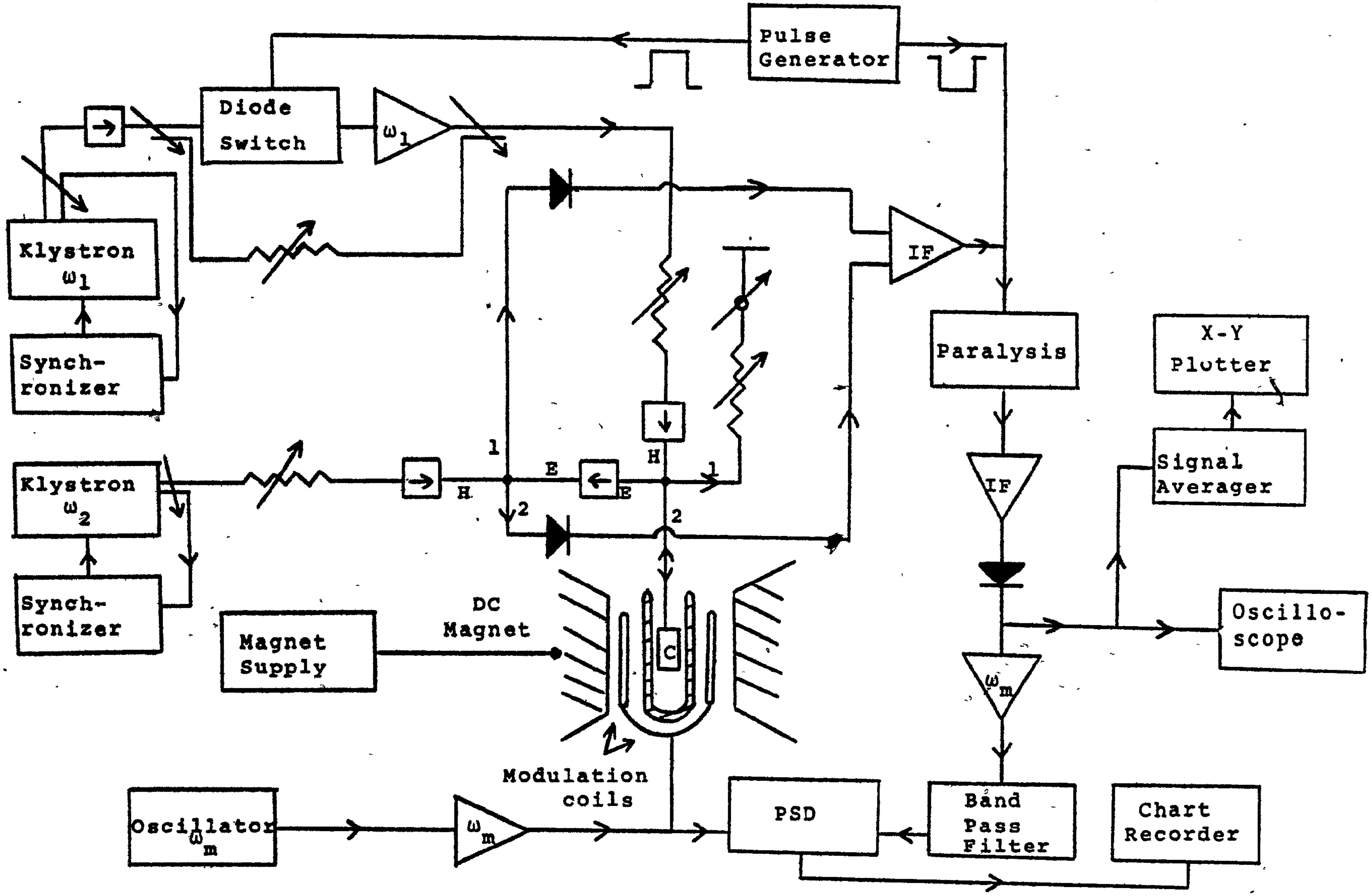
Pulse Generator
Diode Switch
ω1
Klystron ω1
Synch-ronizer
IF
Paralysis
X-Y Plotter
Klystron ω2
Synch-ronizer
1
E
H
H
E
1
2
2
IF
Signal Averager
DC Magnet
Magnet Supply
C
Oscillo-scope
ωm
Modulation coils
Oscillator ωm
ωm
PSD
Band Pass Filter
Chart Recorder

to H. This limited the noise spectrum to a narrow band in the region of 200 Hz by means of phase-sensitive detection and a band pass filter, greatly increasing the sensitivity of the spectrometer.

The magnitude of the DC field was measured using a Harvey Wells Model E502 nuclear magnetic resonance (NMR) gauss meter and a Fluke 1900A frequency counter. The magnetic field was swept at a constant rate until the resonant magnetic field was reached. The microwave frequency of 9.460±0.005 GHz was measured with a calibrated PRD 585A wavemeter. At resonance the paramagnetic sample absorbs microwave energy. This causes the microwave carrier frequency ω_1 to be amplitude modulated at the modulation frequency. The power absorbed by the sample at resonance changes the Q of the cavity and unbalances the microwave bridge. Then the amplitude modulated reflected signal from the cavity enters the balanced mixer magic tee to be mixed with the output of the reference Klystron II, which is stabilized at a frequency ω_2 such that $\omega_1-\omega_2=30$ MHz. This intermediate frequency (IF) signal is detected, amplified and demodulated in order to extract the magnetic field modulation frequency of 200 Hz. The absorption line derivative is finally traced by a chart recorder at the output of a phase sensitive detector which compares the cavity signal with a 200 Hz reference signal.

The spin-lattice relaxation measurements were carried out using a pulse saturation technique described by Bowers and Mims (1959). A microwave amplifier VA - 824B, controlled by a Somerset switching diode X-416, in the main arm of the circuit served to pump the spins and saturate the EPR signal using a peak power of 1.5 Watt. A tektronix pulse generator activated the switching diode as well as a paralysis circuit which cut off the IF frequency to avoid saturation of the amplifier during the pulsing period. Various pulse widths and recurrence rates were employed to check for optimum results. A continuous wave (CW) low power signal was taken directly from Klystron 1 and added to the pulse signal through a directional coupler. This "monitor" power was adjusted to a low value to minimize its effect on the instantaneous spin distribution. Its purpose was to monitor the EPR signal recovery after the end of the microwave pulse; the signal intensity being proportional to the population difference as the spins return to thermal equilibrium.

Since the relaxation measurements were done on the imaginary or absorption part of the magnetic susceptibility χ'', caution must be taken to eliminate the real or dispersion part of the magnetic susceptibility χ'. Thus the saturation measurements were made with the unmodulated magnetic field adjusted to the center of the resonance line where $\chi'=0$, to insure that the shape of the recovery signal was a function of the absorption only. The recovery of the EPR absorption signal after saturation was fed into a "twenty-four channel signal averager" described by Vincent (1973) and plotted by an X-Y recorder. The signal averager consists of a series of memory units (capacitors) tied to the recovery signal. During each sweep, an internal clock oscillator advances a ring counter which controls the memory gates. If the sweeps are synchronized with the repetitive waveform of interest, that waveform is gradually stored in the memory, because the same portion of the waveform is applied to any given capacitor on successive sweeps. The signal-to-noise ratio is also improved because the signal is being integrated during this averaging process. This signal averager marks a significant improvement in the accuracy of spin-lattice relaxation measurements over photographic methods using an oscilloscope tracing of the recovery signal. Relaxation times as small as ~10 microseconds could be measured with good signal intensity. This limit was determined by the minimum signal averager gate size (~6μs) and the IF amplifier rise time (~1μs).

The cryogenic system consisted of concentric Dewars with the outer one containing liquid nitrogen. The main liquid helium Dewar was placed between the pole faces of the magnet and contained the microwave cavity with the sample sitting in a helium exchange gas atmosphere of approximately 35 Torr at 4.2°K to eliminate vibration from the boiling liquid helium. Temperatures in the cavity were measured with an Allen Bradley, (105Ω at 20°C) carbon resistor calibrated against liquid vapor pressure using an Edwards Vacustat as well as a Wallace and Tiernan Model FA145 vapor pressure gauge. Repeating the calibration after an interval of one year, resulted in less than a 1% change in the calibration curve. The resistance of the thermometer was measured on a special Wheatstone bridge circuit which compensated for the resistance of the #40 connecting wires. Since the power dissipated in the thermometer was less than 1 μWatt, the temperature readings within the cavity were not affected. Temperatures in the liquid helium region, which were controlled by a pump and cartesian manostat, were accurate to better than 1%. Stability was good except for a small temperature interval near the λ point of helium.

6. EXPERIMENTAL RESULTS: Ti^{3+} IN CESIUM ALUMINUM ALUM

Octahedrally co-ordinated Ti^{3+} was studied as a dilute substitutional impurity for Al^{3+} in cesium aluminum alum. Section 6.1 reviews the structure of the host crystal. The next section presents the EPR data obtained for this system with special attention given to the model of Shing and Walsh (1974a) for a quasi-Γ_8 ground state. Spin-lattice relaxation measurements which are consistent with the model presented in section 6.2 are given in the next section. The last part of this chapter discusses these results in the light of previous work on this as well as related systems.

6.1 Crystal Structure

The crystal structure of the alums was first determined by Lipson and Beevers (1935) based on x-ray measurements. The alums are a series of double salts with the general formula

$$R^{i}\ R^{iii}\ (R^{iv}\ O_4)_2\ .\ 12\ H_2O \qquad (6.1)$$

where R^{i}, R^{iii} and R^{iv} are monovalent, trivalent and tetravalent ions respectively. Most usually R^{i} and R^{iii} are metallic ions while R^{iv} is one of sulpher, selenium or tellurium. Wyckoff (1923) showed that the space group is T_h^6 (Pa 3) with four formula (6.1) molecules per unit cell.

Lipson (1935) divided the alums into three structural classes according to the size of the monovalent ion. The α alum structure is typical of medium sized monovalent ions such as rubidium alum while the β and γ alum structures are typical of larger (eg. cesium alum) and smaller (eg. sodium alum) sized monovalent ions respectively. The β alum is the most common structure, with the interest here on cesium aluminum alum, $CsAl(SO_4)_2 \cdot 12\ H_2O$.

In all the alums, there are two crystallographically different types of water molecules. One type is always associated with the monovalent cation while the other type is associated with the trivalent cation. The Al^{3+} ion is always surrounded by six water molecules in a slightly flattened octahedron with trigonal symmetry $\bar{3}$. There are four symmetry-equivalent sites for the Al^{3+} ion per unit cell with symmetry axes along <111> directions. This is the environment into which the Ti^{3+} ion is placed when it is a substitutional impurity for Al^{3+}. Cromer et al. (1966) measured the average Al-O distance to be 1.88 Å within the coordination octahedra. They also determined the lattice constant to be 12.352±0.003 Å.

All measurements were performed on single crystals of CsAl alum doped nominally with 0.1 atomic % Ti^{3+}, which were grown by Dr. G. Fredericks of the Chemistry Department, McGill University, from aqueous solution in an inert atmosphere to prevent the oxidation of Ti^{3+} (see Appendix 2). Other samples were also tried with varying success depending on the concentration of Ti^{3+} ions. Doping levels could be qualitatively estimated based on the darkness of the typical violet colour characteristic of the optical absorption band for Ti^{3+}.

6.2 The EPR Spectra

The energy level structure of Ti^{3+} in cesium aluminum alum is shown schematically in Figure 6.1. The free ion ^2D ground term is split by the dominant octahedral cubic crystal field into a ground Γ_{5g} electronic state with the excited Γ_{3g} state at approximately 20,000 cm^{-1} above the ground level. As shown in Chapter 3, the ground Γ_{5g} level is depressed by the Jahn-Teller stabilization energy, E_{JT} due to the dynamic Jahn-Teller coupling to the Γ_{3g} vibrational mode. At this stage, the trigonal crystal field at the Ti^{3+} site would ordinarily be expected to split the vibronic triplet ground state into a Γ_3 and Γ_1 with the Γ_1 singlet lower. This first order effect is opposed by the admixture of the excited Γ_{3g} and ground state Γ_{5g} orbital states by the trigonal field which contributes a second-order splitting of the ground Γ_{5g} in the opposite sense. Abou-Ghantous et al. (1974) showed that the effective trigonal Hamiltonian under the assumption that the Γ_{5g} electronic ground state is strongly coupled to the Γ_{3g} vibrational mode has the form

$$\mathcal{H}_{trig} = \frac{1}{3}\,[\gamma V - \frac{(v')^2}{\Delta}]\,[3\ell_z^2 - \ell(\ell+1)] \qquad (6.2)$$

where V is the trigonal splitting of the Γ_{5g} state to first order, γ is the vibronic reduction factor, v' is the admixture of the excited Γ_{3g} and the ground state by the trigonal field, Δ is the cubic field splitting and the effective orbital angular momentum $\ell=1$. Since the first term within the bracket is reduced by the vibronic reduction factor while the second

FIGURE 6.1

Schematic energy-level diagram of Ti^{3+}

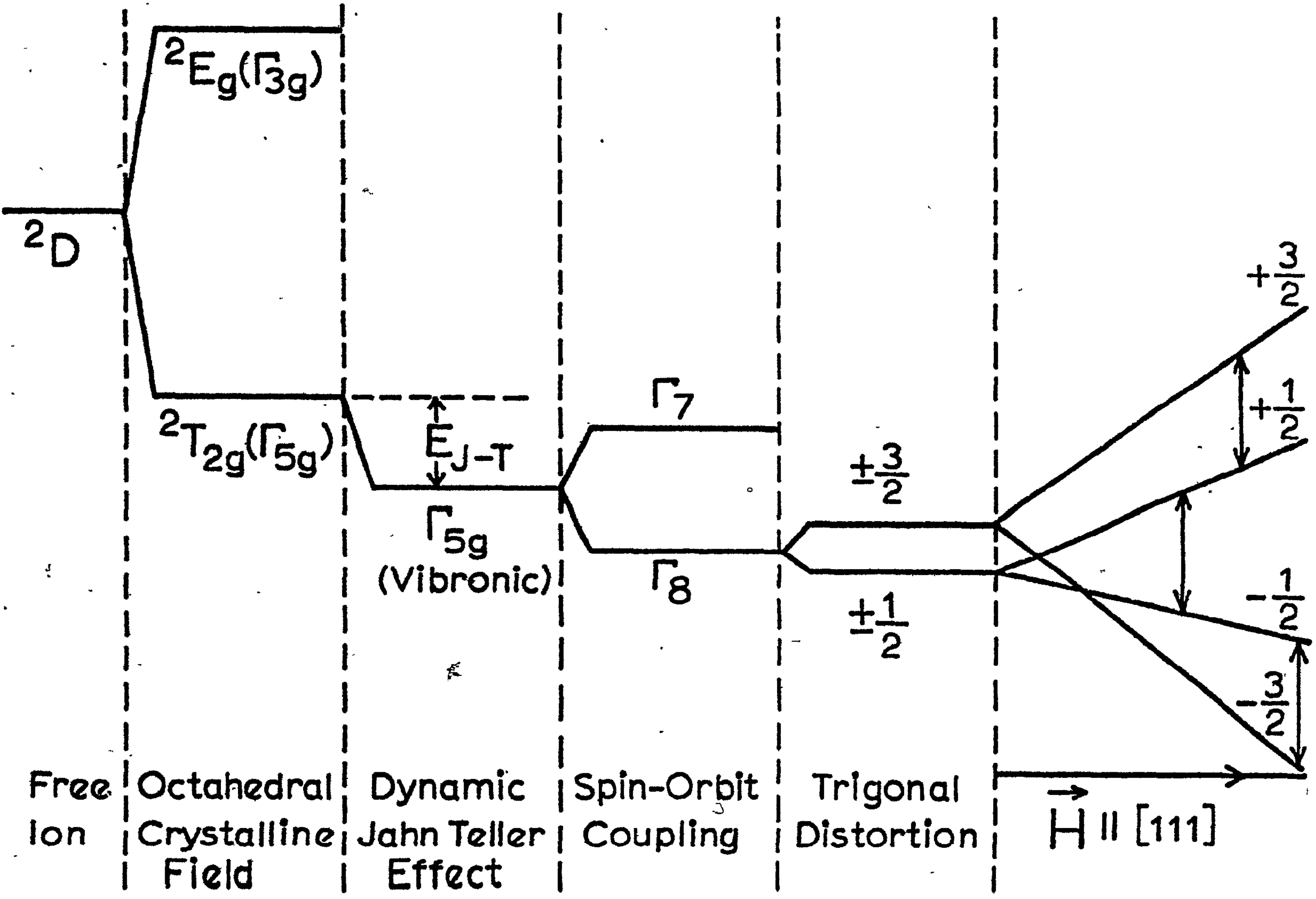
$^2E_g(\Gamma_{3g})$
^2D
$^2T_{2g}(\Gamma_{5g})$
E_{J-T}
Γ_{5g}
(Vibronic)
Γ_7
Γ_8
$\pm\frac{3}{2}$
$\pm\frac{1}{2}$
$+\frac{3}{2}$
$+\frac{1}{2}$
$-\frac{1}{2}$
$-\frac{3}{2}$
Free Ion
Octahedral Crystalline Field
Dynamic Jahn Teller Effect
Spin-Orbit Coupling
Trigonal Distortion
$\vec{H} \parallel [111]$

term remains unaffected by the Jahn-Teller coupling, γv is comparable in magnitude with $(v')^2/\Delta$. For Ti^{3+} in CsAl alum the parameter v is positive which leads to an almost complete cancellation of the effective trigonal field.

The spin-orbit interaction splits the three-fold degenerate Γ_{5g} ground state into a ground Γ_8 state having a four-fold spin degeneracy and an excited Γ_7 state with two-fold spin degeneracy. As pointed out in Chapter 3, the operator representing the spin-orbit interaction $\lambda\vec{L}.\vec{S}$ has its matrix elements reduced by the orbital reduction factor, consequently this splitting is expected to be small. The Γ_8 ground state is split slightly by the residual trigonal field and local crystal strain, resulting in a quasi-Γ_8 quartet which is shown to an exaggerated scale in Figure 6.1. Upon application of an external magnetic field, the quasi-Γ_8 quartet splits according to the linear Zeeman effect. If a finite splitting exists between the $\pm\frac{3}{2}$ and $\pm\frac{1}{2}$ Kramers doublets, then the result is three distinct $\Delta M=\pm 1$ EPR transitions.

The EPR measurements were performed at 9.46 GHz on single crystals of CsAl alum doped with nominal 0.1 atomic % Ti^{3+}. All samples displayed the same quantitative characteristics. Figure 6.2 shows the first derivative representation of the EPR spectrum measured at 2.5°K with $\vec{H}$ along a [111] axis. Observable EPR spectra were obtained only below 3°K due to short relaxation times. The three $\Delta M=\pm 1$ transitions were identified and labeled A, B and C corresponding to the $-\frac{3}{2} \leftrightarrow -\frac{1}{2}$, $+\frac{3}{2} \leftrightarrow +\frac{1}{2}$ and $+\frac{1}{2} \leftrightarrow -\frac{1}{2}$ transitions respectively. Line C has the regular line shape because it is a transition within a Kramers doublet. The other two lines show significant strain broadening because the EPR

FIGURE 6.2

First derivative representation of the EPR spectrum of Ti^{3+} in cesium aluminum alum measured at 9.46 GHz and 2.5°K with $\vec{H}$ along a [111] axis. The labels are A: $-\frac{3}{2} \leftrightarrow -\frac{1}{2}$; B: $+\frac{3}{2} \leftrightarrow +\frac{1}{2}$; C: $+\frac{1}{2} \leftrightarrow -\frac{1}{2}$.

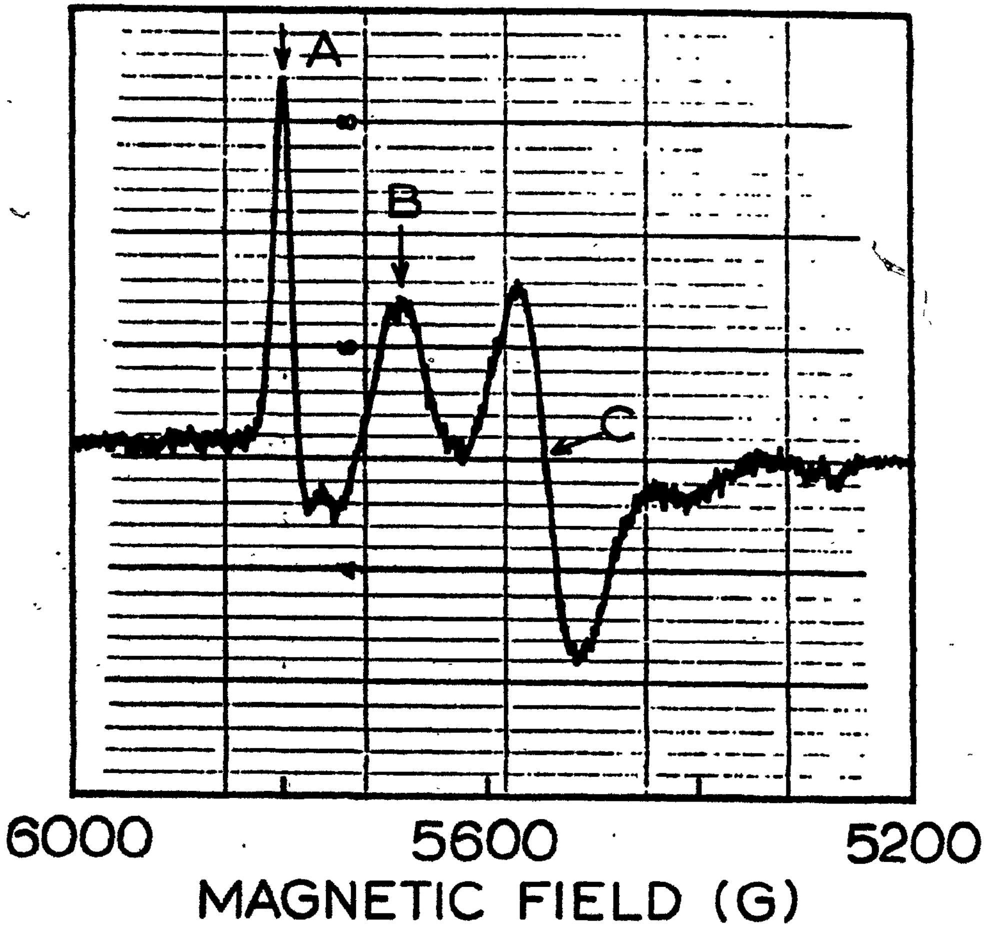
A
B
C
6000
5600
5200
MAGNETIC FIELD (G)

transitions are between non-conjugate vibronic states. Line A($-\frac{3}{2} \leftrightarrow -\frac{1}{2}$ transition) was identified by observing that its intensity increased relative to the other transitions as the temperature was reduced and the upper energy levels slightly depopulated. The very weak low field transitions which complicate the spectrum are not $\Delta M=\pm 2$ or ± 3 transitions. The locations of lines A and B were taken at their extrema while the zero-crossing of line C was used to locate its position. This method was used in the determination of the angular spectra.

Woonton and MacKinnon (1968) observed a spectrum similar to Figure 6.2, but interpreted it in terms of an $S=\frac{1}{2}$ ground state with lower than trigonal Ti^{3+} site symmetry (i.e. twelve nonequivalent sites). This modification of the usual alum structure described by Cromer et al. (1966) can be shown to be unnecessary upon examination of the angular spectra in the {110} and {111} planes. Figure 6.3 shows the angular variation of the EPR spectra for Ti^{3+} in CsAl alum measured in the {110} plane. The $\pm\frac{3}{2} \leftrightarrow \pm\frac{1}{2}$ transitions were observed to have a much larger anisotropy than the $+\frac{1}{2} \leftrightarrow -\frac{1}{2}$ transition. The periodicity was 70° and 110° indicating that the symmetry axes are along <111> directions. Complete EPR spectra could be observed only within the angular range ±30° with respect to the symmetry axis. The angular variation of the EPR spectra in the {111} plane (Figure 6.4) has a periodicity of 60°. The angular spectra in both planes confirms the presence of four symmetry-equivalent Ti^{3+} sites per unit cell with trigonal symmetry axes along <111> directions. Thus the usual alum structure is consistent with the effective $S=3/2$ ground state.

FIGURE 6.3

Experimental angular EPR spectra with $\vec{H}$ in {110}.

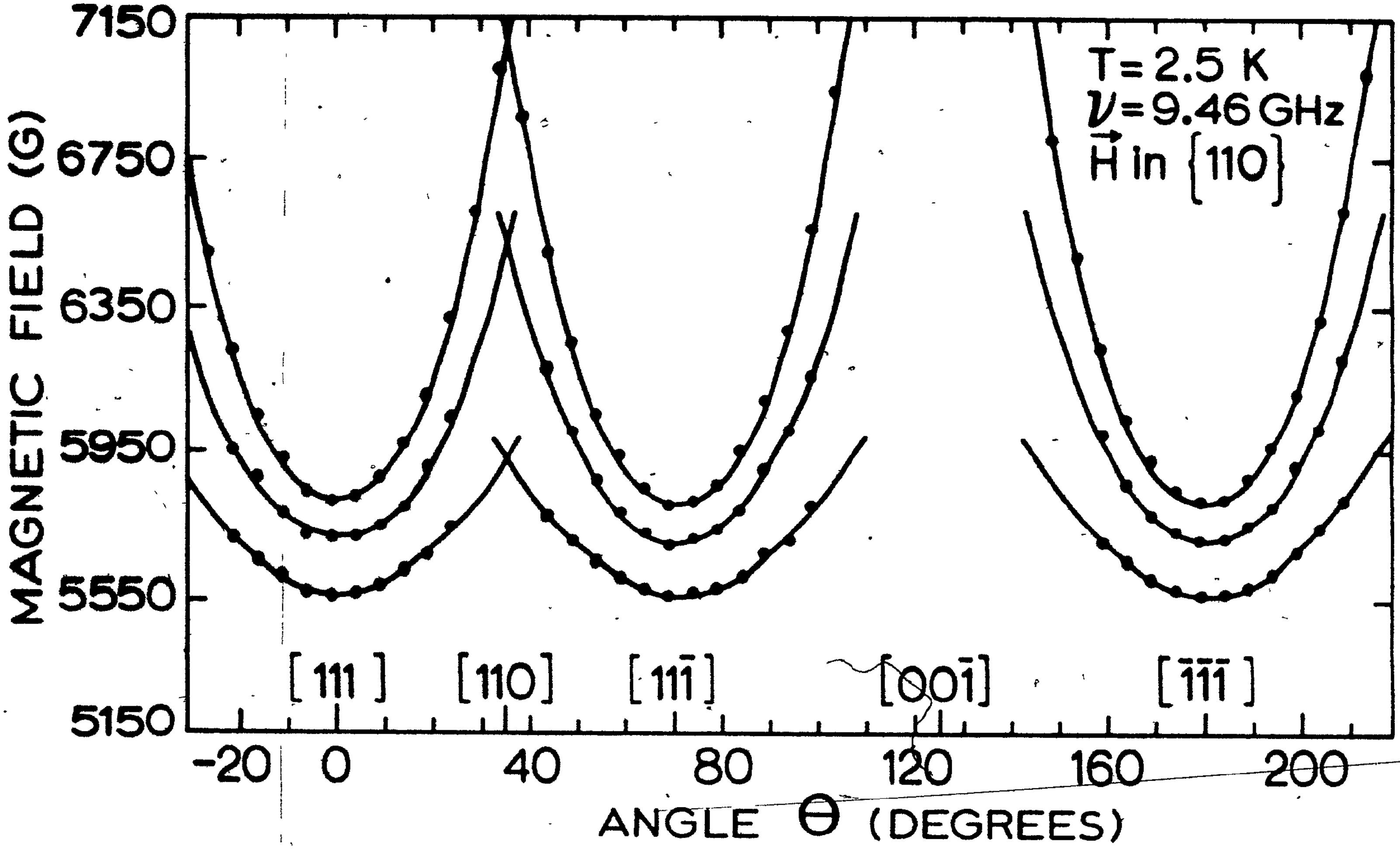
7150
6750
6350
5950
5550
5150
MAGNETIC FIELD (G)
-20
0
40
80
120
160
200
ANGLE Θ (DEGREES)
[111]
[110]
[11$\bar{1}$]
[00$\bar{1}$]
[$\bar{1}\bar{1}\bar{1}$]
T = 2.5 K
ν = 9.46 GHz
$\vec{H}$ in {110}

FIGURE 6.4

Experimental angular EPR spectra with $\vec{H}$ in {111}.

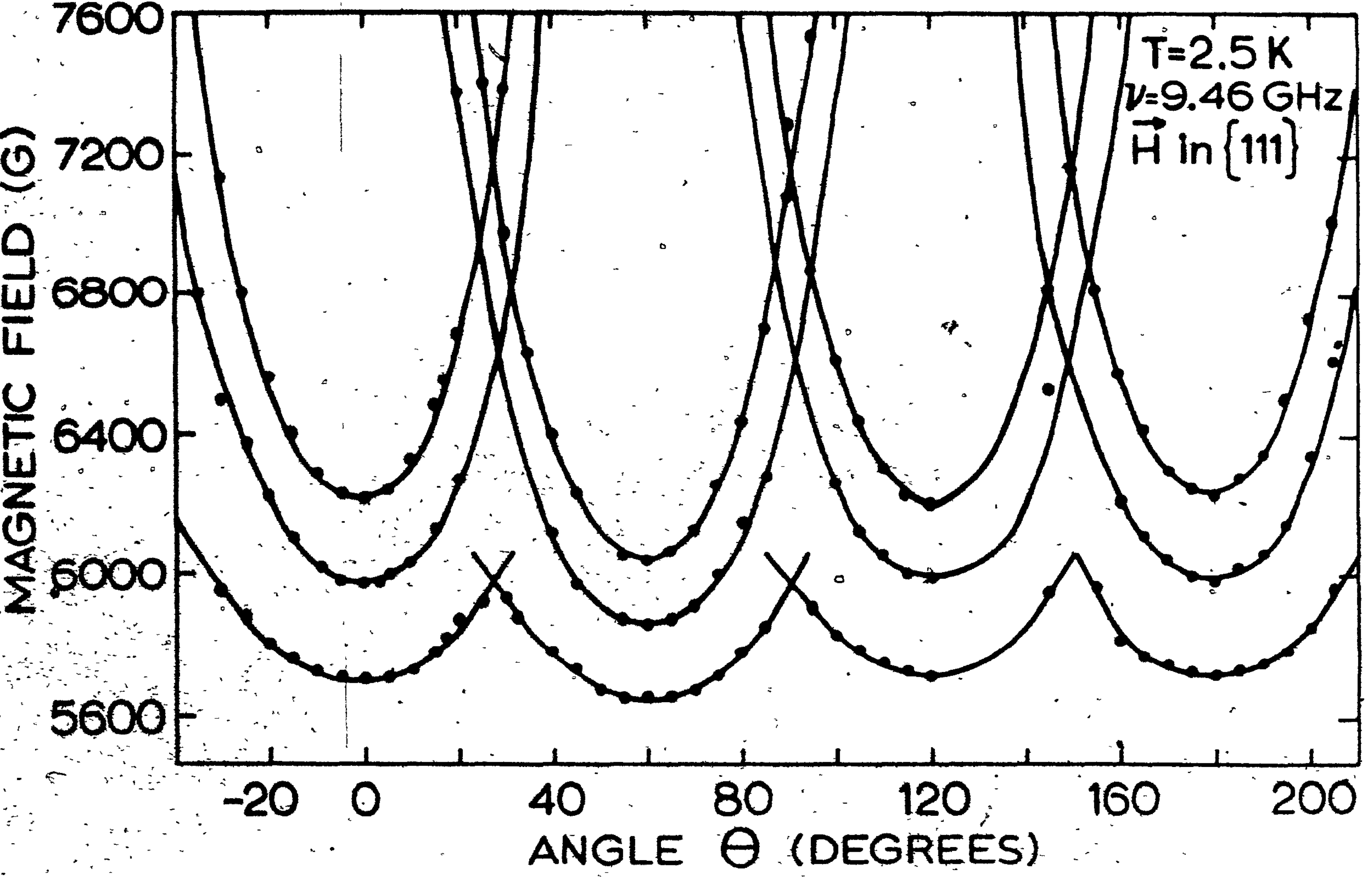
7600
7200
6800
6400
6000
5600
MAGNETIC FIELD (G)
-20
0
40
80
120
160
200
ANGLE Θ (DEGREES)
T=2.5 K
ν=9.46 GHz
$\vec{H}$ in {111}

Shing and Walsh (1974a) have derived a spin-Hamiltonian for the quasi-Γ_8 ground state of Ti^{3+} as a dilute substitutional impurity for Al^{3+} in CsAl alum in terms of an effective spin $S=3/2$. This was based on the introduction of a third order spin angular momentum term into an augmented spin-Hamiltonian for a Γ_8 quartet (Bleaney, 1959). Using a Hamiltonian of the form

$$\begin{aligned}\mathcal{H} &= g_{\parallel}\beta H_z S_z + g_{\perp}\beta(H_x S_x + H_y S_y) \\ &\quad + f\beta(H_x S_x{}^3 + H_y S_y{}^3 + H_z S_z{}^3) \\ &\quad + D\{S_z^2 - \tfrac{1}{3}S(S+1)\}\end{aligned} \tag{6.3}$$

they were able to calculate expected EPR transitions within the quasi-Γ_8 ground state with trigonal symmetry. By diagonalizing the dominant g terms and omitting the unobserved $\Delta M=\pm 2$ and ± 3 transition term, they determined the following spin-Hamiltonian parameters by fitting to the angular spectra;

$$\begin{aligned} g_{\parallel} &= 1.1937 \pm 0.001 \\ g_{\perp} &= 0.6673 \pm 0.005 \\ U_{\parallel} &= \sqrt{5/2}\ f_{\parallel} = -0.0144 \pm 0.002 \\ U_{\perp} &= \sqrt{5/2}\ f_{\perp} = -0.0868 \pm 0.005 \\ D &= 39.3 \pm 1.0\ \text{MHz} \end{aligned} \tag{6.4}$$

The comparison of their calculated angular EPR spectra to the observed EPR spectra is reproduced in Figure 6.5. Since the zero-field splitting factor D was determined to be very small, the almost complete cancellation of the trigonal field was used by Jesion et al. (1974) to calculate the orbital reduction factor γ. Setting $\mathcal{H}_{trig}$ of equation (6.2) equal to zero, they estimated $\gamma=0.03$ which is considerably less than the previous estimate for Ti^{3+} in methylammonium alum (Shing et al. 1974). Since the excited Γ_7 spin orbit level has an energy separation of $\gamma\lambda\vec{L}.\vec{S}$ where the effective orbital and spin angular momenta are 1 and $\frac{1}{2}$ respectively, Jesion et al. (1974) predicted that the excited Γ_7 state is at approximately 6 cm^{-1} above the ground quasi-Γ_8 state.

6.3 Spin-lattice Relaxation*

The spin-lattice relaxation measurements were performed on the same single crystals of cesium aluminum alum doped with nominal 0.1 atomic % Ti^{3+} as were used for the EPR study. The pulse saturation technique described in Chapter 5 was used with a pulse width of one millisecond and a repetition rate adjusted to about fifty times longer than the measured relaxation time of the sample. This allowed the spin system to return to thermal equilibrium before the next pulse. All measurements were conducted by saturating the $+\frac{1}{2} \leftrightarrow -\frac{1}{2}$ transition since this was

---

*Note: The results of this section have been published by Jesion, A., Shing, Y.H., and Walsh, D., 1975. Phys. Rev. Lett. 35, 1, 51.

FIGURE 6,5

Calculated and experimental angular EPR spectra of Ti^{3+} in CsAl alum. Dots are experimental data; solid lines are calculated spectra (Shing and Walsh, 1974a).

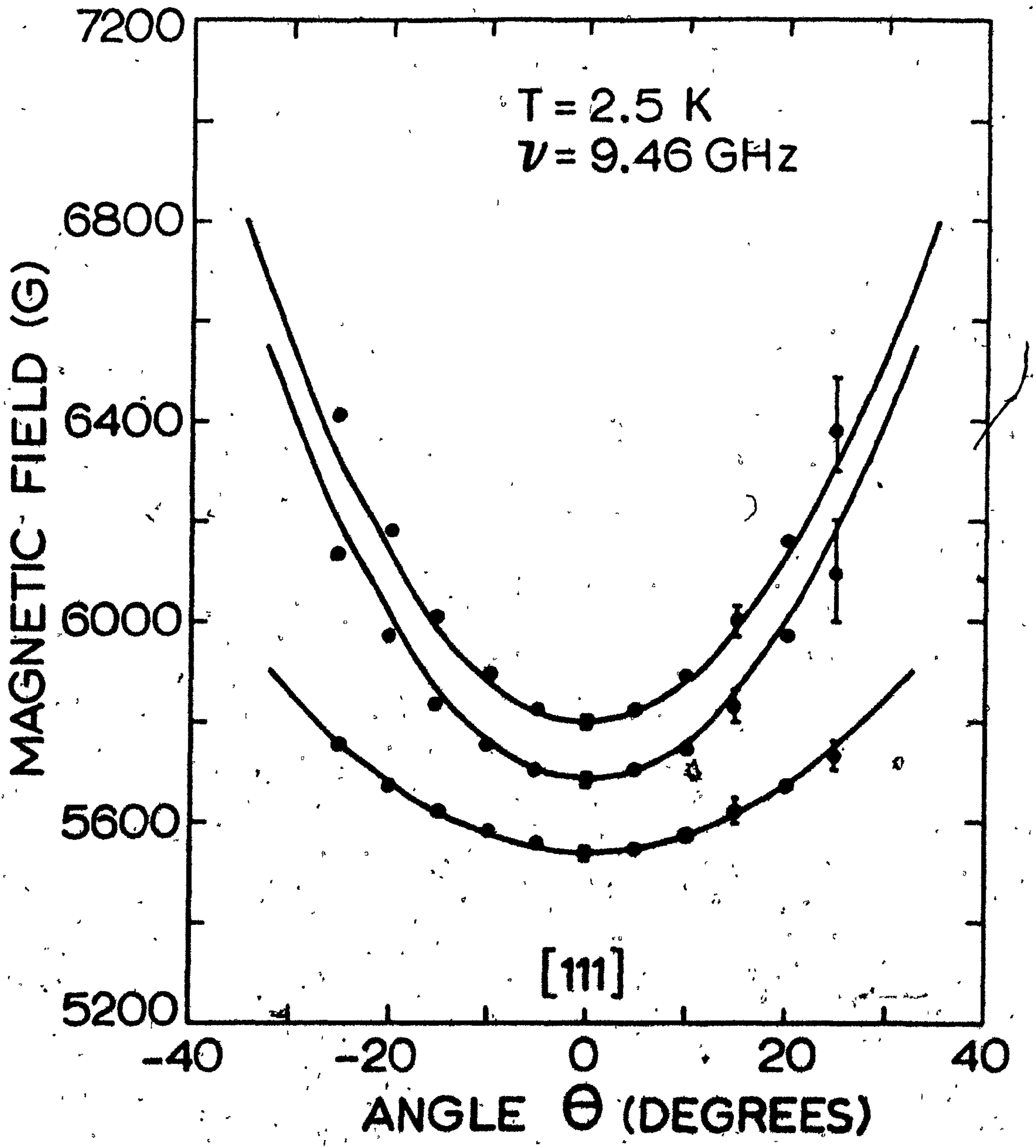
7200
6800
6400
6000
5600
5200
T = 2.5 K
ν = 9.46 GHz
[111]
MAGNETIC FIELD (G)
-40
-20
0
20
40
ANGLE Θ (DEGREES)

least affected by strain broadening. After the saturating pulse, the EPR signal recovery was a simple exponential decay with a time constant τ, the spin-lattice relaxation time. The recovery signal was fed to a 24-channel signal averager (see Chapter 5) and consequently all data points represent the average of approximately 100 recoveries. After plotting the logarithm of the recovery signal amplitude against time, the spin-lattice relaxation time was calculated by linear regression using a Hewlett-Packard 55 hand calculator. The maximum error in the relaxation measurements is 15%.

The temperature dependence of the spin-lattice relaxation rate of Ti^{3+} in CsAl alum measured between 2.63°K and 1.27°K with the DC magnetic field along the [111] axis is shown in Figure 6.6. Relaxation times vary over two orders of magnitude, from approximately 20 microseconds at T=2.6°K to approximately 3 milliseconds at the lowest temperatures reached in the experiments. The temperature interval could not be extended since the rapid increase in the relaxation rate at higher temperatures required the measurement of short relaxation times beyond the capability of the apparatus. The computer best fit to the relaxation rate has the form

$$1/\tau=2.21T^{10.2}+2.14\mathrm{x}10^{5}[\exp(9.93/T)-1]^{-1}+216 \quad (\mathrm{sec}^{-1}) \qquad (6.5)$$

where T is measured in degrees Kelvin. The three terms represent, respectively, the nonresonant Raman rate, the Orbach relaxation rate via an excited state at Δ above the ground level, and the temperature-independent spectral diffusion rate of the

FIGURE 6.6

Temperature dependence of the spin-lattice relaxation rate for 0.1 atomic % Ti^{3+} in CsAl alum at 9.46 GHz with the magnetic field parallel to [111] axis. Dots are experimental data; the solid line is the computed best fit.

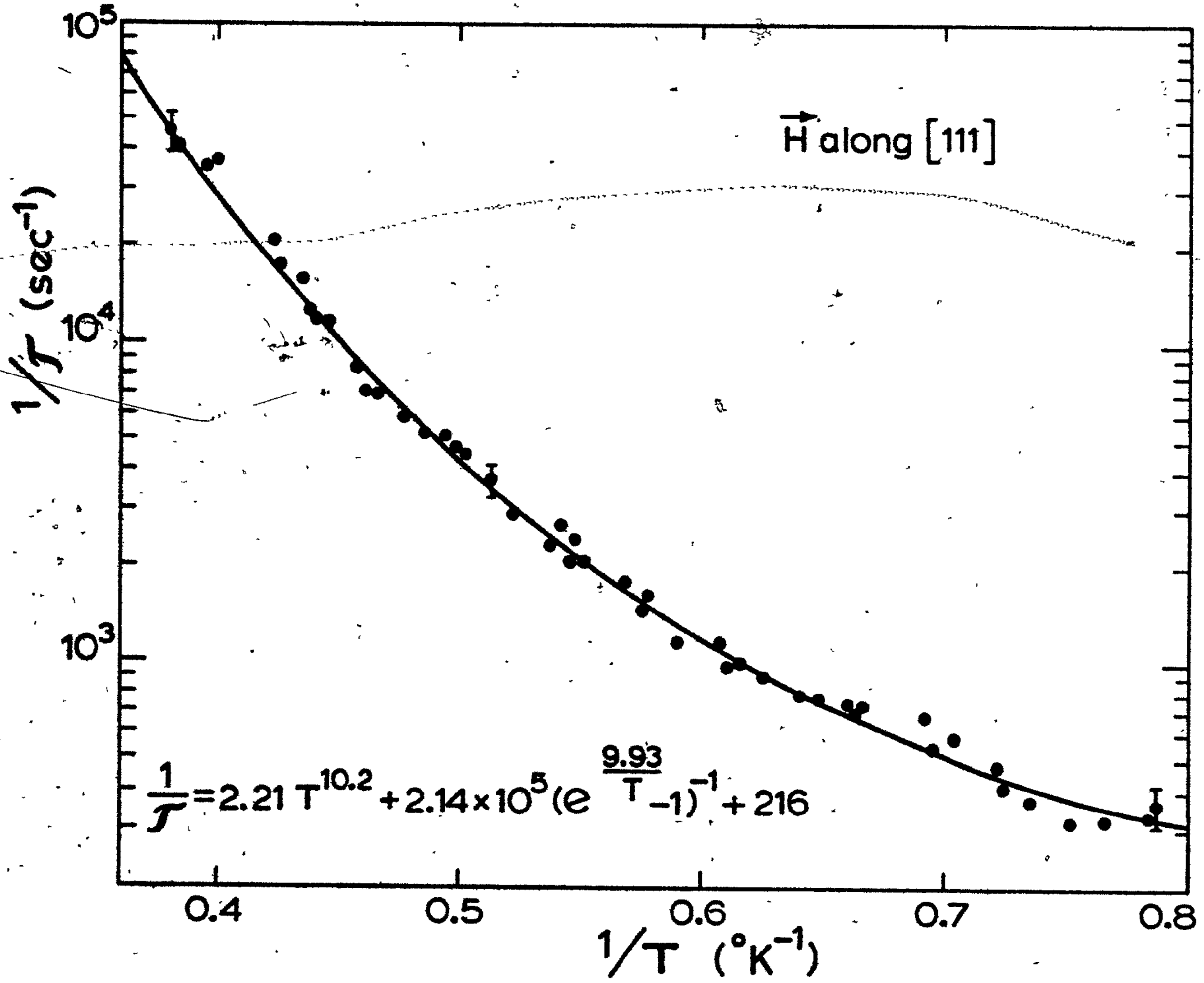10^5
10^4
10^3
$1/\mathcal{T}$ (sec^{-1})
$\vec{H}$ along [111]
$\frac{1}{\mathcal{T}} = 2.21\,T^{10.2} + 2.14\times10^5 (e^{\frac{9.93}{T}} - 1)^{-1} + 216$
0.4
0.5
0.6
0.7
0.8
$1/T$ (°K^{-1})

strain-broadened line. No single process could successfully describe the relaxation data over the whole temperature range. The best fit (6.5) was generated by a least squares computer program which minimizes

$$\chi^2 = \sum_{i=1}^{N} \left[\frac{R_i(T) - R_i'(T)}{S_i} \right]^2 \qquad (6.6)$$

where $R_i(T)$ are the experimental data points, $R_i'(T)$ are the calculated rates using the trial function,

$$R_i'(T) = A\ T^n + B[\exp(\Delta/T) - 1]^{-1} + C\ , \qquad (6.7)$$

S_i is the experimental error of the i^{th} data point and N is number of experimental points in the curve. The values of the parameters A, B, C, n and Δ which minimized χ^2 appear in equation (6.5). The index n is 9 for the nonresonant Raman relaxation mechanism of a Kramers ion. The exponent of the Orbach term and the uncertainty, determines the Γ_7 energy to be $(10 \pm 1.5)°K$ or $(7 \pm 1)\mathrm{cm}^{-1}$ in agreement with the estimate of Δ from the EPR data.

6.4 Discussion

The trigonal field at Al^{3+} sites within CsAl alum is known to be substantial (Cromer et al. 1966). The trigonal distortion angle was estimated to be approximately 1° by G. Donnay and J.D.H. Donnay (private communication). For non Jahn-Teller ions, the trigonal field is typically of the order of 100 cm^{-1}. The almost complete cancellation of this trigonal field is a direct consequence of the dynamic Jahn-Teller coupling of the orbital triplet Γ_5 to the Γ_{3g} vibrational mode. Shing et al. (1974) had previously used this coupling to successfully explain their results for the energy level splitting of Ti^{3+} in methylammonium alum.

In a report on Ti^{3+} substituting for Al^{3+} in CsAl alum, Woonton and MacKinnon (1968) interpreted the appearance in the spectrum of more than four EPR lines with unusual anisotropy as evidence of lower than trigonal Ti^{3+} site symmetry. Dionne and MacKinnon (1968) considered this lower symmetry to be due to an effective displacement of the $[Ti(H_2O)_6]^{3+}$ octahedron perpendicular to the trigonal symmetry axis, giving rise to twelve magnetic complexes in the unit cell. This interpretation, which is based on the assumption that the ground state has an effective spin $S=\frac{1}{2}$, is in disagreement with the usual alum structure of four symmetry equivalent Al^{3+} sites (Bleaney and Trenam, 1952, 1954). However, the model proposed by Shing and Walsh (1974b) demonstrates that the quasi-Γ_8 ground state described by an effective spin 3/2 accounts satisfactorily for both the EPR anisotropy and the existence of twelve resonance lines. Each of the four symmetry equivalent sites per unit cell contributes three $\Delta M=1$ transitions within the quasi Γ_8 state. Thus the twelve EPR lines are explained without lowering the trigonal Ti^{3+} site symmetry.

The properties of a quasi-Γ_8 ground state may account for a number of thermal and magnetic properties of pure CsTi alum. This salt is still magnetically dilute, so that magnetic and exchange interactions between the Ti^{3+} ions should be very small.

Kurti and Simon (quoted by Hebb and Purcell, 1937) reported an anomaly in the specific heat at temperatures of the order of 0.01°K. The ground quasi-Γ_8 ~~state~~ state model may be applied since the small zero-field splitting of the quasi-Γ_8 state provides a sizeable specific heat as the upper Krmers doublet is populated. Bleaney et al. (1955a) characterized the properties of CsTi alum according to an effective spin $S=\frac{1}{2}$, $g_{\parallel}=1.25\pm0.02$, $g_{\perp}=1.14\pm0.02$ and linewidth of 250±50G with four ions per unit cell corresponding to the usual alum structure. The trigonal distortion in CsTi alum will be close but not identical to that in CsAl alum. If the trigonal field cancellation in CsTi alum is more complete, then the ground state would correspond to a Γ_8 quartet with all three $\Delta M=\pm1$ transitions occurring at the same magnetic field. Consequently, only one broad transition will be detected, whose width would be governed by strain and not exchange interactions. This is consistent with the evidence of sizeable strain in the EPR spectra and spin-lattice relaxation temperature dependence for Ti^{3+} in CsAl alum. The existence of a low-lying Γ_7 state may be used to explain the change in the effective magnetic moment as determined from susceptibility data in the range 4-20°K (M.C.M. O'Brien, private communication). The spin-lattice relaxation data of section 6.3 are comparable with earlier measurements for CsTi alum using nonresonant techniques which exhibited an approximate T^8 temperature dependence (Benzie and Cooke, 1951).

The computer fitting to the spin-lattice relaxation data was based on the improved resolution of the experiments using a 24 channel signal averager so that all data points correspond to averages over 100 signal recoveries. Measurements were repeated on several occasions to verify that the results were independent of pulse width and repetition rate. This improved resolution made it possible to extract a detailed temperature dependence from the data, although the temperature interval was small. Below 1.4°K, all the data were consistently of the form

$$\frac{1}{\tau} \gtrsim 200(\mathrm{sec}^{-1}) \qquad (6.8)$$

This established the existence of a limiting value; the temperature-independent spin diffusion relaxation rate. At temperatures above 1.4°K, the relaxation rate could not be described within experimental error by either a Raman or an Orbach process alone. That is, the computer best fit to the data using either process still deviated from some data by approximately 30% which is twice the estimated error in the measurements. For this reason, both processes were used in the trial function (6.7) of the computer least squares program.

If both resonant and nonresonant two-phonon relaxation mechanisms are evident, Marchand (1974) has suggested "interference" terms in the relaxation temperature dependence. When the lowest excited doublet lies well below the Debye limit, these higher order terms are a result of competition for the same phonons to participate in both resonant and nonresonant scattering. In this case the Debye temperature for CsAl alum is 137°K (Fedorov, 1968). Marchand showed that the relaxation rate has the form

$$\frac{1}{\tau} \alpha\ A[\exp(\frac{\Delta}{kT})-1]^{-1}+BT^{9}+CT^{11}+\ .\ .\ . \qquad (6.9)$$

The higher order, interference terms have been omitted from the computer fitting procedure for simplicity. Instead, the exponent n in the Raman term of equation (6.7) was not fixed at 9 but allowed to vary. The "best fit" value, n=10.2 may be interpreted as a superposition of these higher order terms on the "usual" Raman T^9 temperature dependence. In any event, when n was fixed at the value 9, no other computer generated parameters were found to change by more than 10%.

Previous work on non Jahn-Teller systems (Larson and Jeffries, 1966) has indicated that, while the direct process in rare-earth ions may be quite anisotropic, the Orbach process should display little or no angular variation at all. This is because the direct process between a Kramers conjugate pair involves matrix elements of the orbit-lattice interaction which must be taken to second order to include the effects of magnetic field induced admixtures and thus an angular dependence on this magnetic field orientation. However the two phonon relaxation mechanisms involve the absorption and/or scattering of phonons which is independent of the magnetic field orientation. Shing et al. (1973) found that this could not be extended to the Jahn-Teller system Ti^{3+} in methyammonium alum. For Jahn-Teller coupling of an orbital triplet state to Γ_{3g} modes of vibration, the vibronic reduction factor reduces matrix elements of electronic operators which transform like the Γ_{5g} or Γ_{4g}

representation, whereas matrix elements of the Γ_{3g} operators are unaffected. They showed that this preferential coupling of the spin system to the lattice vibrations was responsible for the large angular anisotropy of the Orbach relaxation rate which they observed.

This angular anisotropy was qualitatively confirmed for the Ti^{3+} in CsAl alum system. The anisotropy of the spin-lattice relaxation time τ in the (111) plane at T=1.85°K is shown in Figure 6.7. Measurements were limited by the deterioration of the signal away from the [111] axis. Although the anisotropy is similar to the results of Shing et al. (1973), no analytical work was attempted because of the uncertain nature of the wave functions of the ground and excited states. Also, the CsAl alum host crystal involves a more complicated analysis than the methylammonium alum due to the competing effects of both resonant and nonresonant relaxation mechanisms. Although data is unavailable more than ~30° away from a symmetry axis, the general features of the anisotropy are consistent with their model.

The Raman and Orbach terms of equation (6.5) have comparable magnitudes dominating in the temperature intervals 2.6-1.9°K and 1.9-1.4°K respectively. Figure 6.8 compares the angular anisotropy of the spin-lattice relaxation time in the (111) plane at two temperatures, one in each interval. The curves follow the data and are drawn only as a guide to distinguish the form of the angular anisotropy. At T=1.85°K, the Orbach relaxation rate is larger while the reverse is true at T=2.32°K. The Orbach and Raman relaxation processes should also be expected

FIGURE 6.7

Anisotropy of the spin-lattice relaxation time τ in the (111) plane at T=1.85°K.

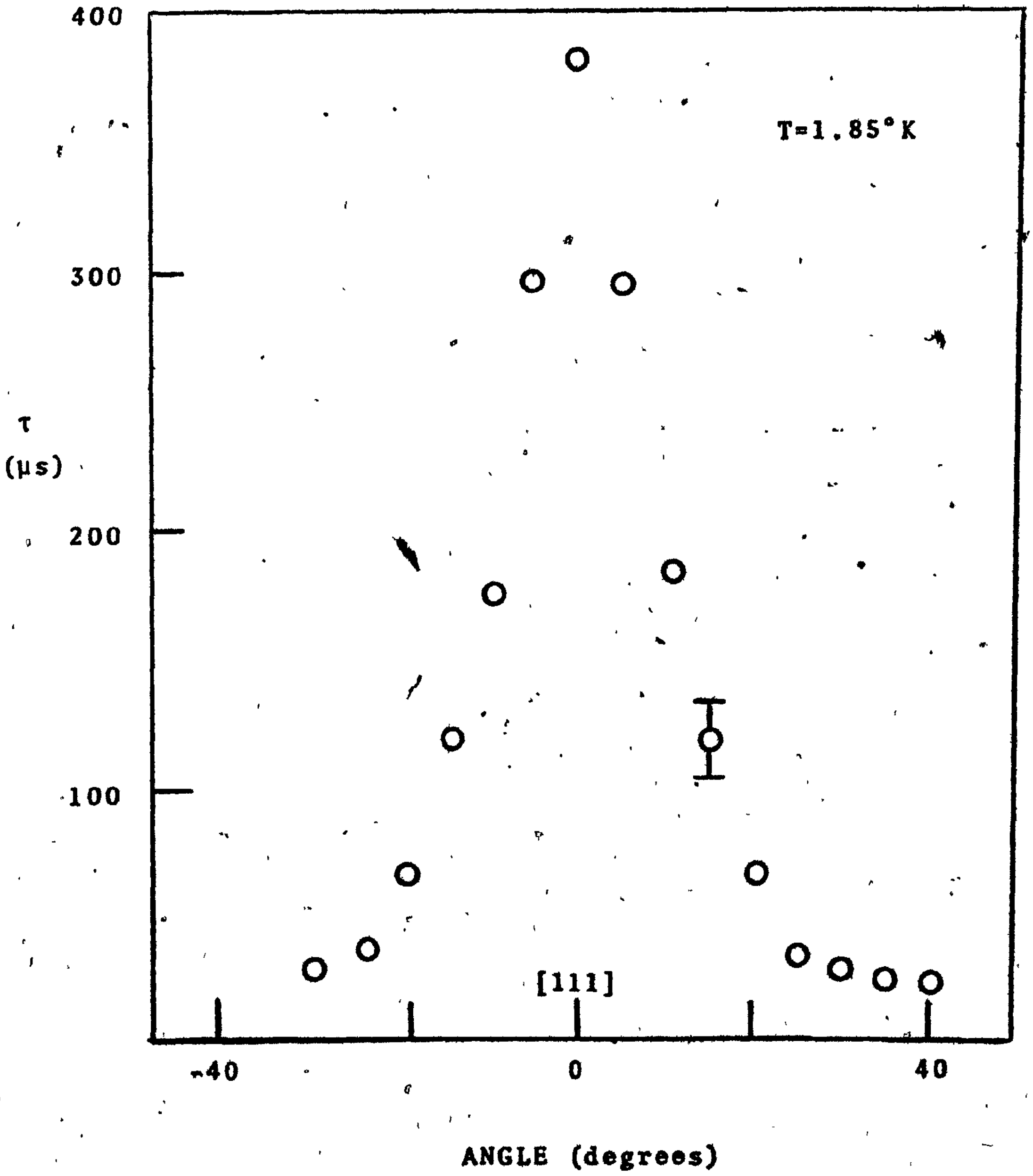
400
300
200
100
τ
(μs)
T=1.85°K
[111]
-40
0
40
ANGLE (degrees)

FIGURE 6.8

Comparison of the angular anisotropy of the spin-lattice relaxation time in the (111) plane at two temperatures.

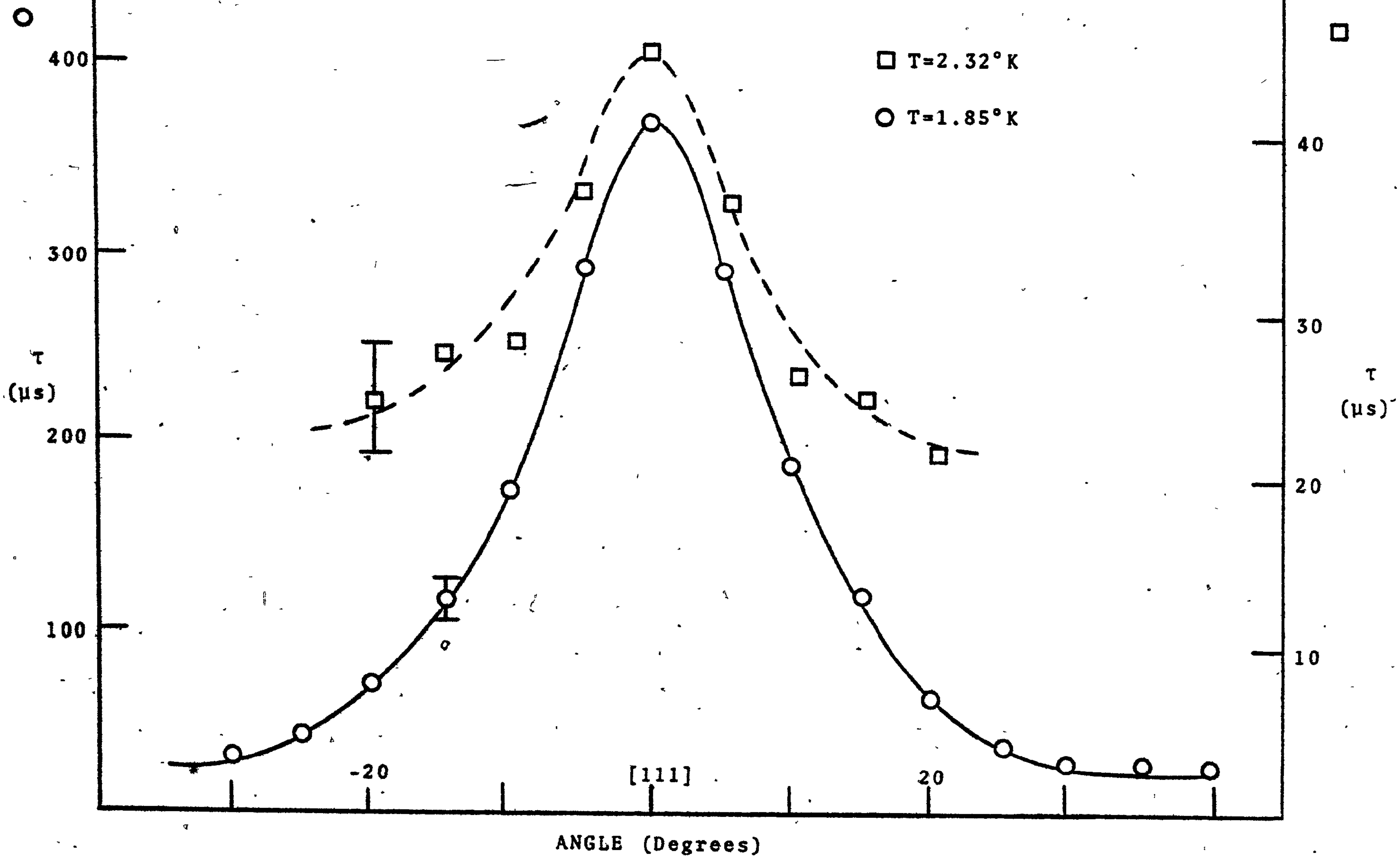
□ T=2.32°K
○ T=1.85°K
○
400
300
τ
(μs)
200
100
□
40
30
τ
(μs)
20
10
-20
[111]
20
ANGLE (Degrees)

to have distinctive differences in their angular anisotropy for Jahn-Teller systems. The reduction of the relaxation time angular anisotropy as T increases reflects the shift in the relative importance of these relaxation mechanisms. At higher temperatures the anisotropy would disappear if the Raman process alone accounted for the relaxation.

7. EXPERIMENTAL RESULTS: Cu^{2+} IN ZINC BROMATE HEXAHYDRATE

This chapter is concerned with the study of octahedrally co-ordinated Cu^{2+} as a dilute substitutional impurity for Zn^{2+} in zinc bromate hexahydrate and follows basically the same format as Chapter 6. The first section summarizes the structure of the host crystal and gives the results of the sample preparation procedure. (This is given in detail in Appendix 3.) Sections 7.2 and 7.3 present the EPR and spin-lattice relaxation data respectively. The discussion of section 7.4 analyses these results and compares them to related systems studied in previous work.

7.1 Crystal Structure and Preparation

Zinc bromate hexahydrate is a member of a group of crystals that have been extensively studied for over fifty years. The space group and cell dimensions were first determined by Wyckoff (1922) from a study of Laue photographs to be $Pa3(T_h^6)$ and 10.31Å respectively. Since the specific gravity is 2.51, he determined the number of molecules of $Zn(BrO_3)_2.6H_2O$ in the unit cell to be four.

The exact structure of zinc bromate hexahydrate was given by Yü and Beevers (1936), at room temperature using the Fourier method of analysis of their x-ray photographs. Arranged on the three-fold axes of the space group are pyramidal BrO_3 groups and octahedral $Zn.6H_2O$ groups. The zinc ion site symmetry is $\overline{3}$, being co-ordinated by six water-oxygen atoms at the corners of a trigonally distorted octahedron (trigonal antiprism). This distortion is small and can be determined from the co-ordinates given by Yü and Beevers (1936). Jesion et al. (1976) found that the interbond angles O-Zn-O, related by the threefold axis, are 88±2 degrees. The co-ordination octahedra of the four zinc ions in the unit cell are oriented differently with respect to crystal axes. However, all four rhombohedral [100] axes make the same angle of 17±2 degrees with respect to the [100] crystal axis.

Crystals with Cu^{2+} as a dilute substitutional impurity for Zn^{2+} in zinc bromate hexahydrate were grown by the slow evaporation of saturated solutions at room temperature. Details of the procedure used to prepare these solutions and samples are described in Appendix 3. A single isotope, ^{65}Cu was used in the preparation, in order to simplify the EPR spectra. Six independent solutions with nominal Cu^{2+} to Zn^{2+} ratios of 10%, 3%, 1%, 0.3%, 0.1% and 0% were prepared. The 0% (pure $Zn(BrO_3)_2.6H_2O$) samples were studied as a control group and produced no EPR spectra. The line intensity was found to vary in the same ratio as the concentration of Cu^{2+} in the solution. Although consistent quantitative data were obtained for all concentrations, samples from the nominal 0.1% and nominal 0.3% solutions produced such poor quality signals as to make extensive EPR and spin-lattice relaxation measurements unreliable. After the completion of the experiments two crystals from each of the remaining groups were analysed using atomic absorption spectroscopy (see Appendix 3). The results are summarized in Table 7.1. The actual Cu^{2+} concentrations were consistently down from the nominal concentration of the parent solutions by a factor of two to five. This compares with a

TABLE 7.1

Analysis of Samples of Cu^{2+} Doped $Zn(BrO_3)_2 \cdot 6H_2O$ by Atomic Absorption Spectroscopy

Nominal concentration of Cu^{2+} in parent solution	Ratio of Cu^{2+} to Zn^{2+}
Percentage	Percentage
1	0.16 ± 0.01
1	0.25 ± 0.01
3	1.44 ± 0.03
3	1.56 ± 0.03
10	3.20 ± 0.04
10	4.44 ± 0.04

similar reduction by a factor of 30 found by Vincent and Walsh (1973) for Cu^{2+} as a substitutional impurity for Mg in lanthanum magnesium double nitrate (LMN).

7.2 The EPR Spectra*

The EPR measurements were performed on single crystals of zinc bromate hexahydrate doped with nominal 1% Cu^{2+}. Although the results quoted in this section were obtained for this concentration, all other samples produced quantitatively similar results. The EPR spectra of crystals with higher Cu^{2+} concentrations were increasingly obscured by larger linewidths while data from crystals with lower Cu^{2+} concentrations were less reliable due to low signal intensity.

At 77°K, the EPR spectrum consists of a single isotropic line with four partially resolved hyperfine components described by the spin-Hamiltonian

$$\mathcal{H}_{77^\circ K} = g\,\beta\vec{H}\cdot\vec{S} + A\,\vec{S}\cdot\vec{I} \qquad (7.1)$$

where $g=2.215 \pm 0.003$ and $A=(31.2 \pm 1.0) \times 10^{-4}\ cm^{-1}$. These parameters of the isotropic spin-Hamiltonian agree within experimental error with those reported by Bleaney et al. (1955c) for the same system at 90°K.

At 4.2°K this isotropic spectrum was no longer observable.

---

*Note: The results of this section have been published by Jesion, A., Shing, Y.H., Walsh, D., and Donnay, J.D.H., 1976. J. Phys. C: Solid St. Phys. 9, L219.

In its place, anisotropic spectra were observed for each of the four differently oriented sites of Cu^{2+} within zinc bromate hexahydrate. The isotropic, high-temperature spectrum is the motionally narrowed average of the low temperature spectra. The transition between these spectra was observed by Bijl and Rose-Innes (unpublished) to remain incomplete down to 7°K. Although a very small absorption was observed between the "parallel" and "perpendicular" spectra at 4.2°K, it was not isotropic and hence could not correspond to the remnants of the high-temperature isotropic spectrum at $g=\frac{1}{3}(g_{\parallel}+2g_{\perp})$. Thus the transition appears to be complete at 4.2°K.

Each Cu site contributes three axial spectra with tetragonal symmetry to the low-temperature anisotropic spectra. These three spectra correspond to tetragonal distortions along the X, Y, and Z axes of the octahedron formed by the co-ordination water-oxygen ions. Thus, for any general magnetic field orientation, twelve anisotropic spectra are expected; each anisotropic spectrum consisting of four allowed hyperfine lines approximately 10G wide. This makes the identification of particular EPR transitions difficult due to the overlapping of many lines within a small magnetic field interval.

When the magnetic field is directed along the crystallographic [100] axis, these twelve anisotropic spectra coalesce into two types of spectra. This is because the co-ordination octahedra of the four Cu^{2+} sites are oriented at the same angle (17 ± 2 degrees) or its supplement (163 ± 2 degrees) with respect to the crystallographic [100] axis. A sample EPR spectrum, with the magnetic field parallel to the crystallographic [100] axis is shown in Figure 7.1a. Parallel and perpendicular spectra correspond to the magnetic field parallel and perpendicular to a principal axis of the g tensor. These principal axes do not correspond to crystallographic symmetry directions but to the co-ordination octahedra of the four Cu^{2+} sites. Since they are all oriented at the same angle with respect to the crystallographic [100] axis, there is a superposition of the spectra of each site. The low field spectrum is the superposition of four spectra corresponding to the "near" parallel spectra of the g-tensor principal axes of the four sites of Cu^{2+}. The high field spectrum is the superposition of two sets of four "near" perpendicular spectra and has double the intensity of the low field spectra. Figure 7.1b shows a spectrum measured with the magnetic field parallel to the g tensor principal axis of one of the Cu^{2+} sites. The four sets of four low-field hyperfine spectra clearly demonstrate the four sites of Cu^{2+} in $Zn(BrO_3)_2.6H_2O$. The parallel spectrum is indicated by the four lines drawn under the spectrum. The perpendicular spectrum is not well resolved because of the gross overlapping of the high field lines.

The way in which the superposition of the four spectra corresponding to each Cu^{2+} site takes place is illustrated by Figure 7.2. The angular variation of only the lowest-field hyperfine line of each of the four sites is plotted in a plane containing a crystallographic [100] axis and one of the g tensor principal axes. With the arrow indicating the position of $g_{\parallel}$, the angle between these two directions was determined to be 12.5 ± 2 degrees. Since the shapes of the EPR lines were distorted

FIGURE 7.1

First derivative representation of the EPR spectrum of Cu^{2+}: $Zn(BrO_3)_2.6H_2O$ measured at 9.46 GHz and 4.2°K with $\vec{H}$ along

(a) a [100] crystal axis,

(b) a principal axis of the g-tensor

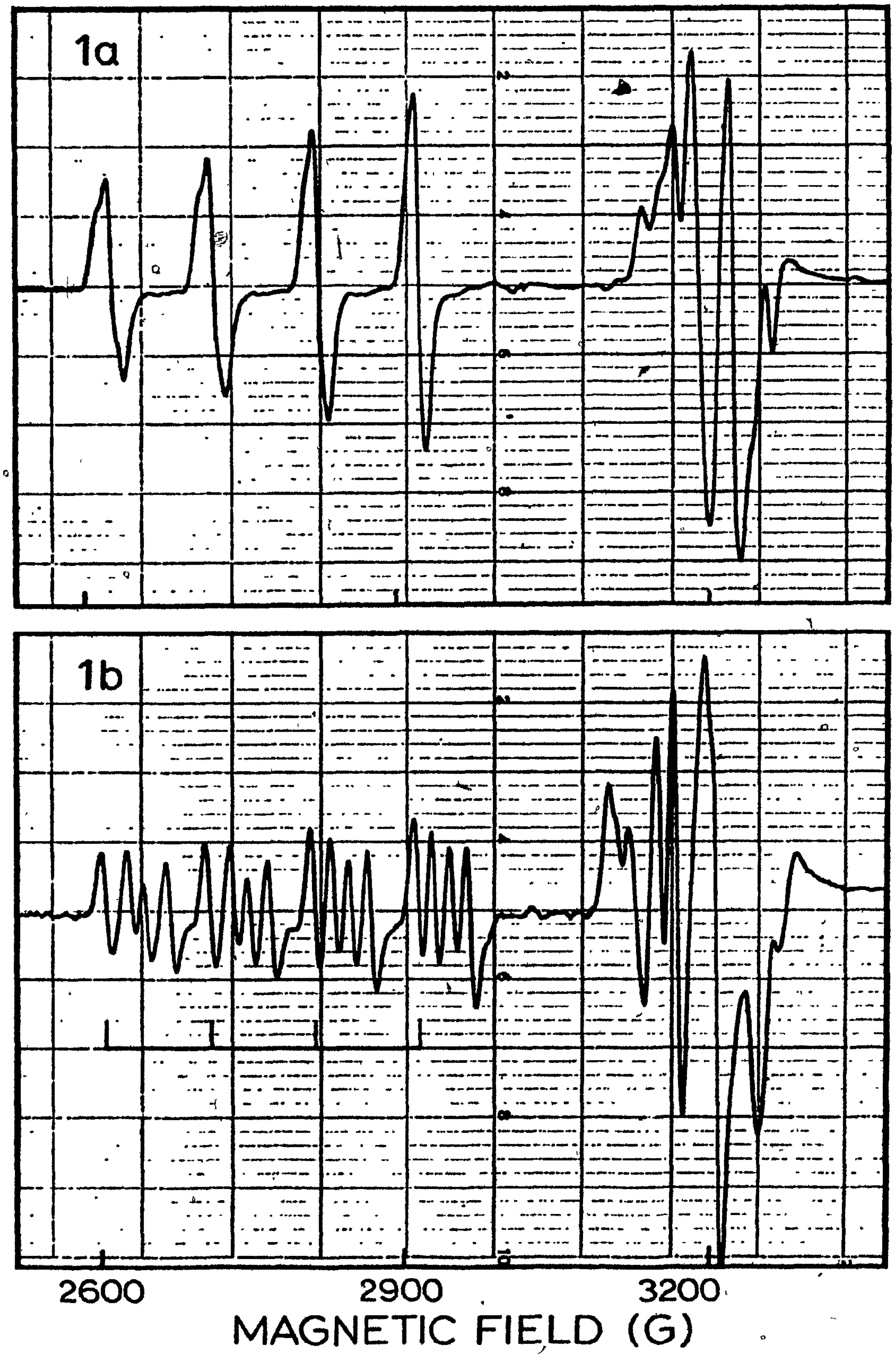
1a
1b
2600
2900
3200
MAGNETIC FIELD (G)

FIGURE 7.2

Angular variation of the lowest-field hyperfine line of the four Cu^{2+} sites in zinc bromate hexahydrate in a plane containing a [100] crystal axis and one of the g-tensor principal axes.

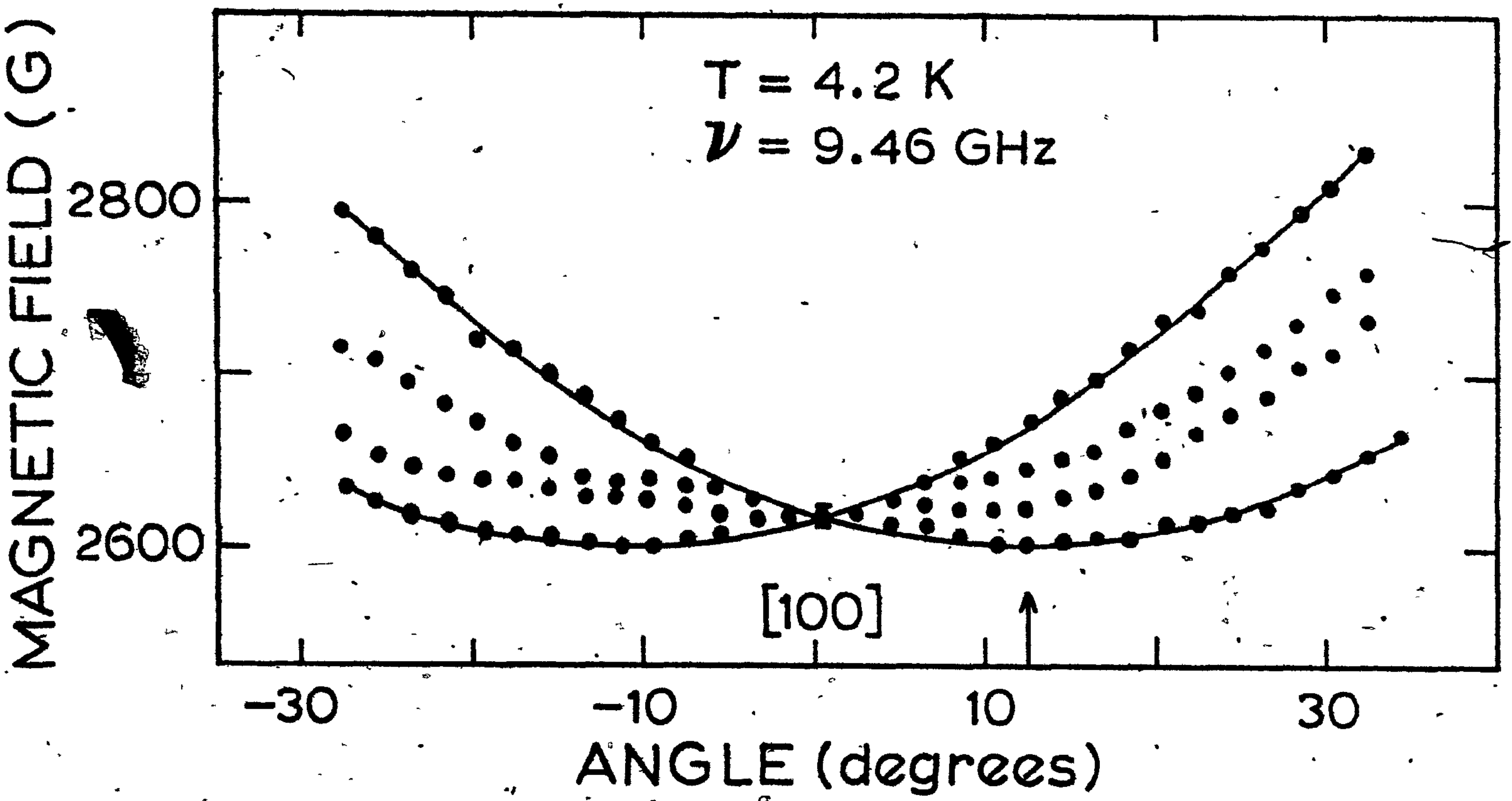
T = 4.2 K
ν = 9.46 GHz
MAGNETIC FIELD (G)
2800
2600
[100]
−30
−10
10
30
ANGLE (degrees)

as the superposition took place, there is a sizeable uncertainty attached to the location of particular lines.

These measured anisotropic spectra can be described by an axial spin-Hamiltonian with $S=\frac{1}{2}$ and nuclear spin $I=\frac{3}{2}$ in the form,

$$\begin{aligned} \mathcal{H} &= g_{\parallel}\beta H_z S_z + g_{\perp}\beta(H_x S_x + H_y S_y) \\ &+ A_{\parallel} S_z I_z + A_{\perp}(S_x I_x + S_y I_y) \qquad (7.3) \\ &+ Q[I_z^2 - \tfrac{1}{3}I(I+1)] \end{aligned}$$

where g, A and Q are the spectroscopic g-factor, the hyperfine parameter and the quadrupole parameter respectively. At 4.2°K, these spin-Hamiltonian parameters were determined to be

$$\begin{aligned} g_{\parallel} &= 2.4507 \pm 0.0005 \\ g_{\perp} &= 2.1009 \pm 0.002 \\ A_{\parallel} &= (117.8 \pm 0.5) \times 10^{-4}\ \text{cm}^{-1} \qquad (7.4) \\ A_{\perp} &= (13.3 \pm 1.5) \times 10^{-4}\ \text{cm}^{-1} \\ Q &= (6.7 \pm 1.5) \times 10^{-4}\ \text{cm}^{-1} \end{aligned}$$

These parameters along with the axial spin-Hamiltonian (7.3) were used to calculate the angular spectra of one particular site. Figure 7.3 shows the agreement with the actual measured

FIGURE 7.3

Calculated and experimental angular EPR spectra of one Cu^{2+} site in zinc bromate hexahydrate. Points are experimental data; full curves are calculated spectra.

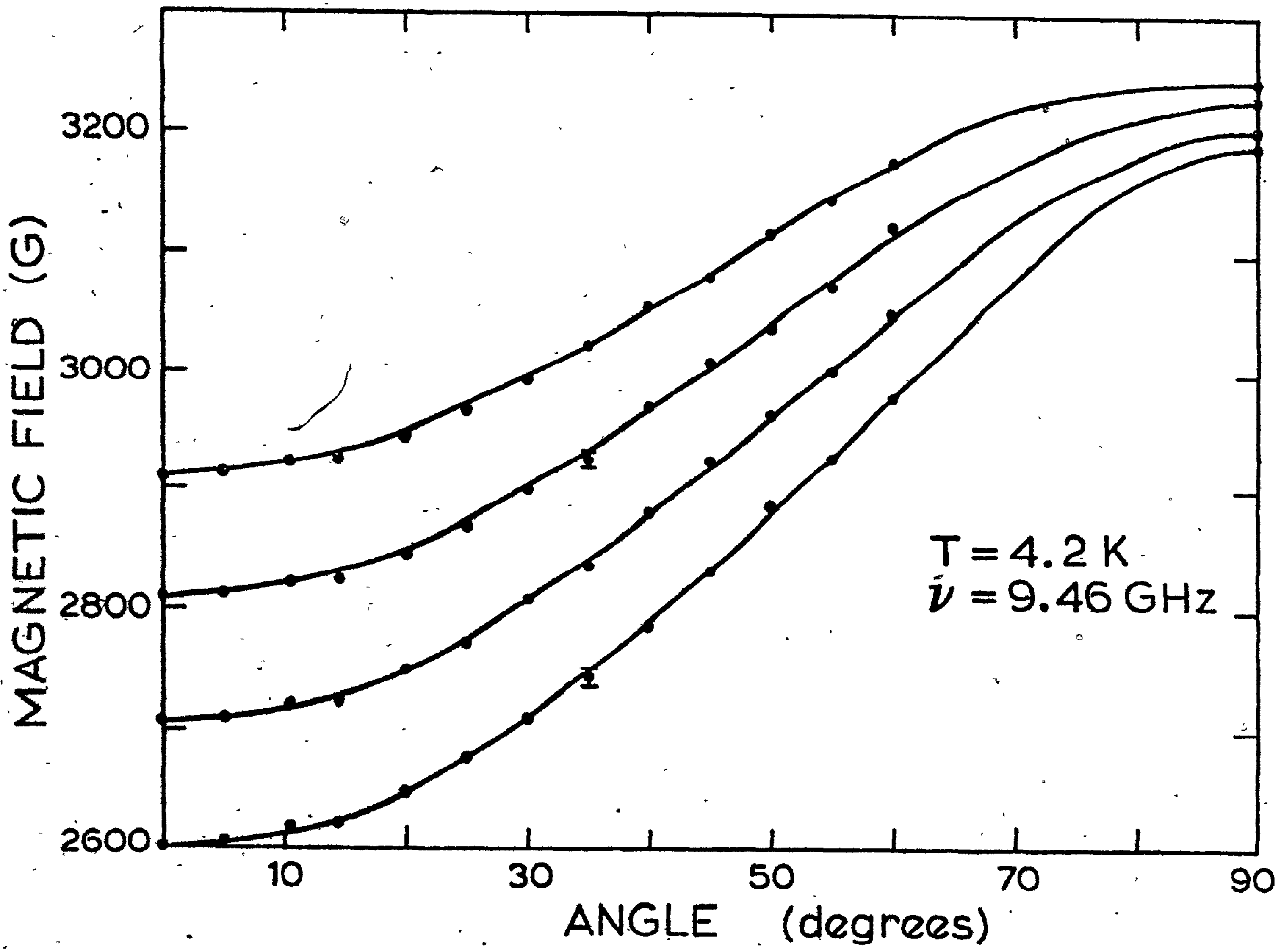
MAGNETIC FIELD (G)
3200
3000
2800
2600
10
30
50
70
90
ANGLE (degrees)
T = 4.2 K
ν = 9.46 GHz

angular variation of the four hyperfine lines of the EPR spectrum of one Cu^{2+} site. The complete angular variation of the anisotropic spectra would include three such spectra with tetragonal symmetry for each of the four Cu^{2+} sites for a total of forty-eight angular dependent lines. Thus it was not possible to trace unambiguously a particular EPR line throughout the entire angular range. The angular variation of the anisotropic spectra shown in Figure 7.3 shows that the ground level of Cu^{2+} in zinc bromate hexahydrate is a strain-stabilized vibronic doublet rather than a quartet, and can be accurately described by a spin-Hamiltonian with tetragonal symmetry (see for example Coffman, 1968). A quartet ground state would have a "cross-over" angular variation which is not observed. This implies that the signs of $A_{\parallel}$ and $A_{\perp}$ must be the same, contrary to the results of Breen et al. (1969) and Dang et al. (1974) who found $A_{\parallel}$ opposite in sign to $A_{\perp}$ for Cu^{2+} in LMN and zinc fluosilicate respectively.

The g-tensor principle axis of the spin-Hamiltonian (7.3) was measured by determining the position corresponding to the maximum value of the spectroscopic g-factor, $g_{\parallel}$. This position was found to be (12.5±2) degrees away from the [100] crystal axis, which is the position where the "near parallel" spectra of the four sites coincide. However, from the crystal structure determination of Yü and Beevers (1936), the angle between the [100] crystal axis and the [100] rhombohedral axis was calculated to be (17±2) degrees. Thus, there is an angular displacement of the g-tensor principle axis of (4.5±4) degrees from the rhombohedral [100] axis.

7.3 Spin-Lattice Relaxation

The spin-lattice relaxation measurements were carried out using the pulse saturation technique outlined in Chapter 5. A pulse width of twenty microseconds was used following the procedure of Breen et al. (1969). Longer pulse widths, particularly over fifty microseconds, produced spurious, pulse-dependent recovery curves corresponding to macroscopic crystal heating effects. These effects were observed for all samples including the undoped zinc bromate hexahydrate control samples, implying that the host crystal was responsible for such phenomena. A twenty microsecond pulse width was found to saturate the EPR transitions without causing crystal heating. The repetition rate was about fifty times longer than the relaxation rate of the crystals to ensure that the spin system returned to its thermal equilibrium before the next pulse.

The recovery signals could be expressed in all experiments as a simple exponential of the form

$$S(t)=A\ e^{-t/\tau} \qquad (7.5)$$

where S(t) is the strength of the recovery signal at time t with t=0 corresponding to the end of the saturating pulse. To extract the spin-lattice relaxation time constant τ, the logarithm of the signal amplitude in arbitrary units was plotted against time. The slope of the resulting plot (τ) was calculated by linear regression using a Hewlett-Packard 55 hand calculator.

Spin-lattice relaxation rates were measured over a temperature range from 4.2°K to approximately 1.3°K for samples grown from the nominal 1%, 3% and 10% Cu^{2+} saturated solutions. These crystals were subsequently analysed and found to have Cu^{2+} to Zn^{2+} ratios of 0.0025, 0.0156 and 0.0444 respectively (see Appendix 3). The DC magnetic field was oriented in the direction of the [100] crystal axis which corresponds to the simplest EPR spectrum where there are superpositions of the "parallel" and "perpendicular" spectra (see Figure 7.1a). This superposition served to enhance the weak observed signal intensity.

All data points are averages of at least twenty measurements, each using a signal averager, (see Chapter 5) equally distributed over the four hyperfine components of the "parallel" spectrum. No systematic difference was observed between the data obtained from each hyperfine component of the "parallel" spectrum, although relaxation rates measured within the "perpendicular" spectrum were generally larger by up to 50%. Such data (based on "perpendicular" spectra) was reported briefly in the paper of Breen et al. (1969) but were not studied in this work. Using pulse saturation techniques and by photographing oscilloscope presentations of the absorption signal recovery, they reported $1/\tau$ proportional to T in the temperature range $10>T>1.3$°K for two samples of Cu^{2+} in zinc bromate hexahydrate. Although their results for $T<2.2$°K fell below the linear extrapolation of the high temperature data, they could not account for this with a phonon bottleneck mechanism since both their samples started to deviate at the same temperature despite a factor of five difference in concentration. No EPR work was reported in their study. Their spin-lattice relaxation data were unreliable because they worked with the complicated "perpendicular" spectrum probably because of the stronger signal intensity. Partial superposition of many EPR lines makes it very uncertain that any particular line is actually saturated. Moreover, photographic techniques fail to provide sufficiently accurate data for a detailed study of the temperature dependence.

Figure 7.4 shows the temperature dependence of the spin-lattice relaxation rate, $1/\tau$ for the zinc bromate hexahydrate crystal doped with nominally 1% Cu^{2+}. The plot shows a slow temperature dependence; the relaxation times varying from approximately 50 μs at 1.3°K to approximately 12 μs at 4.2°K. The data follows an approximate $T^{1.2}$ temperature dependence since the relaxation rate quadruples as the temperature is tripled. Thus the relaxation mechanisms that exhibit such fast temperature dependences as T^9 or T^5 are clearly unsuitable for describing the data. Similarly the coth $(^{h\nu}/2kT)$ function which asymptotically approaches a linear temperature dependence for $kT>>h\nu$ appears to be too "slow" to describe the data. The $T^{1.2}$ rate could be interpreted as a sum of two terms as follows

$$\frac{1}{\tau} \cong AT^{1.2} = BT+CT^2 \tag{7.6}$$

where A, B and C are adjustable constants and the linear and quadratic terms represent a direct relaxation mechanism and a phonon bottleneck respectively. However this appears to be unlikely since a phonon bottleneck can be avoided by working with

FIGURE 7.4

Spin-lattice relaxation rate as a function of inverse temperature for nominal 1% Cu^{2+}: $Zn(BrO_3)_2 \cdot 6H_2O$. The solid line represents the computer best fit to the data.

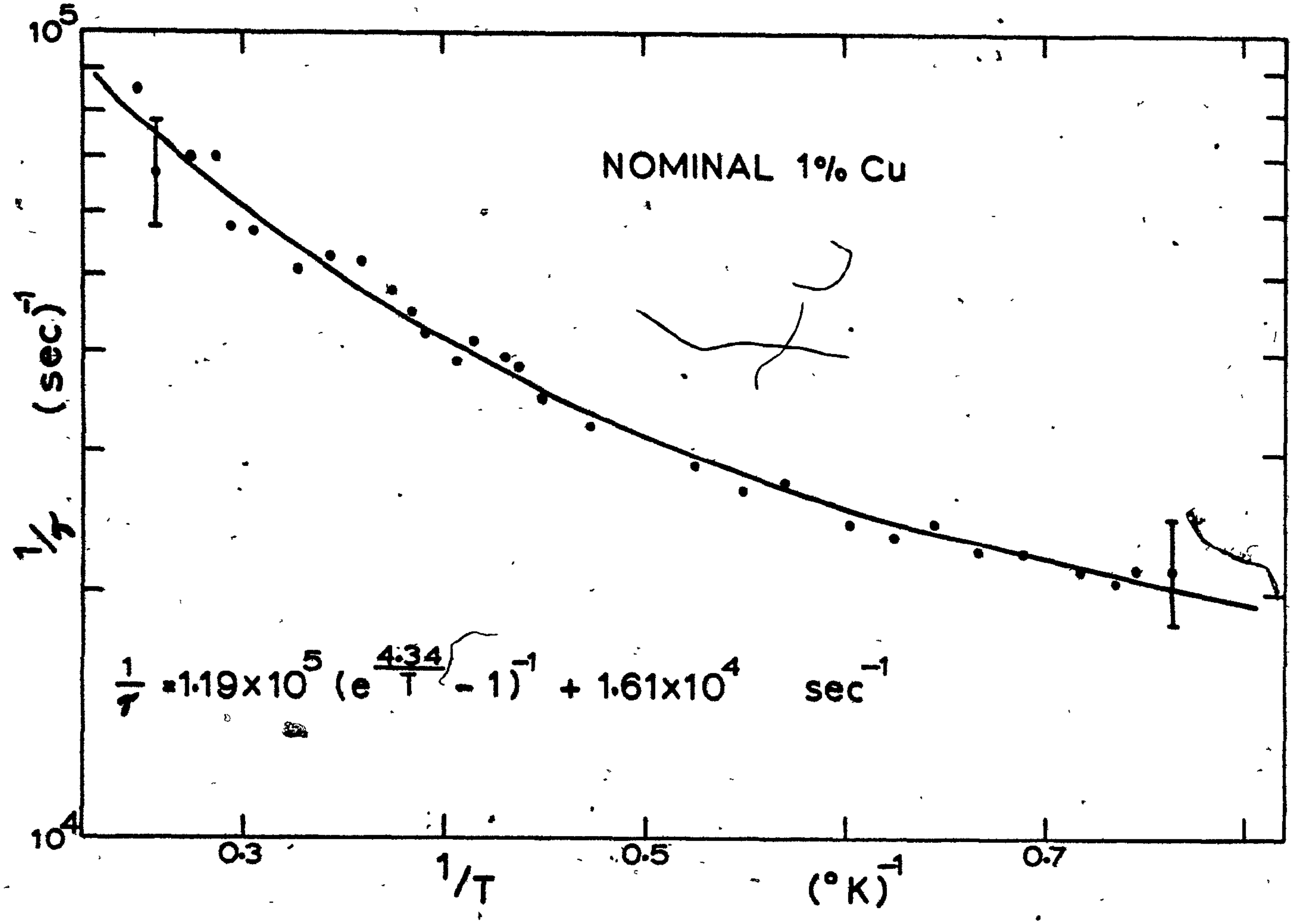
NOMINAL 1% Cu
$\frac{1}{\tau} = 1{\cdot}19\times10^{5}\,(e^{\frac{4{\cdot}34}{T}} - 1)^{-1} + 1{\cdot}61\times10^{4}$ sec^{-1}
10^5
10^4
$1/\tau$ (sec)$^{-1}$
0·3
0·5
0·7
$1/T$ (°K)$^{-1}$

low concentrations so as to minimize the spin heat capacity. Since Adde et al. (1969) have shown that a phonon bottleneck produces a linear dependence of τ on concentration, which was not observed here in subsequent measurements, equation (7.6) was discarded in the interpretation of the data.

The computer best fit to the data obtained for all samples was of the form

$$\frac{1}{\tau} = A[\exp(\Delta/kT-1)]^{-1}+B \qquad (7.7)$$

where the first term represents an Orbach type relaxation process via a near-by excited state at Δ above the ground level and the second term represents a temperature-independent spin-spin relaxation. A sizeable spin-spin relaxation rate may be expected due to the short duration of the saturating pulse. The solid line in Figure 7.4 represents the computer best fit of the form (7.7) while the error bars represent an estimated 15% uncertainty in the values of the relaxation time τ. This is repeated for the nominal 3% and nominal 10% samples in Figures 7.5 and 7.6 respectively. The relaxation data was almost identical for the nominal 1% and 3% samples although their actual Cu^{2+} concentrations differed by a factor of six. Relaxation times for the nominal 10% sample were only approximately 35 microseconds at the lowest temperatures reached in the experiments. This was probably due to an enhancement of the spin-spin exchange since the actual Cu^{2+} concentration was 18 times larger than that of the nominal 1% sample. For all samples, the parameters A, B and Δ of equation (7.7) were found by the least squares method described in section

FIGURE 7.5

Spin-lattice relaxation rate as a function of inverse temperature for nominal 3% Cu^{2+}: $Zn(BrO_3)_2 \cdot 6H_2O$. The solid line represents the computer best fit to the data.

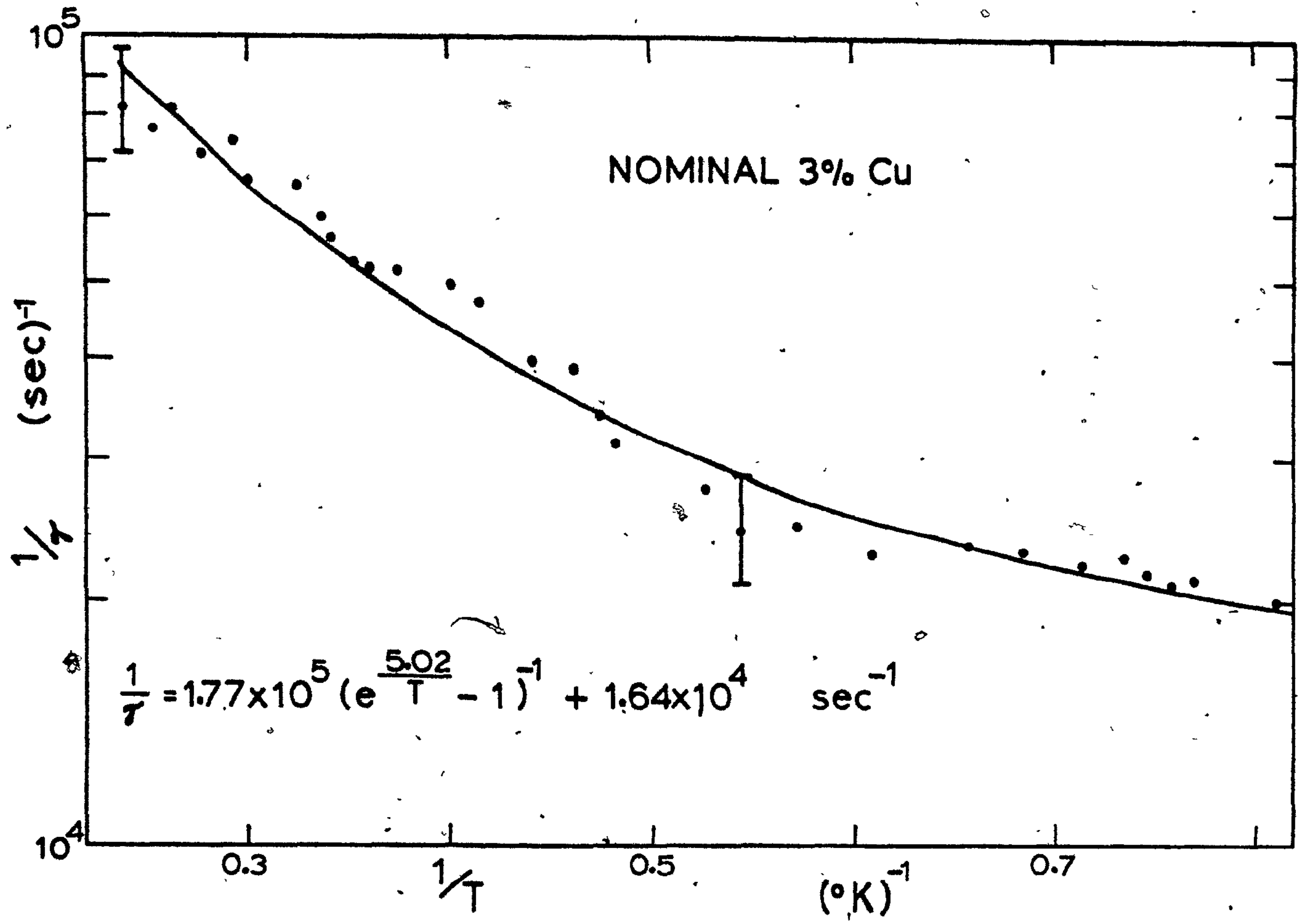
NOMINAL 3% Cu
$\frac{1}{\tau} = 1.77 \times 10^5 (e^{\frac{5.02}{T}} - 1)^{-1} + 1.64 \times 10^4 \quad sec^{-1}$
$1/\tau$ (sec)$^{-1}$
10^5
10^4
0.3
0.5
0.7
$1/T$ (°K)$^{-1}$

FIGURE 7.6

Spin-lattice relaxation rate as a function of inverse temperature for nominal 10% Cu^{2+}: $Zn(BrO_3)_2 \cdot 6H_2O$. The solid line represents the computer best fit to the data.

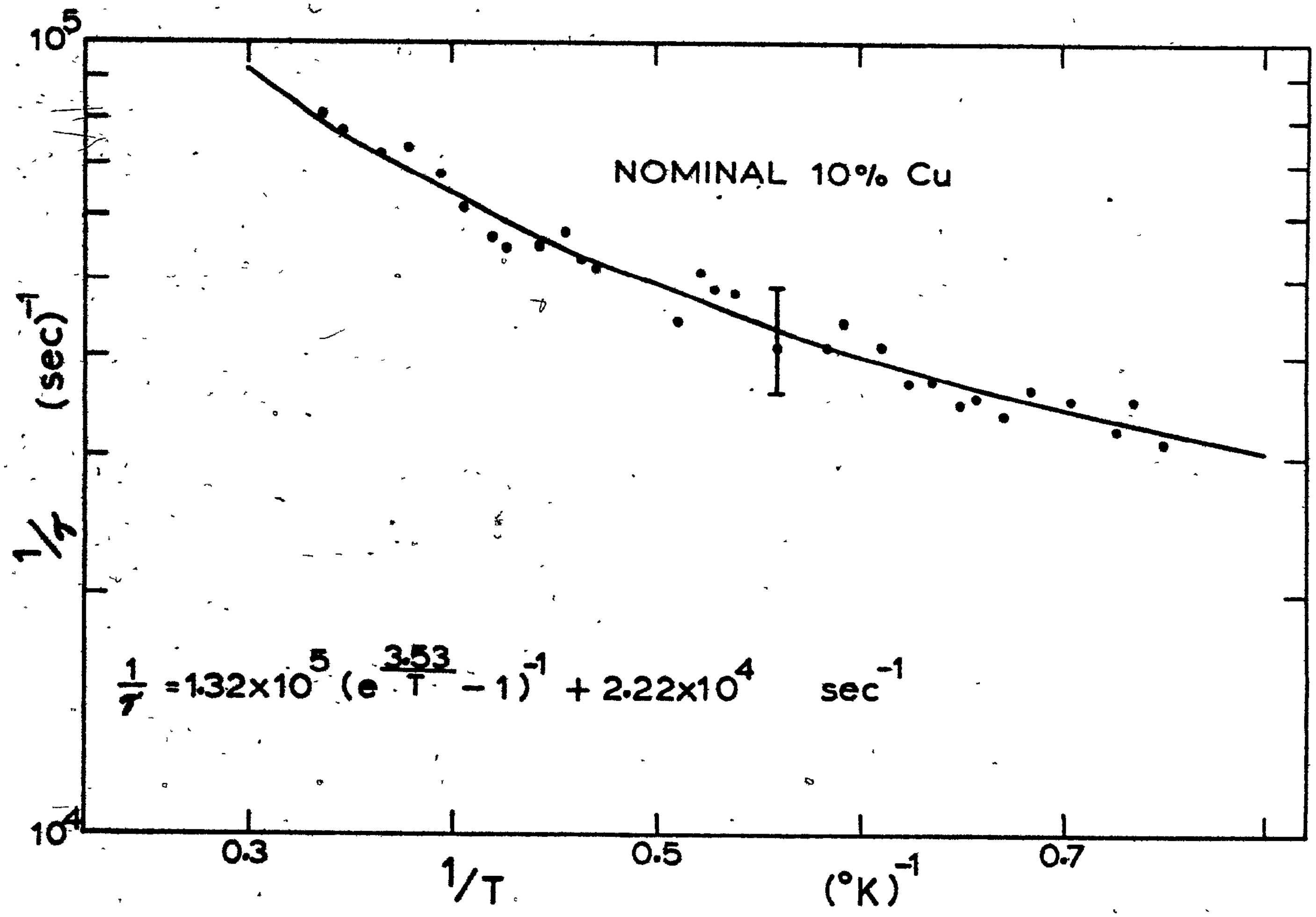
NOMINAL 10% Cu
$\frac{1}{\tau} = 1.32\times10^{5}\,(e^{\frac{3.53}{T}} - 1)^{-1} + 2.22\times10^{4}$ sec^{-1}
10^{5}
10^{4}
$1/\tau$ (sec)$^{-1}$
0.3
0.5
0.7
$1/T$ (°K)$^{-1}$

6.3, using a trial function of the form (7.7). The results are shown in Table 7.2.

7.4 Discussion

The EPR spectra described in section 7.2 are consistent with a Jahn-Teller model which considers the orbital doublet electronic ground state coupled to the Γ_{3g} vibrational modes. An axial spin-Hamiltonian with tetragonal symmetry of the form (7.3) can successfully describe the angular variation of the EPR spectra. The same spin-Hamiltonian was used by Bleaney et al. (1955c) to describe the EPR properties of several cupric salts with trigonal symmetry. Spin-Hamiltonian parameters for octahedrally co-ordinated Cu^{2+} in four similar hydrated salts are compared in Table 7.3. Consistent g-values are a result of crystallographic similarities in the immediate environment of the Cu^{2+} ion. As mentioned in section 7.2, no evidence was found to support the assignment of opposite signs to $A_{\parallel}$ and $A_{\perp}$ for the zinc bromate hexahydrate host. Careful study of the angular variation of the EPR spectra showed no "cross-over" indicating that the ground state (in which the resonance is observed) is a strain-stabilized vibronic doublet.

At low temperatures the effect of the trigonal field is superimposed on that of the frozen in Jahn-Teller tetragonal distortions. This has the effect of tipping the principal directions of the g and A tensors away from the <100> axes and giving them a rhombic character. Such modifications were discussed by Williams et al. (1969) for Cu^{2+} in LMN. They predicted (but could not measure) that the principal axis for $g_{\parallel}$ would be tilted

TABLE 7.2

Best Fit Parameters to the Spin-Lattice Relaxation Rate of the Form $\frac{1}{\tau} = A[\exp(\Delta/kT)-1]^{-1}+B$ For $Cu^{2+}:Zn(BrO_3)_2.6H_2O$

Nominal % Cu (actual % Cu)		A sec^{-1}	B sec^{-1}	Δ °K
1	(0.25)	1.19×10^5	1.61×10^4	4.34
3	(1.56)	1.77×10^5	1.65×10^4	5.02
10	(4.44)	1.32×10^5	2.22×10^4	3.53

(Maximum uncertainty in all parameters: 15%)

TABLE 7.3

Spin-Hamiltonian Parameters for Octahedrally Co-ordinated Cu^{2+}

HOST	T. °K	$g_{\parallel}$	$g_{\perp}$	$A_{\parallel}$ $\times 10^{-4} cm^{-1}$	$A_{\perp}$ $\times 10^{-4} cm^{-1}$	Q $\times 10^{-4} cm^{-1}$	REFERENCE
$Zn(BrO_3)_2.6H_2O$	4.2	2.4507 ±0.0005	2.1009 ±0.002	117.8 ±0.05	13.3 ±1.5	6.7 ±1.5	This Work
$Mg_3Bi_2(NO_3)_{12}.24H_2O$	20	2.454 ±0.003	2.096 ±0.003	110±1	17±2	-	Bleaney et al. (1955c)
$La_2Mg_3(NO_3)_{12}.24H_2O$	20	2.465 ±0.001	2.099 ±0.001	-111.7 ±0.5	16.0 ±0.5	10.5 ±0.5	Breen et al. (1969)
$ZnSiF_6.6H_2O$	4.2	2.460 ±0.005	2.100 ±0.005	±107±2	∓14±2	-	Dang et al. (1974)

by an angle $\Delta\theta$ in a plane containing the tetragonal axis and trigonal axis, from [100] towards [111]. Their approximation was of the form

$$\Delta\theta \approx \frac{10}{3}\sigma \tag{7.8}$$

where σ is $\frac{1}{\sqrt{2}}$ times the ratio of the matrix element of the trigonal field V_3 between the T_{2g} and E_g states, to the cubic field splitting Δ between these orbital states. This dimensionless parameter σ was subsequently found to be 0.045 ± 0.01 for Cu^{2+} in LMN while Dang et al. (1974) who closely follow the same procedure estimated $\sigma \approx 0.06$ for Cu^{2+} in zinc fluosiliciate. Williams et al. go on to predict that a non-zero σ should cause an anisotropy in the waist of the g-tensor,

$$g_1 - g_2 = 4P\sigma \tag{7.9}$$

where $P = \lambda/\Delta$, λ being the spin-orbit coupling constant. P may be evaluated to first order by using the g-values obtained in the paper of O'Brien (1964). Her equation (28) is

$$\begin{aligned} g_1 = g_2 = g_\perp &= 2 - 2P - \frac{2P}{8w} \\ g_3 = g_\parallel &= 2 - 8P + \frac{4P}{8w} \end{aligned} \tag{7.10}$$

where $w^2 = \frac{9\beta}{8\alpha}$, α is the moment of inertia factor defined by

$$\alpha = \frac{\hbar^2}{2\mu\rho_o}$$

and β is one half the barrier height. Values for α and β were first estimated by Opik and Pryce (1957) as 8 cm^{-1} and 600 cm^{-1} respectively. Carrying out the calculation using the measured g-values (7.4), the parameters P and w are -0.0544 and -1.7317 respectively for Cu^{2+} in zinc bromate hexahydrate. Since no anisotropy in the waist of the g-tensor was observed, the maximum value of σ can be estimated from the uncertainty in the measurement of g as follows;

$$|g_1 - g_2| = 4P\sigma < 0.004 \qquad (7.11)$$

thus

$$\sigma < 0.018$$

Such a value of σ together with equation (7.8) implies a maximum value of $\Delta\theta$ equal to $3\frac{1}{2}$ degrees which is consistent with the EPR data of section 7.2 which distinguishes such an angular displacement of $\Delta\theta = 4.5 \pm 4$ degrees. The Cu^{2+} in zinc bromate system marks the first experimental observation of the tilting of the principal axis for $g_{\parallel}$ away from the <100> axes for such systems. In the zinc fluosilicate host, Dang et al. used measurements of the anisotropy of the spin-lattice relaxation rate to put an upper bound of $3\frac{1}{2}$ degrees on $\Delta\theta$, but were also unable to observe such a displacement.

The principle values of the g-tensor, $g_{\parallel}=2.4507$ and $g_{\perp}=2.1009$ may also be used to estimate Ham's quenching parameter q. Since $\frac{1}{2}<q<1$ for a dynamic Jahn-Teller effect with only linear coupling and no warping, the value of q relative to $\frac{1}{2}$ provides a useful criterion as to the strength of the Jahn-Teller coupling (Ham, 1968). Using the definitions

$$\begin{aligned} g_a &= 2.0023 - \frac{4\lambda}{\Delta} \\ g_b &= -\frac{4\lambda}{\Delta} \end{aligned} \tag{7.12}$$

we have (following Abragam and Bleaney, 1970),

$$\begin{aligned} g_{\parallel} &= g_a + 2q\ g_b \\ g_{\perp} &= g_a - q\ g_b \end{aligned} \tag{7.13}$$

Thus, using the principle values of the g tensor determined in section 7.2,

$$\begin{aligned} g_a &= 2.2175 \\ q\ g_b &= 0.1166 \end{aligned} \tag{7.14}$$

from which q is obtained as

$$q = \frac{q\ g_b}{g_a - 2.0023} \simeq 0.54 \tag{7.15}$$

Since the limiting value of q is 0.5 for strong Jahn-Teller coupling, the above values are consistent with an intermediate to strong Jahn-Teller effect. The value of g_a in equation (7.14) corresponds to the high temperature isotropic spectrum (which is the motionally narrowed average of the low temperature anisotropic spectra), $g=2.215\pm0.003$, within experimental error.

Jesion et al.(1976) were unable to distinguish between the model of Ham (1968) based on random strain with dominant tetragonal components and the model of Vincent and Walsh (1973) based on a weak co-operative Jahn-Teller tetragonal distortion on the basis of EPR measurements alone. The spin-lattice relaxation data of section 7.3 seem to support the former model. Vincent and Walsh observed a concentration-dependent relaxation rate for Cu^{2+} in LMN and deduced from this a concentration-dependent strain parameter, F. However this was not observed over a wide concentration range for Cu^{2+} in zinc bromate hexahydrate (0.25% Cu^{2+} to 4.44% Cu^{2+}). In addition, the data for each sample could not be fitted to a function of the form

$$\frac{1}{\tau} = A \coth\left(\frac{\Delta}{2kT}\right) \qquad (7.16)$$

which was used in their analysis. Here Δ is the energy splitting to some well-defined low-lying excited level.

Mangum and Hudson (1966) reported a resonant relaxation process for several rare-earth relaxation rates in $LaCl_3$ with the values of Δ varying from sample to sample for Sm and Eu. They suggested the possibility of an inhomogeneously broadened excited state resulting in the lowering of an effective Δ due to cross-relaxation. Young and Stapleton (1966) examined this suggestion by means of a model in which Δ varied, from one paramagnetic site to another, according to a Gaussian distribution. Even a wide distribution of Δ values will not necessarily broaden the EPR of the ground doublet excessively if only Kramers transitions are considered which is the case also for Cu^{2+} here. By assuming that the i^{th} ion relaxed at a rate given by

$$(1/\tau)_i = A\Delta_i^3 \exp(\Delta_i/kT) \qquad (7.17)$$

and that a spin-spin interaction acted to bring the spin system into equilibrium as it relaxed to the lattice, they obtained an observed effective Δ which is a function of temperature.

The spin-lattice relaxation data of section 7.3 is consistent with the above model. Fitting the data to a resonant relaxation process plus spin-spin interaction, the values obtained for Δ are listed in Table 7.2. No concentration dependence was observed within the experiemental error and fitting procedure. The values of Δ probably reflect some average value $\langle\Delta\rangle$ over a distribution of excited energy levels due to the effects of variable random strain on the energy level structure at the Cu^{2+} sites. Although the value of Δ may be subject to local fluctuations for various samples, the effective average value $\langle\Delta\rangle$ is approximately 3.1 cm^{-1} (4.3°K).

For Cu^{2+} in LMN, Vincent and Walsh (1973) observed a recovery signal which was the sum of two exponential decays corresponding to phonon-assisted tunneling via two excited states (see Figure 4.4). If the tunneling splitting 3Γ is very small, both excited doublets overlap considerably and only a single exponential decay can be observed. This appears to be the case in the bromate host, so that tetragonal strain plays the dominant role in determining the energy level structure. A rough estimate of the tetragonal strain parameter F may be made using equation (4.14),

$$E_1=(\frac{F}{2}-\Gamma)$$

$$E_2=-\frac{1}{2}(\frac{F}{2}-\Gamma)+\frac{1}{2}(\frac{9F^2}{4}+3F\Gamma+9\Gamma^2)^{1/2}$$

$$E_3=-\frac{1}{2}(\frac{F}{2}-\Gamma)-\frac{1}{2}(\frac{9F^2}{4}+3F\Gamma+9\Gamma^2)^{1/2}$$

For a typically small value of the tunneling splitting such as $3\Gamma=0.01\ \text{cm}^{-1}$ and using $\langle\Delta\rangle = 3.1\ \text{cm}^{-1} = E_1 - E_3$, this implies $F\approx 2.0\ \text{cm}^{-1}$ (2.9°K).

Although a poor recovery signal intensity was observed for Cu^{2+} in zinc bromate hexahydrate compared to LMN which was studied with the same apparatus, the relaxation rate was increased by approximately one order or magnitude. The Orbach-type relaxation mechanism depends on the resonant scattering of phonons with energy Δ equal to the splitting between the excited and ground states. If one assumes a distribution of such excited energy levels, the relaxation rate must be enhanced because the number of phonons which can participate in the relaxation is increased. Since the overall relaxation rate is the summation over all possible mechanisms, this may account for such an increase in the observed relaxation rate, while the signal intensity suffers due to a somewhat incoherent superposition of recovery signals.

8. SUMMARY

For many years the unusual EPR spectra and fast relaxation rates of octahedrally co-ordinated Ti^{3+} in the alums at liquid helium temperatures were not well understood. Static crystal field theory predicted that the ground state should be a Kramers doublet with the first excited state over 100 cm^{-1} above this level (Van Vleck, 1958). When the dynamic Jahn-Teller coupling of the Γ_{3g} vibrational mode is taken into account, (Ham, 1965) some of the low-temperature magnetic properties of Ti^{3+} doped CsAl alum as well as CsTi alum can be explained consistently.

The paramagnetic resonance spectra of Ti^{3+} as a dilute substitutional impurity for Al^{3+} in CsAl alum has been measured at 9.46 GHz at temperatures below 3°K. The unusual angular variation of the EPR spectra has been interpreted in terms of a quasi-Γ_8 quartet ground state with the usual alum structure (Shing and Walsh, 1974a). This is a consequence of the almost complete cancellation of the trigonal crystal field and led to an estimate for the orbital reduction factor, $\gamma \approx 0.03$ and the energy level splitting to the first excited Γ_7 state, $\Delta \approx 6$ cm^{-1}. Accurate spin-lattice relaxation measurements using a 24-channel signal averager were also performed on the above system in the temperature range 1.27°K to 2.63°K to determine the temperature dependence of the relaxation process. Both nonresonant and resonant two-phonon relaxation mechanisms were observed. The computer best fit to the relaxation data confirmed the predicted energy level splitting between the ground and first excited states to be 7 ± 1 cm^{-1}. This agreement supports the Jahn-Teller model in which there is a strong coupling of the Γ_{5g} electronic state to the Γ_{3g} vibrational mode as well as the approximate cancellation of the trigonal field producing a quasi-Γ_8 ground state.

Both the $Ti^{3+}(3d^1)$ and the $Cu^{2+}(3d^9)$ ions have ^2D ground states as free ions, although the cubic crystal field inverts their energy level structure in octahedral co-ordination. Although the former has received considerable attention with respect to a possible Jahn-Teller instability, it was the Cu^{2+} in zinc fluosilicate system which first exhibited an unambiguous Jahn-Teller effect (Bleaney and Ingram, 1950). Since then, octahedrally co-ordinated Cu^{2+} ions have been extensively studied to test models of the electron-phonon interaction in insulating crystals. Cu^{2+} in the hydrated salt, zinc bromate hexahydrate is a member of a family of Jahn-Teller systems first studied by Bleaney et al. (1955c) which can be interpreted in terms of a dynamic Jahn-Teller coupling of the Γ_{3g} electronic state to the Γ_{3g} vibrational modes of the co-ordination octahedron (O'Brien, 1964 ; Ham ,1968).

The EPR spectra of Cu^{2+} as a dilute substitutional impurity for Zn^{2+} in zinc bromate hexahydrate have been measured at 9.46 GHz below 4.2°K for the first time. The angular variation of the EPR spectrum shows that the ground state is a strain-stabilized vibronic doublet with tetragonal symmetry. At 4.2°K, the spin-Hamiltonian parameters were determined to be

$$g_{\parallel}=2.4507\pm0.0005 \qquad A_{\parallel}=(117.8\pm0.5)\times10^{-4} \quad cm^{-1}$$

$$g_{\perp}=2.1009\pm0.002 \qquad A_{\perp}=(13.3\pm1.5)\times10^{-4} \quad cm^{-1}$$

$$Q=(6.7\pm1.5)\times10^{-4} \quad cm^{-1}$$

As well as determining that the principal axis of the g-tensor deviates from the [100] crystal axis by 12.5±2 degrees, an angular displacement of 4.5±4 degrees between the g-tensor principal axis and the [100] local axis was measured for the first time. Spin-lattice relaxation measurements were carried out on three crystals with different Cu^{2+} concentrations. The relaxation rate was found to be independent of the Cu^{2+} concentration provided that the impurity level remained dilute. A resonant two-phonon mechanism with an average energy level splitting of 3.1 cm^{-1} was found from the computer best fit to the data. Both the EPR and spin-lattice relaxation data have been discussed primarily in terms of Ham's model (1968) of random strain with dominant tetragonal components.

APPENDIX 1

MECHANISMS OF SPIN-LATTICE RELAXATION

The temperature dependence of the spin-lattice relaxation rate of paramagnetic ions has been a topic of considerable experimental and theoretical interest for over forty years. A large number of relaxation mechanisms have been investigated in the literature with extensive reviews such as Stevens (1967) and Orbach and Stapleton (1972) providing a framework for the study of spin-lattice relaxation processes. In Appendix 1 the main features of this topic are briefly outlined with references to the original papers where the detailed work was published.

Waller (1932) was the first to consider the problem of spin-lattice and spin-spin interactions in paramagnetic salts. His model pictured relaxation transitions as a result of the modulation of the dipolar interaction by lattice vibrations. This led to calculated spin lattice relaxation rates $1/\tau$ proportional to H^2T for the direct process and T^{+7} for the Raman process. However the magnitude of his calculated rates were found to be much greater than that experimentally observed, particularly in dilute magnetic salts.

The foundations of the present theory of spin-lattice relaxation based on phonon modulation of the crystalline electric field were laid by Kronig (1939) and Van Vleck (1939b). The former considered magnetic field admixtures of excited states to overcome Kramers theorem in spin $\frac{1}{2}$ states. He obtained $1/\tau$ proportional to H^4T for the direct process and H^2T^7 for the Raman process, while for spins greater than $\frac{1}{2}$ these were H^2T

and T^7 respectively. Van Vleck assumed that the cubic crystalline field arises from an octahedron of point charges or dipoles. He derived the spin-phonon coupling constants as well as discussing Jahn-Teller distortions of the octahedron. The next year, Van Vleck (1940) presented a general development of the spin-lattice relaxation problem. He extended the work of his previous paper with special attention to $S=\frac{1}{2}$ systems (titanium alum) where he avoided the Kramers cancellation using dynamic effects. In this case the relaxation rate $1/\tau$ was calculated to be proportional to T^9.

Van Vleck (1941a, b) also considered the heating of phonons with energies resonant to the spin system due to spin-lattice relaxation transitions. He considered the energy balance between relaxation heating and cooling due to radiation into the heat bath and predicted a significant bottleneck for the direct process in many salts. The phonon-phonon interaction which transmits heat from the narrow energy region resonant to the spin system to the rest of the phonon spectrum was shown to be insufficient to break the bottleneck at low temperatures. Scott and Jeffries (1962) derived a spin-lattice relaxation rate in the presence of a phonon bottleneck, $\frac{1}{\tau} \alpha T^2$ which they verified experimentally for Pr^{3+} in double nitrate.

Spin diffusion is a flow of heat through the spin system via the spin-spin interaction when the spin temperature in one region of a crystal is raised above the average value. This adds a constant (i.e. temperature independent) term to the spin-lattice relaxation rate. Bloembergen et al. (1959) were first to discuss such relaxation transitions brought about by dipolar or exchange forces.

In 1961, Finn et al. reported the first observation of the resonance relaxation of a low-lying doublet by real transitions to an intermediate state higher in energy by $\Delta >> kT$. They verified that the spin-lattice relaxation rate $\frac{1}{\tau}$ is proportional to $\exp(-\Delta/kT)$ for cerium magnesium nitrate with $\Delta = 34°K$. Independently, Manenkov and Prokhorov (1962) predicted relaxation rates proportional to $[\exp(\frac{\Delta}{kT})-1]^{-1}$ from their analysis of spin doublet states lying at energy Δ below another spin level. This temperature dependence was shown to be due to the resonance process via intermediate states, and a special case of the direct process in multilevel systems.

Numerous relaxation mechanisms have been studied both theoretically and experimentally which display T^n temperature dependence where n=3, 5 or other values. Orbach and Blume (1962) showed that when the phonons which take part in the Raman relaxation process between two degenerate states possess energies greater than the separation of a third state, the relaxation rate is proportional to T^5 instead of the usual T^7 or T^9 rate.

Using a Jahn-Teller model where the crystal vibrations cause an octahedral Jahn-Teller complex to reorient between three strain stabilized tetragonal distortions, Williams et al. (1969) predicted a spin-lattice relaxation rate of the form

$$1/\tau = aT + bT^3 + cT^5 + d\exp(-\Delta/kT)$$

for temperatures above the strain splittings due to random crystal strain. Experimental results on such systems include the observation of $\frac{1}{\tau}=aT+bT^2$ by Lee and Walsh (1968), $\frac{1}{\tau}=aT+bT^5$ by Breen et al. (1969), $\frac{1}{\tau}=a\ \coth(\Delta/2kT)$ by Vincent and Walsh (1973) and $\frac{1}{\tau}=aT^3$ by Dang et al. (1974).

APPENDIX 2

PREPARATION OF CESIUM ALUMINUM ALUM CRYSTALS CONTAINING SMALL AMOUNTS OF Ti^{3+}

The procedure outlined here was used by Dr. G. Fredericks of the Chemistry Department, McGill University to prepare samples of CsAl alum with Ti^{3+} as a dilute substitutional impurity for Al^{3+}. These samples were grown in the summer of 1973 while the bulk of the EPR and spin-lattice relaxation measurements were carried out in 1974 and early 1975. Doping levels of Ti^{3+} could be estimated by the darkness of the typical violet colour characteristic of the optical absorption band for Ti^{3+}. Very "lightly coloured" samples invariably produced poor EPR signals, thus providing an easy check on the Ti^{3+} concentration. Most samples have retained their original colour (Ti^{3+} concentration) for over three years at this writing.

The first stage was the preparation of the host cesium aluminum alum, $CsAl(SO_4).12H_2O$. Forty grams of aluminum sulphate, $Al_2(SO_4)_3.18H_2O$ and twenty-four grams of cesium sulphate, Cs_2SO_4 were dissolved in one litre of deionized water. This was accomplished by mixing the above in a beaker and heating to 90°C on a hot plate. After concentrating the solution to 800ml, the beaker was covered with a watch glass and placed in an ice bath for twenty-four hours.

Upon crystallization, the small crystals were filtered onto a sintered glass filter crucible of medium porosity. The crystals were then redissolved in one litre of deionized water by heating to 90°C. Following this, the beaker was allowed to sit at 0°C for twenty-four hours causing crystals to form. These were then filtered off and dried with filter paper. All crystals were stored in a tightly stoppered glass container. This yielded fifty-nine grams of crystals with volumes in the range one to five cubic millimeters. Upon analysis, the Al and SO_4 content were 4.71% and 33.33% compared with the theoretical values of 4.75% and 33.83% respectively. Larger crystals were obtained by redissolving the CsAl alum previously obtained and allowing crystals to form at 25°C over a period of seven days. This produced crystals of volume approximately twenty-five cubic millimeters.

The next step was to prepare a supply of accessible Ti^{3+} ions. Solutions of Ti^{3+} ions in sulphuric acid were prepared by dissolving basic titanium sulphate, $TiOSO_4.H_2SO_4.8H_2O$ in dilute sulphuric acid and passing the resulting filtered solution through a Jones Reductor in a nitrogen atmosphere. The Jones Reductor consists of a column of amalgamated, granulated zinc contained in a glass tube, through which a solution to be reduced may be drawn.

The desired quantity of alum to be doped was weighed out and transferred to a 500ml suction flask to which the appropriate volume of Ti^{3+} solution was added. The flask was closed with a one-hole rubber stopper fitted with a glass tube which dipped into the mixture. While continuously bubbling nitrogen through the solution to prevent oxidation of the Ti^{3+} ions, the flask was then heated in a water bath to 60°C. After the crystals had dissolved, the flask was closed under slight pressure and transferred to an inert atmosphere. Crystals usually began to form within twenty-four hours, being removed when they reached the desired size. Several samples were analysed for their titanium, aluminum and sulpher content. Titanium was determined colorometrically as a peroxide complex; aluminum and titanium were precipitated simultaneously as the oxides while the sulphate content was determined gravimetrically as the barium sulphate. All analyses were within 1% of the calculated composition.

APPENDIX 3

PREPARATION OF ZINC BROMATE HEXAHYDRATE CONTAINING SMALL AMOUNTS OF Cu^{2+}

To avoid possible complications in the EPR spectra due to the different quadrupole moments of the copper isotopes, only one isotope was used in the doping process. All chemicals used in the following preparation were reagent grade while only distilled, deionized water was used in solution.

Approximately 181.5 milligrams of ^{65}Cu was obtained from Oak Ridge National Laboratories. The powdered copper was heated in an open crucible to form the oxide CuO. The resulting powder was accurately weighed and reheated until no change in the weight was evident upon further heating. This CuO was then converted to suphate by adding dilute sulphuric acid solution (using just enough nitric acid to ensure the complete dissolution of the copper oxide). After the solution was heated "to fumes" to break down HNO_3 and other possible nitrates into gasses, the resulting powder produced a light blue coloured solution typical of copper sulphate.

Since barium bromate, $Ba(BrO_3)_2$ was not commercially available, it was produced using the following reaction

$$BaCl_2 + 2KBrO_3 \rightarrow Ba(BrO_3)_2 \downarrow + 2KCl$$

Since the barium bromate is at least two orders of magnitude less soluble than the other reagents, the precipitate was washed several times to insure that only the barium bromate remained. The precipitate was found to melt at 259±2°C which is in agreement with the melting temperature of 260°C for barium bromate.

To increase the solubility of the barium bromate for subsequent use, it was dissolved in water near the boiling point. This hot barium bromate solution was slowly added to the individually prepared zinc sulphate and ^{65}Cu sulphate solutions to precipitate barium sulphate as shown below

$$Ba(BrO_3)_2 + ZnSO_4 \rightarrow BaSO_4\downarrow + Zn(BrO_3)_2$$

$$Ba(BrO_3)_2 + CuSO_4 \rightarrow BaSO_4\downarrow + Cu(BrO_3)_2.$$

The precipitates were filtered and washed with water which was returned to the respective sulphate solutions to prevent the loss of Zn^{2+} and Cu^{2+} ions. This was repeated until a further drop of barium bromate solution produced no more precipitate. This completed the conversion of the copper and zinc sulphate solutions into copper and zinc bromate solutions, respectively. These solutions were diluted for combination into six groups according to the ratio of moles of Cu^{2+} ions to moles of Zn^{2+} ions, namely 10%, 3%, 1%, 0.3%, 0.1% and 0% or pure zinc bromate.

The six solutions were allowed to evaporate and reach saturation at room temperature, at which point single crystal samples of various sizes were withdrawn as they formed. It was found that the solutions containing higher concentrations of Cu^{2+} took on a greenish-blue colour which darkened with the age of the solution. This indicated that Zn^{2+} was preferentially accepted into the crystals thereby building up the Cu^{2+} concentration within samples that were withdrawn later from the solution. All samples used in the experiments were taken before the parent solutions became "old".

After obtaining the relaxation data, the actual Cu^{2+} concentration of the samples were determined by D. Jeffries of the Chemistry Department, McGill University using atomic absorption spectroscopy. Three sets of standards were made, each consisting of four solutions of 10, 30, 60 and 100 ppm (^{65}Cu equivalent). The background media were 10^4ppm, 10^3ppm and 200ppm $Zn(BrO_3)_2 \cdot 6H_2O$ respectively for the three standards. No significant differences were observed in the calibration curves of absorption vs. ppm Cu among the three sets of standards. Furthermore, a solution of 2×10^4 ppm $Zn(BrO_3)_2 \cdot 6H_2O$ containing no copper gave a reading of zero absorption. The absorption measurements were made on a Unicon model SP90A Atomic Absorption instrument with a copper source lamp. The monochromater was set for the 327.4 nm line of Cu. The results of this analysis are shown in Table V.1.

BIBLIOGRAPHY

Abou-Ghantous, M., Bates, C.A., and Stevens, K.W.H., 1974. J. Phys. C: Solid St. Phys., 1, 325.

Abragam, A., and Bleaney, B., 1970. Electron Paramagnetic Resonance of Transition Ions, (Clarendon Press, Oxford).

Abragam, A., and Pryce, M.H.L., 1950. Proc. Phys. Soc. (London) A63, 409.

__________, 1951. Proc. Roy. Soc. A205,135.

Adde, R., Geshwind, S., and Walker, L.R., 1969. In Proc. 15th Colloque AMPERE, (North-Holland, Amsterdam).

Bates, C.A., and Bentley, J.P., 1969. J. Phys. C: Solid St. Phys., 2, 1947.

Benzie, J. and Cooke, A.H., 1951. Proc. Roy. Soc. A209, 269.

Bersuker, I.B., 1963. Soviet Phys. - JETP. 16, 933.

Bethe, H., 1929. Ann. d. Physik 3, 133.

Bijl, D., 1950. Proc. Phys. Soc. (London) A63, 405.

Bleaney, B., 1959. Proc. Phys. Soc. (London) 73, 939.

Bleaney, B., Bogle, G.S., Cooke, A.H., Duffus, R.J., O'Brien, M.C.M. and Stevens, K.W.H., 1955a. Proc. Roy. Soc. (London) A68, 57.

Bleaney, B., and Bowers, K.D., 1952. Proc. Phys. Soc. (London) A65, 667.

Bleaney, B., Bowers, K.D., and Ingram, D.J.E., 1955b. Proc. Roy. Soc. 228, 147.

Bleaney, B., Bowers, K.D., and Trenam, R.S., 1955c. Proc. Roy. Soc. 228, 157.

Bleaney, B., and Ingram, D.J.E., 1950. Proc. Phys. Soc. (London) A63, 408.

Bleaney, B., and Stevens, K.W.H., 1953. Reports Prog. Phys. 16, 108.

Bleaney, B., and Trenam, R., 1952. Proc. Phys. Soc. 65, 560.

__________, 1954. Proc. Roy. Soc. A223, 1.

Bloembergen, N., Shapiro, S., Pershan, P.S. and Artman, J.O., 1959. Phys. Rev., 114, 445.

Bowers, K.D., and Mims, W.B., 1959. Phys. Rev. 115, 285.

Breen, D.P., Krupka, D.C., and Williams, F.I.B., 1969. Phys. Rev. 179, 241.

Coffman, R.E., 1968. J. Chem. Phys. 48, 2, 609.

Cromer, D.T., Kay, M.J., and Larson, A.C., 1966. Acta. Cryst. 21, 383.

Dang, L.S., Buisson, R., and Williams, F.I.B., 1974. J. de Phys., 35, 49.

de Haas, W.J., and du Pré, F.K., 1938. Physica 5, 969.

Dionne, J.F., 1964. Can. J. Phys. 42, 2419.

__________, 1966a. Can. J. Phys. 44, 2329.

__________, 1966b. Phys. Rev. 139, A1648.

Dionne, J.F., and MacKinnon, J.A., 1968. Phys. Rev. 172, 325.

Fedorov, F.I., 1968. Theory of Elastic Waves in Crystals, (Plenum, New York).

Feher, G., 1957. Bell Telephone Tech. J. 36, 449.

Finn, C.B.P., Orbach, R., and Wolf, W.P., 1961. Proc. Phys. Soc. (London) 77, 261.

Gill, J.C., 1965. Proc. Phys. Soc. 85, 119.

Gladney, H.M., and Swalen, J.D., 1965. J. Chem. Phys. 42, 1999.

Gorter, C.J., Teunissen, P., and Dijkstra, L.J., 1938. Physica 5, 1013.

Ham, F.S., 1965. Phys. Rev. 138, A1727.

__________, 1968. Phys. Rev. 166, 307.

__________, 1971. Phys. Rev. B4, 3854.

__________, 1972. Electron Paramagnetic Resonance, ed., S. Geschwind, Plenum Press, New York.

Hebb, M.H., and Purcell, E.M., 1937. J. Chem. Phys. 5, 338.

Jahn, H.A., and Teller, E., 1936. Phys. Rev. 49, 874.

__________, 1937. Proc. Roy. Soc. (London) A161, 220.

Jesion, A., Shing, Y.H., and Walsh, D., 1974. In Proc. 18th Colloque AMPERE,(Univ. of Nottingham Press, Nottingham, England).

__________, 1975. Phys. Rev. Lett. 35, 1, 51.

Jesion, A., Shing, Y.H., Walsh, D., and Donnay, J.D.H., 1976. J. Phys. C: Solid St. Phys. 9, L219.

Kramers, H.A., 1930. Proc. Acad. Sci. Amst. 33, 959.

Kronig, R. de L., 1939. Physica 6, 33.

Larson, G.H., and Jeffries, C.D., 1966. Phys. Rev. 145, 311.

Lee, K.P.,and Walsh, D., 1968. Phys. Letters 27A, 17.

__________, 1971. Can. J. Phys. 49, 1620.

Lipson, H., 1935. Proc. Roy. Soc. A151, 347.

Lipson, H., and Beevers, C.A., 1935. Proc. Roy. Soc. A148, 664.

Longuet-Higgins, H.C., Opik, U., Pryce, M.H.L., and Sack, R.A., 1958. Proc. Roy. Soc. (London) A244, 1.

Low, W., and Suss, J.T., 1963. Phys. Lett. 7, 5, 310.

Macfarlane, R.M., Wong, J.Y., and Sturge, M.D., 1968. Phys. Rev. 166, 250.

Manenkov, A.A., and Orbach, R., 1966. eds., Spin-Lattice Relaxation in Ionic Solids, (Harper & Row, New York).

Manenkov, A.A., and Prokhorov, A.M., 1962. Soviet Phys. - JETP, 15, 951.

Mangum, B.W., and Hudson, R.P., 1966. J. Chem. Phys. 44, 704.

Marchand, R.L., 1974. Phys. Rev. B9, 11, 4613.

Moffitt, W., and Liehr, A.D., 1957. Phys. Rev. 106, 1195.

Moffitt, W., and Thorson, W., 1957. Phys. Rev. 108, 1251.

Mulliken, R.S., 1933. Phys. Rev. 43, 279.

O'Brien, M.C.M., 1964. Proc. Roy. Soc. (London) A281, 323.

Opik, U., and Pryce, M.H.L., 1957. Proc. Roy. Soc. (London) A238, 425.

Orbach, R., 1961a. Proc. Roy. Soc. A264, 458.

__________, 1961b. Proc. Roy. Soc. A264, 485.

Orbach, R., and Blume, M., 1962. Phys. Rev. Lett. 8, 478.

Orbach, R., and Stapleton, H.J., 1972. in Electron Paramagnetic Resonance, ed. S. Geschwind, (Plenum, New York).

Poole, C.P., 1967. Electron Spin Resonance, (Interscience, New York).

Reynolds, R.W., Boatner, L.A., Abraham, M.M., and Chen, Y., 1974. Phys. Rev. B10, 9, 3802.

Rumin, N., Vincent, C., and Walsh, D., 1973. Phys. Rev. B7, 1811.

Scott, P.L., and Jeffries, C.D., 1962. Phys. Rev. 127, 32.

Shing, Y.H., Vincent, C., and Walsh, D., 1973. Phys. Rev. Lett. 31, 17, 1036.

__________, 1974. Phys. Rev. B9, 340.

Shing, Y.H., and Walsh, D., 1974a. Phys. Rev. Lett. 33, 1067.

__________, 1974b. J. Phys. C: Solid St. Phys. 7, L346.

Stevens, K.W.H., 1953. Proc. Roy. Soc. (London) A219, 542.

__________, 1967. Rep. Prog. Phys. 30, 1, 189.

Stoneham, A.M., 1965. Proc. Phys. Soc. (London) 85, 107.

Tanabe, Y., and Kamimura, H., 1958. J. Phys. Soc. Japan 13, 394.

Van Vleck, J.H., 1939a. J. Chem. Phys. 1, 61.

__________, 1939b. J. Chem. Phys. 7, 72.

__________, 1940. Phys. Rev. 57, 426.

__________, 1941a. Phys. Rev. 59, 724.

__________, 1941b. Phys. Rev. 59, 730.

__________, 1958. Discuss. Faraday Soc. 26, 96.

Vincent, C., 1973. Ph.d. Thesis, Department of Physics, McGill University.

Vincent, C., and Walsh, D., 1974. Phys. Rev. B8, 4935.

Waller, I., 1932. Z. Physik 79, 370.

Williams, F.I.B., Krupka, D.C., and Breen, D.P., 1969. Phys. Rev. 179, 255.

Woonton, G.A., and MacKinnon, J.A., 1968. Can. J. Phys., 46, 59.

Wyckoff, R.W., 1922. Amer. J. Sci. 4, 188.

__________, 1923. Amer. J. Sci. 5, 209.

Young, B.A., and Stapleton, H.J., 1966. Phys. Lett. 21, 498.

Yü, S.H., and Beevers, C.A., 1936. Z. Kristallogr., 95, 426.